

5. DESCRIPTION OF POTENTIAL ENVIRONMENTAL IMPACTS OF PROPOSED ACTIVITY AND ASSESSMENT OF THEIR SCALE AND SIGNIFICANCE

5.1. List of Potential Transboundary Environmental Impacts of Navigation Route Project as Identified by the Inquiry Commission, and Analysis of Key Impact Factors in the Transboundary Context

One of the main outputs produced by the Inquiry Commission is the justified list of potential transboundary environmental impacts of the proposed navigation route, ranked in terms of their likelihood and significance [16]. Presented below is the list of impacts identified and considered by the Inquiry Commission, where the impacts are ranked in terms of their likelihood, significance and sufficiency/adequacy of available information. This approach enables a better focus on the most significant transboundary impacts and more efficient design/implementation of additional research activities and surveys required to provide a complete picture of impacts that might be associated with the proposed navigation route.

1) *Likely significant* adverse transboundary impacts:

- (1) Impact of dredging or deepening of the rifts on the distribution of the flow discharge between the Bystre and Starostambulske Branches and on the water level dynamics along the Bystre Branch, resulting in loss of floodplain habitats important for fish (spawning and nursery) and birds (nesting, feeding);
- (2) Impact of habitat loss by coverage of riparian dump sites and dredging through the offshore sandbar and measures for bank protection on birdlife and fish;
- (3) Impact on the increase of suspended sediment concentration, downstream of the dredging site on fish;
- (4) Impact on the turbidity of marine waters as a result of dumping of spoil at the dump-site at sea, under conditions of southbound alongshore currents;
- (5) Impact of repeated maintenance dredging hampering the recovery processes of affected areas for fish in the long term;
- (6) Cumulative impact of loss and/or disturbance of habitats and by shipping traffic on fish and bird life on a large scale and long time.

2) *Hardly likely significant (inconclusive)* adverse transboundary impacts:

- (7) Impact of increased salt penetration in the Bystre Branch;
- (8) Impact of dredging the sandbar and construction of the retaining dam on the migratory behaviour of sturgeon and shed.

3) *Unlikely significant* adverse transboundary impacts:

- (9) Impact of dredging on the hydro-morphological developments over larger distances and time scales
- (10) Impact of dredging on the distribution of the discharges and the associated water level dynamics between the Chilia and the Tulcea branches;
- (11) Impact of dredging in the sandbar section of the Bystre Branch;
- (12) Impact of dredging on the increase of nutrient concentrations;
- (13) Impact of toxic sediment contamination;
- (14) Impact of overall increase of nutrients, heavy metals and organic micro-pollutants;
- (15) Impact from fish entrainment in dredgers;
- (16) Impact of the dump site in the Black Sea on fish.

4) **Likely** adverse transboundary impact but *insufficient information to judge significance*:

- (17) Impact of dredging on the turbidity of the river and marine waters;
- (18) Impact on the coastal morphology of the Romanian coastal section between the Chilia and the Sulina Branches from the construction of the retaining dam and the maintenance dredging of the Bystre sandbar section;
- (19) Impact of the navigation on fish and bird life;
- (20) Impact of increase of suspended sediment concentration at and near the dredging site;
- (21) Impact on migratory fish, passing the dredging area and/or shifting between different habitats across the border during dredging operations;
- (22) Impact of morphological modifications (e.g. bank protection), resulting from dredging activities, causing more uniform and degraded habitat conditions;
- (23) Effect of the dump site in the Black Sea on the benthic fauna at and around the dump site in relation to the increased suspended sediment concentrations and deposition, loss of habitat and burial of fish food organisms.

5) **Unlikely** adverse transboundary impact but *insufficient information to judge significance*:

- (24) Presence of toxic concentrations of zinc and copper.

5.2. The Methodological Framework, Programme and Key Data Inputs for Further In-Depth Study Undertaken as Part of the Present Assignment

5.2.1. The Methodological Framework for the Modelling Exercise Carried Out to Examine and Predict the Impact of the Seaward Access Channel Construction and Operation on the Distribution of Flow Between the Bystre and Starostambulske Branches

5.2.1.1. One-Dimensional Model of Flow Distribution in the Danube Delta's River Network

The one-dimensional hydraulic regime model for the Danube Delta [17] is based on the use of the complete Saint-Venant equation with respect to a one-dimensional river network [18]. The fact that the model is one-dimensional implies that all hydraulic characteristics are averaged over the river cross-section, i.e. flow velocities are assumed to be equal at each point of a river traverse. The following equations were used to model the Danube Delta system [19]:

$$\begin{aligned} \frac{\partial A}{\partial t} + \frac{\partial Q}{\partial x} &= 0 \\ \frac{\partial Q}{\partial t} + \frac{\partial}{\partial x} \left(\frac{Q^2}{A} \right) + gA \frac{\partial y}{\partial x} + gA \frac{Q|Q|}{K^2} &= 0 \end{aligned} \quad (5.2.1)$$

where t is time interval (s),

x is the modelled along the watercourse axis (m),

$Q(x, t)$ refers to the flow discharge rate (m³/s),

$A[y(x, t)]$ is the cross-section area (m²),

$y(x, t)$ is a free water surface level relative to the Baltic datum (m),

g is the gravitational acceleration (m/s²),

K is the discharge characteristics of the river channel, calculated by the following formula.

$$K = \frac{1}{n} AR^{2/3},$$

where A is the cross-section area,

R is the hydraulic radius which for wide river channels is assumed to be equal to the average depth,

n is the roughness factor.

Based on the set of equations (5.2.1), the flow discharges $Q(x,t)$ and free-surface water levels $y(x,t)$ are derived as a function of time at each point of river network. The set of equations (5.2.1) was solved using the methods developed as part of the CHARIMA package [18]. The equations (5.2.1) were solved using the finite difference method on the basis of the Preisman scheme [19] that featured the following forms of the time and space derivatives:

$$\begin{aligned} \frac{\partial Q}{\partial t} &= \frac{1}{\Delta t} \left[\Theta(Q_{i+1}^{n+1} - Q_{i+1}^n) + (1 - \Theta)(Q_i^{n+1} - Q_i^n) \right] \\ \frac{\partial Q}{\partial x} &= \frac{1}{\Delta x} \left[\varphi(Q_{i+1}^{n+1} - Q_i^{n+1}) + (1 - \varphi)(Q_{i+1}^n - Q_i^n) \right] \end{aligned} \quad (5.2.2)$$

The subscripts i and $i+1$ refer to two successive spatial grid points; the superscripts n and $n+1$ are two successive time steps; ∂x is the distance between the points i and $i+1$; ∂t is a specified time step; Θ and φ are weighting factors whose values lie within the range 0 to 1. By introducing the set (5.2.2) into the set of equations (5.2.1), a non-linear system of algebraic equations can be produced for $Q(x,t)$ and $y(x,t)$, for each modelled grid point, as follows;

$$\begin{aligned} &\frac{1}{2\Delta t} (A_{i+1}^{n+1} - A_{i+1}^n) + \frac{1}{2\Delta t} (A_i^{n+1} - A_i^n) + \frac{Q}{\Delta x} (Q_{i+1}^{n+1} - Q_i^{n+1}) + \frac{1-Q}{\Delta x} (Q_{i+1}^n - Q_i^n) = 0 \\ &\frac{1}{2\Delta t} (Q_{i+1}^{n+1} - Q_{i+1}^n) + \frac{1}{2\Delta t} (Q_i^{n+1} - Q_i^n) + \left[\alpha\theta \left(\frac{Q_i^{n+1}}{A_i^{n+1}} + \frac{Q_{i+1}^{n+1}}{A_{i+1}^{n+1}} \right)^2 + \alpha(1-\theta) \left(\frac{Q_i^n}{A_i^n} + \frac{Q_{i+1}^n}{A_{i+1}^n} \right)^2 \right] \\ &+ \left[\frac{\theta}{\Delta x} (Q_{i+1}^{n+1} - Q_i^{n+1}) + \frac{1-\theta}{\Delta x} (Q_{i+1}^n - Q_i^n) \right] - \alpha \left[\frac{Q}{4} \left(\frac{Q_i^{n+1}}{A_i^{n+1}} + \frac{Q_{i+1}^{n+1}}{A_{i+1}^{n+1}} \right) + \frac{1-Q}{4} \left(\frac{Q_i^n}{A_i^n} + \frac{Q_{i+1}^n}{A_{i+1}^n} \right) \right] \\ &+ \left[\frac{\theta}{\Delta x} (A_{i+1}^{n+1} - A_i^{n+1}) + \frac{1-\theta}{\Delta x} (A_{i+1}^n - A_i^n) \right] + g \left[\frac{Q}{2} (A_i^{n+1} + A_{i+1}^{n+1}) + \frac{1-Q}{2} (A_i^n + A_{i+1}^n) \right] + \\ &\left[\frac{\theta}{\Delta x} (y_{i+1}^{n+1} - y_i^{n+1}) + \frac{1-\theta}{\Delta x} (y_{i+1}^n - y_i^n) \right] + g \left[\frac{Q}{2} (A_i^{n+1} + A_{i+1}^{n+1}) + \frac{1-Q}{2} (A_i^n + A_{i+1}^n) \right] + \\ &\theta \left[\beta \frac{Q_i^{n+1} |Q_i^{n+1}|}{(K_i^{n+1})^2} + (1-\beta) \frac{Q_{i+1}^{n+1} |Q_{i+1}^{n+1}|}{(K_{i+1}^{n+1})^2} \right] + (1-\theta) \left[\beta \frac{Q_i^n |Q_i^n|}{(K_i^n)^2} + (1-\beta) \frac{Q_{i+1}^n |Q_{i+1}^n|}{(K_{i+1}^n)^2} \right] = 0 \end{aligned} \quad (5.2.3)$$

Given that each real river system has a complicated configuration featuring various sections with different hydrologic characteristics, the system (5.2.3) cannot be used for all points of river network at one go and without initial preparatory steps. This means that the entire river network should be first divided into sections with similar hydrological characteristics that are called branches (similar hydrological characteristics imply that a section in question has no drastic variations in channel widths and water depth over its entire length). Branch connections represent the river network nodes, and all branch inflows and channel bifurcations are classified as nodes per se. The river network endpoints are also classified as nodes. The set of equations (5.2.1) and resultant algebraic

system (5.2.3) are only valid and relevant with respect to each separate branch. As regards the nodes, they require additional nodal continuity equations to be formulated as follows:

$$Q_m(t^{n+1}) + \sum_{l=1}^{L(m)} Q_{m,l}(t^{n+1}) = 0, \quad m = 1, 2, \dots, M \quad (5.2.4)$$

where M is the total number of nodes within a river network; $L(m)$ is the number of branches linked through a node m ; $Q_{m,l}(t^{n+1})$ refers to flow discharge rate in each branch and at the point of confluence at the moment of time t^{n+1} ; $Q_m(t^{n+1})$ describes additional external inflow to a node m at the moment of time t^{n+1} .

Given that a flow discharge rate estimated at the moment of time t^{n+1} can be described as:

$$Q_{m,l}(t^{n+1}) = Q_{m,l}(t^n) + \Delta Q_{m,l},$$

where $Q_{m,l}(t^n)$ is the discharge rate at the moment of time t^n ; and $\Delta Q_{m,l}$ is a discharge rate increment, the equation (5.2.4) can be formulated as follows:

$$Q_m(t^{n+1}) + \sum_{l=1}^{L(m)} Q_{m,l}(t^n) + \sum_{l=1}^{L(m)} \Delta Q_{m,l} = 0, \quad m = 1, 2, \dots, M \quad (5.2.5)$$

To calculate discharge rates $Q(x,t)$ and free-surface water levels $y(x,t)$ at all points of the river network for a specified time interval, the sets of equations (5.2.3) and (5.2.5) should be solved taking into account the upstream and downstream boundary conditions, and also inner boundary conditions (in this specific case, upstream boundary conditions are defined as flow discharge rates recorded in Kilia, and the downstream boundary conditions refer to the water levels recorded at the sections where the Delta branches empty into the Sea).

Considering the non-linear character of the (5.2.3) system, it should be solved using the stepwise iteration method, where each iteration is used to solve a linearized system derived by presenting the (5.2.3) system as the Taylor series related to the discharge increments ΔQ and free-surface water level increments Δy , and rejecting those members that are higher than the first order infinitesimal. With this approach, the linearized system can be generally re-formulated as follows

$$\begin{aligned} A_0 \Delta y_{i+1} + B_0 \Delta Q_{i+1} &= C_0 \Delta y_i + D_0 \Delta Q_i + G_0 \\ A'_0 \Delta y_{i+1} + B'_0 \Delta Q_{i+1} &= C'_0 \Delta y_i + D'_0 \Delta Q_i + G'_0, \end{aligned} \quad (5.2.6)$$

where ΔQ and Δy are flow discharge and free-surface water level increments in each specified point and at each iteration, and factors $A_0, B_0, C_0, D_0, G_0, A'_0, B'_0, C'_0, D'_0, G'_0$ are calculated as a function of pre-calculated dependent variables and cross-section areas in each specified point of river network at the moment of time t^n or at a previous iteration. The cumbersomeness is the only reason why the factor-related formulas are not presented herein. The linear system is used to calculate the factor values at each successive iteration, and the process continues to the point where the difference in values of target functions derived in two successive

iterations becomes sufficiently small. The result of this process are the values of target variables at the $n+1$ time step.

The cross-section area $A[y(x,t)]$ for a free-surface water level value $y(x,t)$ at each modelled point is derived from tables listing all modelled points of river network and point-specific cross-section areas estimated for a range of fixed depth intervals DH that describe the real river channel. The preparation of tables with input data is a separate exercise, and the real cross-section area at each point is estimated using the linear interpolation procedure with respect to two nodes showing similar or close water depths.

The linearized system can be solved using a pre-defined relationship between node-specific flow discharge and water level increments. This relationship can be derived from the set of equations (5.2.6), and formulated as follows:

$$\Delta Q_{I(l)} = E_1 \Delta y_1 + F_1 + H_1 \Delta y_{I(l)}, \quad (5.2.7)$$

where the index 1 refers to the first point, and the index $I(l)$ refers to the last point of a branch l , and coefficients E_1, F_1, H_1 can be expressed with the help of coefficients used in the set (5.2.6). by introducing the formula (5.2.7) into the equation (5.2.5), the matrix equation can be derived to calculate a water level increment at each node:

$$[A] [\Delta Y] = [B], \quad (5.2.8)$$

where $[\Delta Y]$ is a vector of node-specific water level increments,

$[A]$ is a matrix whose elements are formed by the coefficients E_i and H_i , specified for each node of a river network,

$[B]$ is a vector defined as a function of external inflows $Q_m(t^{n+1})$, the most recent estimates of node-specific flow discharges, and node-specific values of coefficient F_i .

The resultant equation (5.2.8) is solved relative to $[\Delta Y]$ by using any of the methods adopted to resolve the linear equation sets. The next step is the calculation of flow discharge increment (ΔQ) values for river network nodes using the equation (5.2.7), followed by the calculation of flow discharges and free-surface water levels for internal points within each branch. This is a one-iteration procedure used to solve the set of equations (5.2.1). The iteration process continues to the point where the results produced in two successive iterations coincide with sufficient precision. The result produced is the solution of the set of equations (5.2.1) at the $n+1$ time step.

To carry out the modelling exercise for the Ukrainian part of the Chilia Branch, the part of river network lying downstream of Kilia was divided into 43 branches schematically presented in Figure 5.1, which also shows the locations of hydrological stations (yellow triangles). Those river sections where real cross-section areas were known were marked accordingly, and cross-section area estimates were produced for all other sections using available data on the average width and depth of each such section. The calibration of the hydraulic regime model (i.e. the selection and adjustment of model parameters, to include, first and foremost, the roughness factor) was carried out using the available hydrological measurement data for August and September 2002. the model was further verified using the 2001 and 2002 hydrological measurement data.



Figure 5.1. The Map Showing the Modelled Part of Danube River Network, with Indexed River Branches and Hydrological Stations

The calculation procedure employed branch-specific roughness factor values derived during the model calibration (Table 5.1).

Table 5.1. Roughness Factor Values Used in the Calculation Process

Branch Number	1	2	3	4	5	6	7	8	9	10
Roughness Factor	0.0265	0.0367	0.026	0.026	0.0267	0.0267	0.0287	0.0377	0.0377	0.0387
Branch Number	11	12	13	14	15	16	17	18	19	20
Roughness Factor	0.027	0.027	0.027	0.027	0.027	0.027	0.027	0.038	0.038	0.038
Branch Number	21	22	23	24	25	26	27	28	29	30
Roughness Factor	0.038	0.015	0.015	0.015	0.038	0.038	0.038	0.038	0.038	0.016
Branch Number	31	32	33	34	35	36	37	38	39	40
Roughness Factor	0.017	0.017	0.015	0.036	0.016	0.015	0.036	0.036	0.015	0.03
Branch Number	41	42	43							
Roughness Factor	0.03	0.0169	0.0169							

For the model verification, the 2007 flow discharge estimates were produced for the free water surface conditions, for various branches of the Danube Delta based on the 2001 bathymetry data and design parameters specified for the proposed navigation route in the Bystre Branch. The upper boundary conditions were defined on the basis of the 2007 flow discharge measurement data collected by the Ismail Hydrometeorological Observatory at the Vylkove Monitoring Station (Chilia Branch), provided courtesy of the USRIEP Institute (Table 5.2).

Table 5.2. Flow Discharges in the Danube River (Chilia Branch, Near Vylkove)
($W = 90.2 \text{ km}^3$, $M=3.50 \text{ l/s km}^2$, $H=110 \text{ mm}$, $F=817,000 \text{ km}^2$), in m^3/s

Day	Month											
	1	2	3	4	5	6	7	8	9	10	11	12
1	1900	<u>2550</u>	4000	4450	2530	2770	2140	<u>1910</u>	1720	<u>3420</u>	<u>2500</u>	3890
2	1930	2770	3980	4540	2510	2760	2090	1780	1730	3370	2520	3860
3	1930	2950	3950	4590	2500	2680	2060	1710	1750	3270	2600	3880
4	1930	2990	3850	4620	2450	2590	2020	1630	1750	3140	2710	3940
5	1920	3120	3740	4650	2380	2520	1980	1590	1750	2960	2840	4080
6	1930	3170	3640	<u>4670</u>	2310	2480	1960	1560	1760	2820	2960	4210
7	1890	3200	<u>3470</u>	4580	2270	2480	1920	<u>1530</u>	1760	2690	3040	4250
8	1860	3240	3480	4540	2230	2470	1870	<u>1530</u>	1760	2600	3200	4370
9	1850	3150	3500	4460	2210	2450	1860	1590	1830	2540	3410	4510
10	<u>1830</u>	3040	3480	4380	2210	2470	1870	1630	1710	2520	3590	4460
11	1860	2980	3510	4290	2180	2460	1850	1650	<u>1660</u>	2500	3710	4420
12	1910	2920	3680	4200	2140	2500	1840	1670	1680	2500	3790	4410
13	2000	2890	3840	4030	2120	2570	1800	1700	1760	2490	3710	4500
14	2060	2870	3970	3920	2120	2660	1740	1760	1850	2470	3600	4600
15	2120	2850	4070	3720	<u>2100</u>	2760	<u>1730</u>	1760	1870	2440	3470	<u>4630</u>
16	2200	2820	4140	3590	2140	<u>2810</u>	1790	1730	1930	2410	3330	4550
17	2260	2750	4160	3500	2210	2760	1810	1730	2040	2390	3190	4460
18	2300	2720	4140	3420	2210	2720	1870	1740	2160	2350	3110	4470
19	2340	2800	4130	3360	2210	2690	1930	1740	2350	2310	3090	4530
20	2430	3000	4130	3240	2230	2640	2000	1750	2570	2280	3180	<u>4550</u>
21	2470	3170	4190	3080	2250	2600	2060	1720	2770	2250	3320	4540
22	2500	3350	4240	2940	2320	2560	2140	1690	2910	2260	3480	4500
23	2540	3540	4270	2880	2400	2470	2210	1640	3070	2230	3630	4510
24	2590	3710	4150	2820	2460	2400	2310	1620	3180	<u>2230</u>	3780	4560
25	2630	3810	4080	2740	2540	2310	<u>2340</u>	1590	3310	2270	4040	4550
26	<u>2660</u>	3940	4150	2690	2560	2230	<u>2340</u>	1600	3410	2300	4230	4490
27	<u>2660</u>	3940	4280	2650	2560	<u>2190</u>	2290	1650	3530	2420	<u>4290</u>	4400
28	2600	<u>3970</u>	4200	2580	2610	2240	2160	1660	<u>3600</u>	2430	4280	4280
29	2560		4280	2560	2650	2260	2090	1690	3570	2470	4180	4180
30	2550		4340	<u>2550</u>	2680	2250	2040	1700	3490	2510	4010	4010
31	2540		<u>4400</u>		<u>2730</u>		1970	1700		2520		<u>3750</u>
10-Day Period												
1	1900	3020	3710	4550	2360	2570	1980	1650	1750	2930	2940	4150
2	2150	2860	3980	3730	2170	2660	1840	1720	1990	2410	3420	4510
3	2570	3680	4230	2750	2520	2350	2180	1660	3280	2350	3920	4340
Mean	2220	3190	3980	3670	2360	2530	2000	1680	2340	2560	3430	4330
Maximum	2660	3980	4410	4670	2740	2810	2340	1930	3600	3430	4290	4630
Minimum	1830	2520	3430	2540	2100	2180	1720	1520	1650	2220	2500	3710

Figures 5.3 to 5.5. graphically illustrate the resultant flow discharge estimates for the Vylkove section and the Bystre Branch, and estimated water levels under the free water surface conditions for the Kilia section, compared against the actual measurement data.

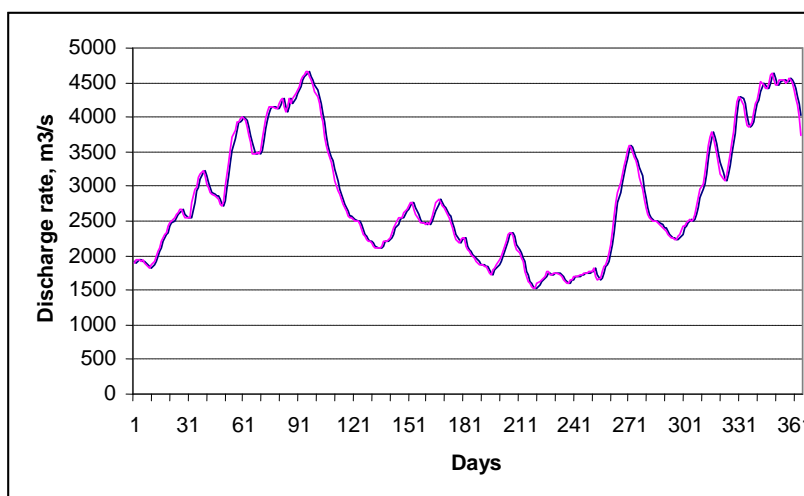


Figure 5.3. The Comparison of Estimated Flow Discharge Rates (Blue Line) with the 2007 Measurement Data, Vylkove Section

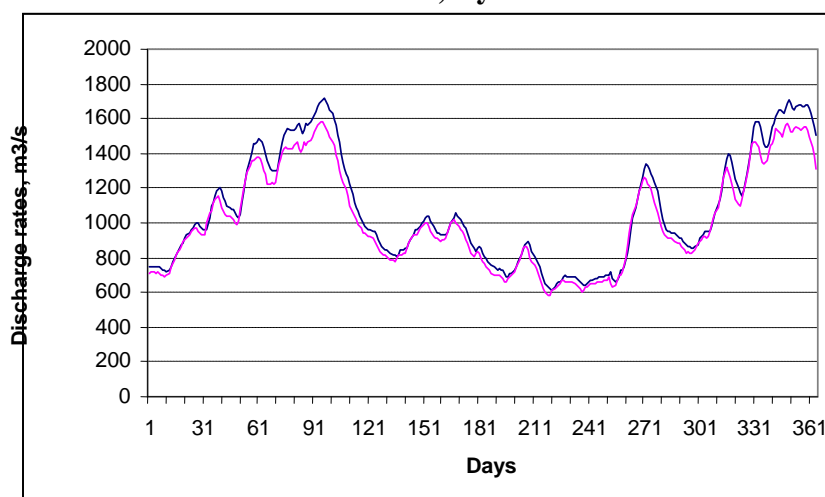


Figure 5.4. The Comparison of Estimated Flow Discharge Rates (Blue Line) with the 2007 Measurement Data, Bystre Branch

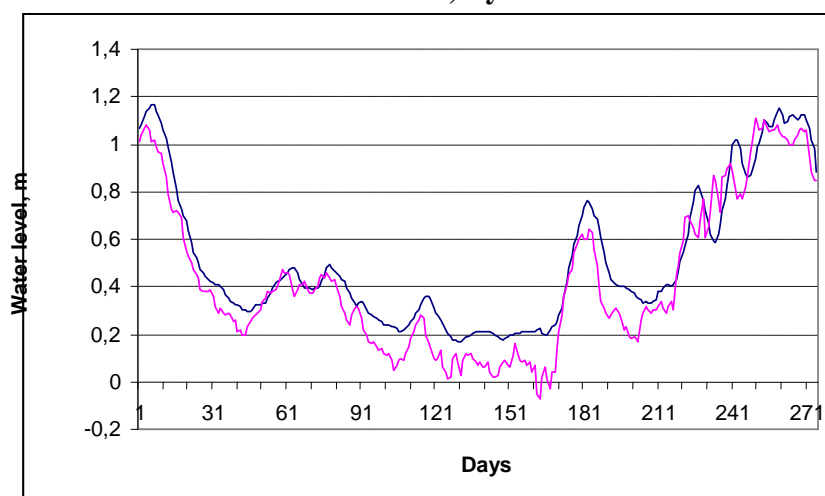


Figure 5.5. The Comparison of Estimated Free-Surface Water Levels (Blue Line) with the 2007 (April-December) Measurement Data, Kilia Section

5.2.1.2. Two -Dimensional Hydraulic Regime Model for the Delta's River Network and Coastal Areas of the Sea, Based on the Unstructured Grids

In 2008, new numerical model COASTOX-UN was developed in the IMMSP, NASU, Kyiv, to solve the shallow-water equations on the triangular unstructured grids. Unstructured grids allow to carry out net thickening effectively anywhere it is necessary to describe narrow channels, and in this way give an opportunity to model hydraulic river-sea systems. The model utilizes unstructured grid with triangular elements, when the equations are solved using the finite-volume methods and Godunov-type scheme. This scheme is explicit and conservative. It has TVD properties and the second order accuracy, both in space and time. At that the second order in time is achieved using the Runge-Kutta method of predictor-corrector type, and the second order in space is achieved by two different methods used to calculate fluxes at the predictor-corrector steps. At the first stage, the Godunov type scheme is used with approximate Riman HLL and Roe solvers. At the second stage, these fluxes are calculated directly downflow using the Riemann problem states. Based on SEA scheme [20], the algorithm has a number of the modifications described in [21]. The model was tested on a lot of 1-dimensional tests, including the dam-break test [22], the “steady transcritical flow with a shock over a hump” test [20, 23], the test “a small perturbation of a steady-state solution” [20, 23], and 2-dimensional tests as well as such as various ones on the dam-break [23-25], the “recirculation flow after sudden expansion” test (Mohamadian et al., 2005), and the “oblique hydraulic jump” test [20, 23]. For all these tests, the model demonstrated sufficient level of precision.

The last test results are represented in Figure 5.6. Its analytical solution is as follows: behind the front, the depth and current velocity are 1.5m and 7.9525 m/s, respectively; the front angle is $\beta_0 = 30^\circ$. The modelled solution is as follows: the depth and current velocity beyond the front equal respectively 1.4993m and 7.9508m/s, the front angle is $\beta_0 = 30^\circ$.

The model was tested as well on actual measurement data collected in December 1999 for the San Francisco bay [26], where regular tidal waves generated specific hydrodynamic regime, when all water was going through narrow place and spreading farther in the bay. In that way strong tidal currents sprang up. The modelling net and comparison of the natural and modelled results are shown at the Figures 5.7 and 5.8.

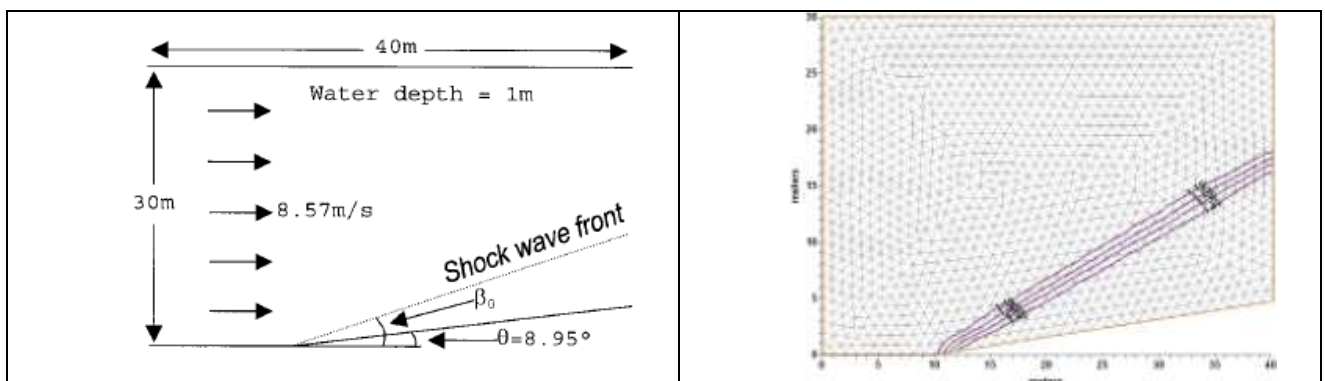


Figure 5.6. The “Oblique Hydraulic Jump” Test Results: the Test Scheme (Left), and the Net with Calculated Water Levels (Right)

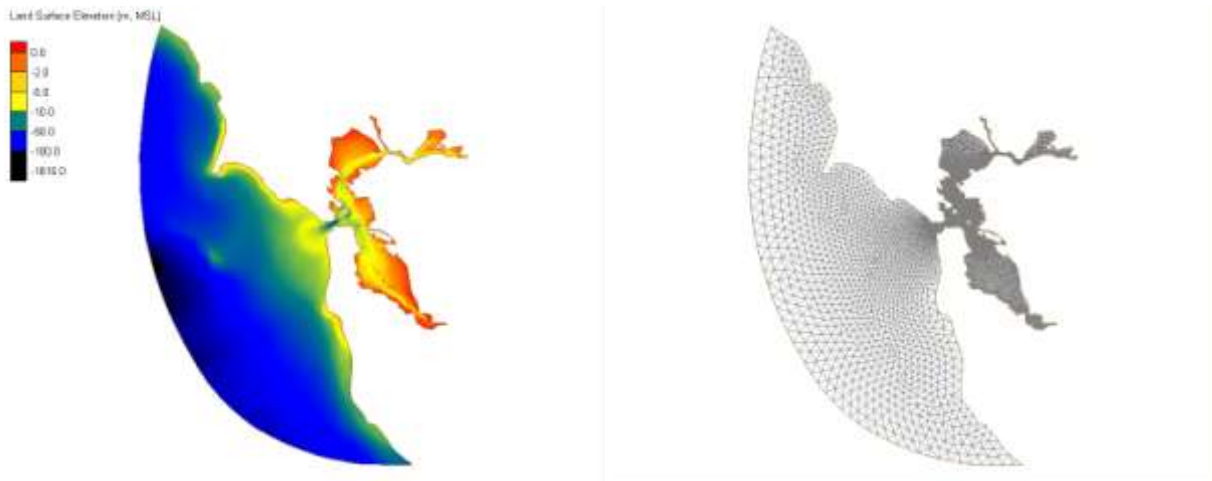


Figure 5.7. Bathymetry and the Modelled Area Net (the San Francisco Bay Area)

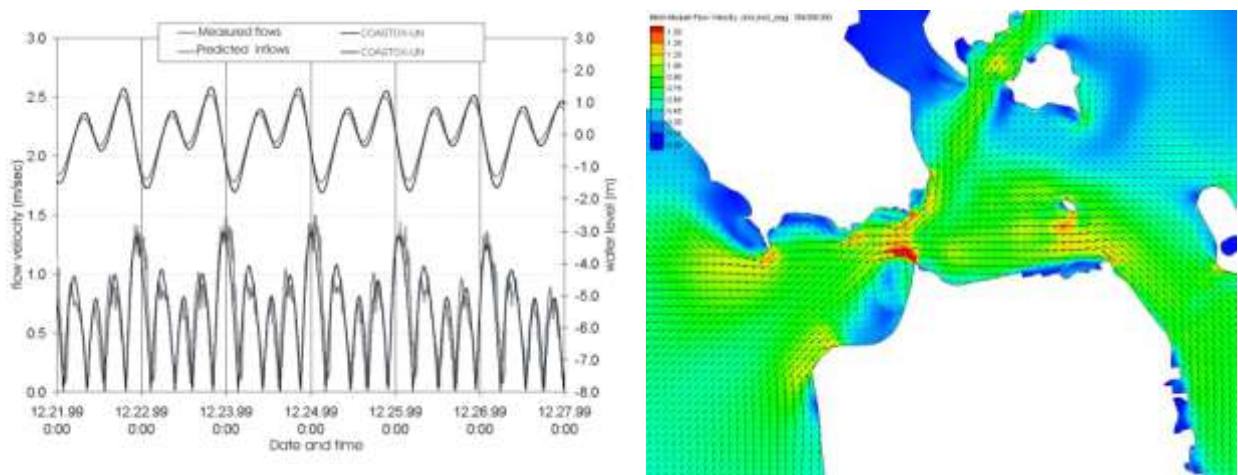


Figure 5.8. (Left) Measured and Calculated Water Levels and Flow Velocities (Left); (Right) Pattern of Currents in the Area Where the San Francisco Bay Joins the Ocean (m/s)

The tested 2-dimensional model was adapted for the hydrodynamics calculations for the Ukrainian part of the Danube Delta, both fluvial and maritime, as a single hydrodynamic system.

A common grid was built to describe the sea and coastal section between the Starostambulske Branch and Bystre Branch. It also includes the Starostambulske and Bistre Branches up to Vylkove (Figures 5.9–5.11). It should be noted that smaller Delta branches (Skhidny, Tsygansky, Musura and Lebedynka) were not modelled due to the lack of sufficient depth measurement data, and appropriate flow discharge rates were specified instead. The water level in the open sea was assumed as equal to -0.21 m.

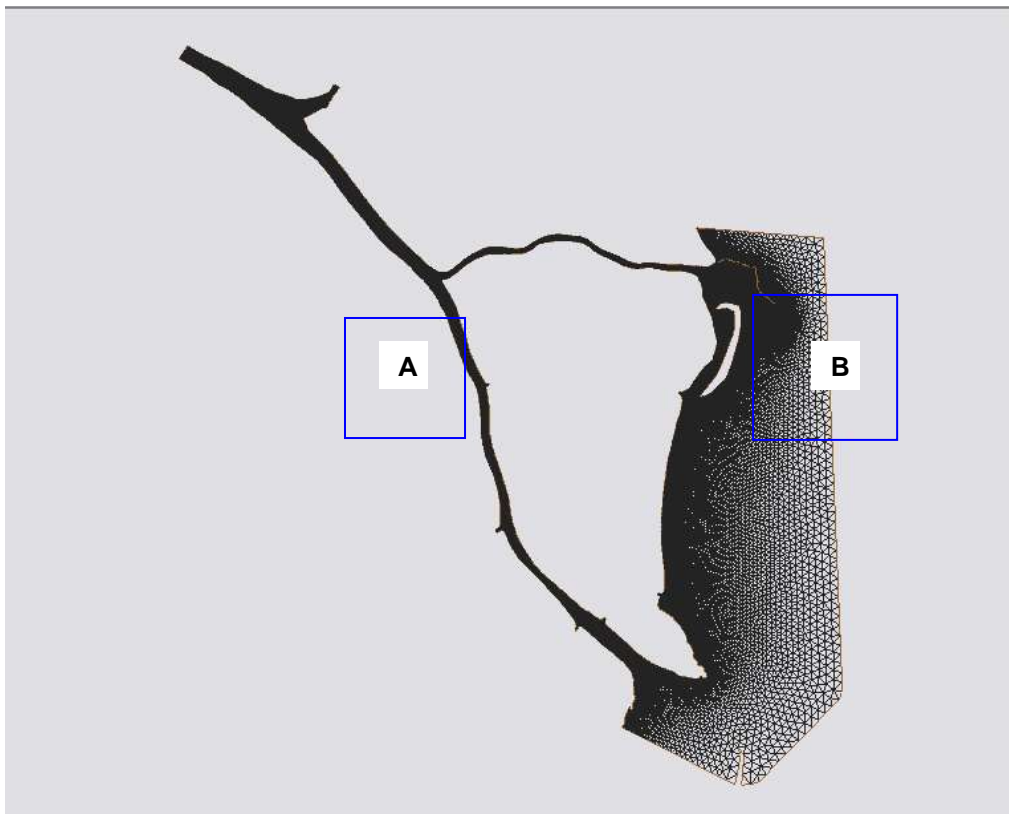


Figure 5.9. The Common Grid for the Modelled Area

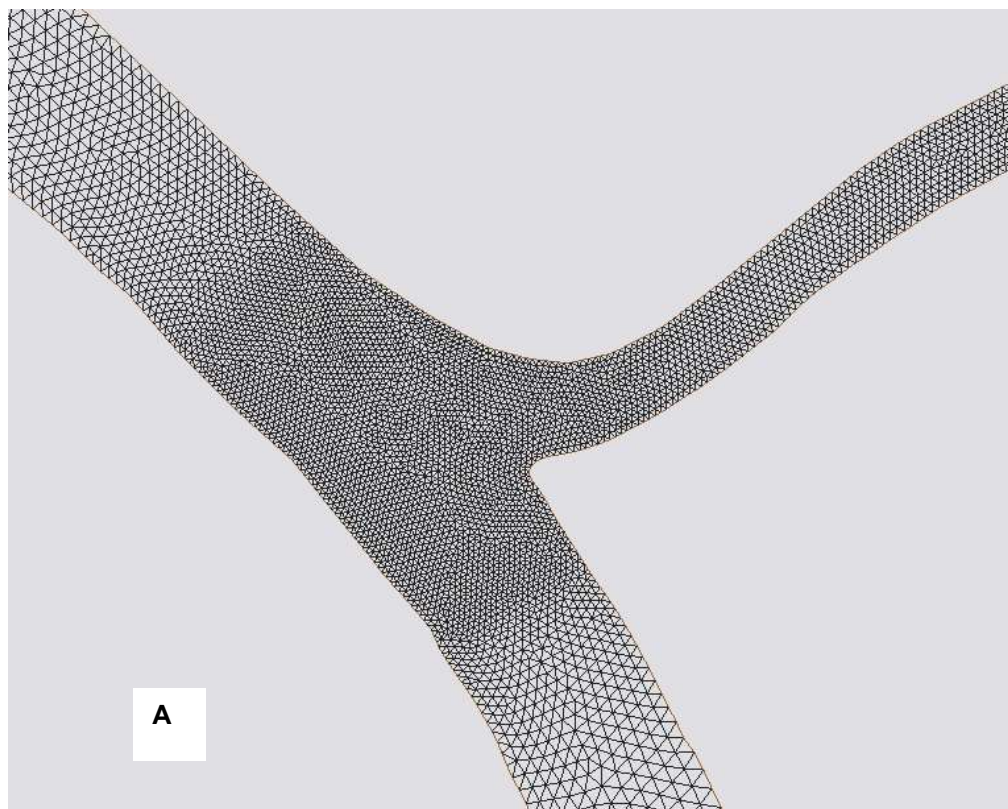


Figure 5.10. The Grid for the Bifurcation of the Bystre and Starostambulske Branches

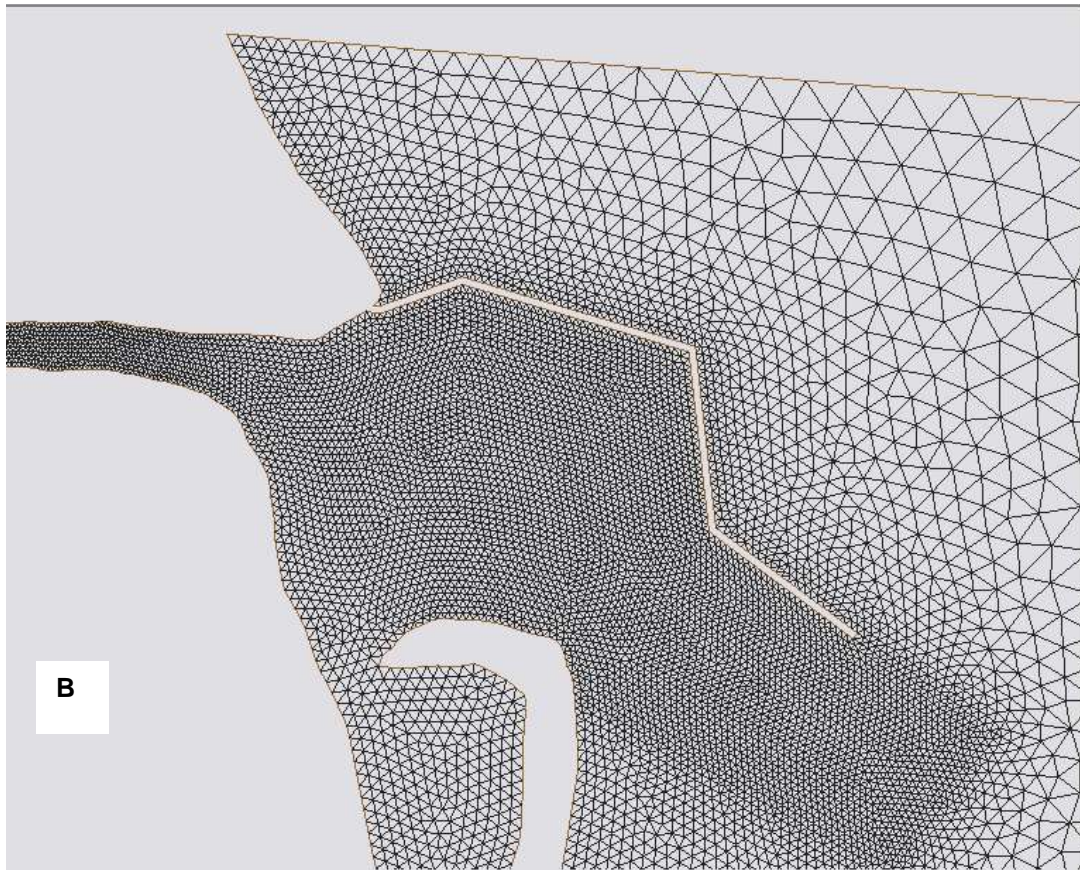


Figure 5.11. The Bystre Branch Grid with the Completed Dam

Three different navigation route (NR) options were considered as follows:

The ‘Before’ Option: without NR, the 2003 topography.

The ‘D’ Option: with a long dam at the Bystre Branch outflow, and the navigation route in place and operational in the Bystre and Starostambulske Branches up to Vylkove; the 2003 topography.

The ‘D+FD’ Option: the same as the ‘D’ Option plus a flow guide dam located at the bifurcation of the Bystre and Starostambulske Branches.

5.2.2. Modelling Methodology Used to Examine the Transport of Suspended Sediments from the Dumping Site

The transport and distribution of suspended sediments under the impact of marine currents were examined with the use of the 3D sediment transport model and numerical technique.

5.2.2.1 Lagrangian Multi-Size Sediment Transport Model

The 3D Lagrangian model [33] simulates transport of non-cohesive, cohesive sediments and mixture of fractions of different size of cohesive/non-cohesive sediments in 2D and 3D modes. The water column and bottom are divided into a set of layers: water layer, active layer, several active bed layers and the non-erodible bed layer (see Figure 5.12).

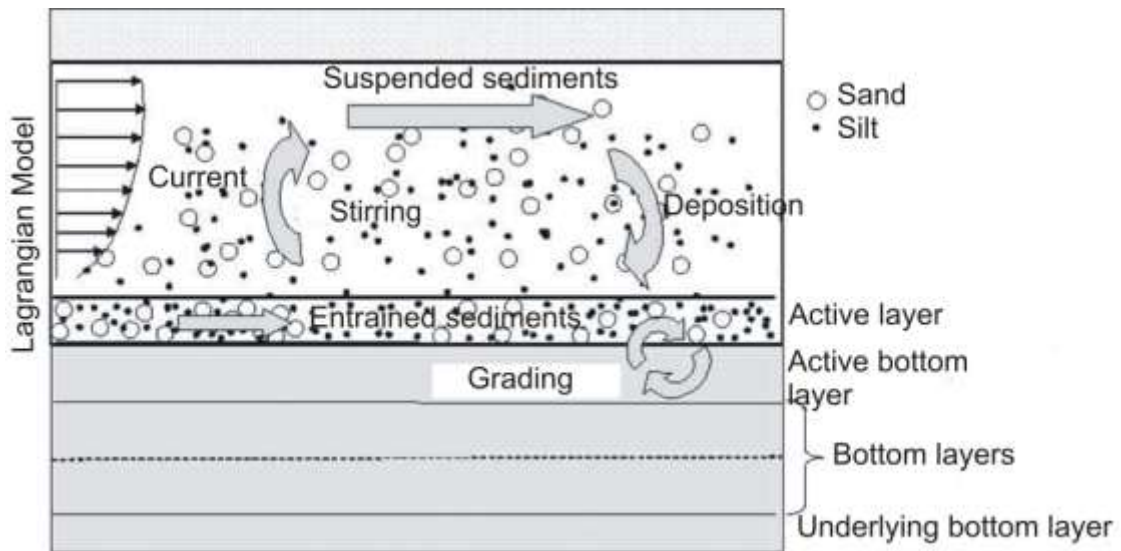


Figure 5.12. Sediment Transport Processes

The suspended sediments are transported by currents and waves in the water layer. The active layer is interface between bed and flow. In the active layer sediments are entrained in water layer or deposited into upper active bed layer that is first bed layer interacted with water layer through active layer. The bed load of non-cohesive sediments also occurs in the active layer. The sorting of fractions non-cohesive sediments in the active layer can result in stronger erosion process. If thickness of active layer become zero then upper bed layer becomes active layer.

Model allows calculation of arbitrary number of sediment size fractions. Because of the different rate of resuspension for size classes the distribution of sand size fractions in active layer differs from distribution in upper active layer that results in armoring effect. The effect of moving ripples is not taken into account in the current model.

Due to the different properties of cohesive and non-cohesive sediments, the exchange with bed is not similar and the processes of erosion and deposition of both kinds of sediments can be interrelated. Following approach by van Ledden [34, 35] we assume that erosion of mixtures of cohesive (“mud”) and non-cohesive sediments (“sand”) is non-cohesive if clay content is below critical. Above critical clay content the bed behaves cohesively. In the non-cohesive regime exchange of sand and mud with bottom is independent, whereas in cohesive regime an erosion of mud and sand occurs simultaneously as cohesive sediment. The deposition is independent process for cohesive and non-cohesive sediments. The number n of fractions of non-cohesive sediment (≥ 0.063 mm) and one fraction of cohesive sediment are described by model. The model accounts for mixed grain size sediments with an arbitrary number of sand size fractions. The content of sand size fraction p_{si} is defined as the ratio of the mass of particles of one particular class size inside the active bed layer elemental area to the mass of all sediments particles contained in the elemental area of active bed layer. Basic constraint is

$$p_m + \sum_{i=1}^n p_{si} = 1 \quad (5.5.9)$$

Here p_m is relative content of mud and p_{si} is relative content of n sand fractions. One of two erosion regimes is considered depending on the critical mud content $p_{m,cr}$: non-cohesive and cohesive regimes.

The Lagrangian technique was used to simulate transport of sediments, deposition and re-suspension. The sediment concentration is represented by a collection of particles and transport problem is solved as particle tracking problem. The mass of suspended sediments and sediments in the active layer in the computational domain was divided on large number of particles of equal mass. Each particle has the following three properties during the simulation:

1. State (either ‘‘Suspended’’ or ‘‘Settled’’)
2. Size class (1 to n -th, ‘‘0’’ th class is reserved for clay)
3. Source class (1 to n_s -th)

The ‘‘Settled’’ particles are placed in the active layer, where they can move as bed load or stay on the bed. The active bed layer supply new particles to active layer when particle budget in this layer is negative at the cost of particle emigration to the suspended sediments or bed load transport or it absorbs particles when active layer thickness exceed given value at the cost particle immigration. Active layer thickness is adjusted to flux particles into water and it is variable in space and time It can only be increased automatically by model due to flow condition changes. Active bed layers are intermediate layers between infinite bed layer and sediments in the water or in the moving bed load layer.

To simulate suspended sediment transport we use Random Dispersion Model (RDM) where position of particle is simulated as a random Markov process [36]. The equations describing increment of particle position $(d\bar{x}, dz) = (dx, dy, dz)$ over each time increment dt is given by

$$\begin{aligned} dx &= udt + \sqrt{2K} d\xi_x, \\ dy &= vdt + \sqrt{2K} d\xi_y, \\ dz &= wdt + w_s dt + \left(\frac{\partial K_z}{\partial z} \right) dt + \sqrt{2K_z} d\xi_z, \end{aligned} \quad (5.5.10)$$

where u, v and w are velocity components in the horizon $d\xi_x, d\xi_y, d\xi_z$ are random varieties with zero mean and variance dt . It is assumed that variation of the diffusivity in horizontal much less than in vertical direction.

For the discrete time step $\Delta t = t_{k+1} - t_k$ the solution is split on two subsequent step. At first the random displacement of particle $(\Delta x_r, \Delta y_r, \Delta z_r)$ is calculated as

$$\begin{aligned} \Delta x_r &= \sqrt{2K\Delta t} P_x, \\ \Delta y_r &= \sqrt{2K\Delta t} P_y, \\ \Delta z_r &= \left(\frac{\partial K_z}{\partial z} \right) \Delta t + \sqrt{2K_z\Delta t + \left(\frac{\partial K_z}{\partial z} \right)^2 \Delta t^2} P_z, \end{aligned} \quad (5.5.11)$$

where P_x, P_y and P_z are random number uniformly distributed on $[-1;1]$, coefficients of diffusion K, K_z are calculated at k time step. At the next step, the displacement of particle by mean velocity and settling is calculated by 2nd order method of Runge-Kutta.

The velocity, vertical and horizontal diffusivity are adopted from hydrodynamics model. For interpolation of velocity and depth fields from mesh nodes of hydrodynamics model to point of

each particle location optionally two interpolation methods are used: linear and non-linear.

5.2.2.2. Non-Cohesive Regime of Transport of Sand/Mud Mixture

Under the non-cohesive regime, the exchange of sand and mud with bottom is independent. The rate of exchange of sand between active layer and water represents source/sink caused by erosion/deposition. It is related to the difference between equilibrium concentration for the i -th sand class $\rho_s C_{ai}^s$ at reference level $z = a$ above the sediment bed that corresponds to the sediment capacity of the steady and uniform flow with the same local parameters and actual near bottom concentration $C_i^s(a)$:

$$K_z \frac{\partial C_{s,i}}{\partial z} = w_{s,i} C_{a,i}, \quad (5.5.12)$$

Here ρ_s is sand grain density [37a]. A set of approaches were developed for equilibrium concentration. The van Rijn [37, 37a] model is one of the most popular. In this model the nondimensional reference concentration [37a] is

$$C_{ai}^s = \frac{0.015 D_i T_i^{1.5}}{a D_{*,i}^{0.3}} \quad (5.5.13)$$

The reference level, $a = \max\{\sigma h, k_s\}$, where k_s is the roughness height, σ is the sigma level close to bottom, D_i is the grain diameter,

$$D_{*,i} = D_i \left[\frac{(s-1)g}{\nu^2} \right]^{1/3}, \quad T_i = \frac{u_*^2}{u_{*,cr,i}^2 (1 + p_m^\beta)} - 1. \quad (5.5.14)$$

Here s is specific gravity of particles; $u_{*,cr}$ is the critical bed shear velocity for initiation of bed motion, that is computed using the Shields criterion

$$u_{*,cr,i} = \sqrt{(s-1)g D_i \Theta_{cr,i}}, \quad (5.5.15)$$

where Θ_{icr} is mobility parameter which is defined by van Rijn [37a] as

$$\Theta_{cr,i} = \begin{cases} 0.24 D_{*,i}^{-1} & , D_{*,i} \leq 4 \\ 0.14 D_{*,i}^{-0.64} & , 4 < D_{*,i} \leq 10 \\ 0.04 D_{*,i}^{-0.1} & , 10 < D_{*,i} \leq 20 \\ 0.013 D_{*,i}^{0.29} & , 20 < D_{*,i} \leq 150 \\ 0.055 & , D_{*,i} > 150 \end{cases} \quad (5.5.16)$$

The settling velocity is provided by van Rijn [37a] as

$$\frac{w_{s,i}}{g D_i^2 / \nu} = \begin{cases} \frac{D_{*,i}^{3/2}}{18} : & D_i \leq 0.1 \\ \frac{10}{D_{*,i}^{3/2}} \left(\sqrt{1 + 0.01 D_{*,i}^3} - 1 \right) : & 0.1 < D_i \leq 1 : \\ 1.1, & D_i > 1. \end{cases} \quad (5.5.17)$$

The source rate for the non-cohesive sediments is calculated for each mesh element and for each sand sizes. The total number of particles of given size to be settled or eroded are calculated for each element. Deposition and erosion are simulated by giving to particle the appropriate label (either ‘‘Suspended’’ or ‘‘Settled’’). Particles that have labels ‘‘Settled’’ do not transported in the water column and treated by bed load routine. Because of the different rate of re-suspension for size classes the distribution of sand size fractions in active layer differs from distribution in upper active layer that results in armoring effect.

The bed load transport of sand is assumed to decrease linearly in the non-cohesive regime with increasing mud content in sand bed [34].

$$\bar{Q}_i^{(s)} = \left(1 - \frac{P_m}{P_{m,cr}}\right) \bar{Q}_i \quad (5.5.18)$$

where \bar{Q}_i is the bed load transport for non-cohesive sediments. The bed load transport for i-th class of sand grains is simulated with the use of a formula of van Rijn [37] and is computed for each area element. The bed load transport rate can be defined as the product of number of moving particles in the element N_{bi} , particle velocity U_{bi} , volume of particle V_p divided on element area S_E . The velocity of particle is calculated following van Rijn [37] as

$$U_{bi} = u_* \left(10 - 7 \sqrt{\frac{\theta_{icr}}{\theta}}\right), \quad (5.5.19)$$

where the Shields parameter θ is

$$\theta = \frac{u_*}{(s-1)gD_i}, \quad (5.5.20)$$

and $s = 1 - \rho_s / \rho_w$, ρ_s , ρ_w are densities of grains and water, respectively, g is gravity, D_i is grain diameter, θ_{icr} is mobility parameter [37]. The total number of particles to be moved in the element is computed from relation for bed load transport [37].

$$N_{bi} = S_E \frac{|Q_i|}{V_p U_{bi}} \quad (5.5.21)$$

This amount of randomly chosen particles in given element area moves and in each time step distribution of particles between elements is recalculated. When in given element area thickness of active layer is more or less given value, the surplus of mass deposits to the active bed layer or new particles enter in this element area from the active bed layer. The thickness of active bed layer is changed accordingly to mass budget.

For the erosion process of mud in non-cohesive regime, the erosion formula by [50] is assumed to be valid

$$E^{(m)} = P_m E_0 \left(\frac{u_*^2}{u_{ce}^{(m)2}} - 1 \right), \quad (5.5.22)$$

$$D^{(m)} = 0 \quad (5.5.23)$$

where E_0 [$\text{kg m}^{-2}\text{s}^{-1}$] is erosion parameter, $u_{ce}^{(m)2} = \tau_{ce}^{(m)} / \rho_w$ is the critical bottom shear velocity for erosion, $\tau_{ce}^{(m)}$ is critical bottom erosion stress. Because the mud content can vary, the right side of (10) was multiplied on p_m . In the non-cohesive regime clay and silt particles easily washed out from the top layer [51] and $u_{*ce}^{(m)}$ should be much less $u_{*ce}^{(m)}$ in cohesive regime. Deposition rate as a flux of sediment from water to the bed is formulated as [52] for $C^{(m)} < C_c^{(m)}$

$$E^{(m)} = 0 \quad (5.5.24)$$

$$D^{(m)} = \frac{W_s^{(m)} C^{(m)}}{H} \left(1 - \frac{u_*^2}{u_{cd}^{(m)2}} \right) \quad (5.5.25)$$

where $W_s^{(m)}$ is the settling velocity, $u_{cd}^{(m)2} = \tau_{cd}^{(m)} / \rho_w$ is a critical shear velocity for deposition, $\tau_{cd}^{(m)}$ is critical shear stress for deposition, $C^{(m)} = C_0 H$, where $C_0 = 0.3 \text{ kg m}^{-3}$ is critical volume concentration.

5.2.2.3. Cohesive Regime of Transport of Sand/Mud Mixture

In the cohesive regime ($p_m \geq p_{m,cr}$), the erosion of both mud and sand are described by [50] formula with correction to mud and sand content

$$E^{(m)} = p_m E_0 \left(\frac{u_*^2 - u_{ce}^{(m)2}}{u_{ce}^{(m)2}} \right) \quad (5.5.26)$$

$$E_i^{(s)} = p_{s,i} E_0 \left(\frac{u_*^2 - u_{ce}^{(m)2}}{u_{ce}^{(m)2}} \right) \quad (5.5.27)$$

Deposition fluxes for mud and sand are independent. For the cohesive regime, the bed load transport is suppressed, i.e. $\vec{Q}_i^{(s)} = 0$. The bed level ζ change is governed by erosion/deposition processes and sand bed load transport as

$$(1 - \varepsilon) \frac{\partial \zeta}{\partial t} = \frac{1}{\rho_s} \sum_{i=1}^n \left(\nabla \vec{Q}_i^{(s)} - E_i^{(s)} + D_i^{(s)} \right) - \frac{1}{\rho_m} (E^{(m)} + D^{(m)}), \quad (5.5.28)$$

where ε is porosity.

5.2.2.4. Model Testing on Analytical Solution

To test the model we used one dimensional test with constant flow condition. We simulate vertical diffusion and settling of sediment until stationary profile set in. We consider stationary flow in uniform channel. Vertical diffusion coefficient can be expressed as:

$$K(z) = \chi u_* z \left(z - \frac{z}{h} \right)$$

where χ - von Karman constant, u_* - friction velocity, h - channel depth.

In Eulerian form equation that describes diffusion and settling of sediment particles has the form:

$$\frac{\partial C}{\partial t} - w_s \frac{\partial C}{\partial z} = - \frac{\partial}{\partial z} K(z) \frac{\partial C}{\partial z}$$

with boundary condition

$$K(z) \frac{\partial C}{\partial z} \Big|_{z=z_b} = -w_s C_a$$

This equation has stationary analytical solution:

$$C(z) = C_a \left(\frac{h-z}{z} \frac{z_{bot}}{h-z_{bot}} \right)^{\frac{w_s}{\chi u_*}}$$

Also this equation was solved using implicit second order finite difference scheme.

Lagrangian model was validated using parameters: $h = 0.4m$; $u_* = 0.05m/s$; $C_a = 1kg/m$; $w_s = 0.01m/s$; $\chi = 0.4$; $m_p = 3 \cdot 10^{-8}kg$ Number of Lagrangian particles was around 1 000 000.

Results on numerical modelling by Lagrangian and Eulerian model with analytical profiles showed on the Figure 5.13. The modelling results showed a sufficient level of consistency between Lagrangian and Eulerian approaches and with stationary analytical solution.

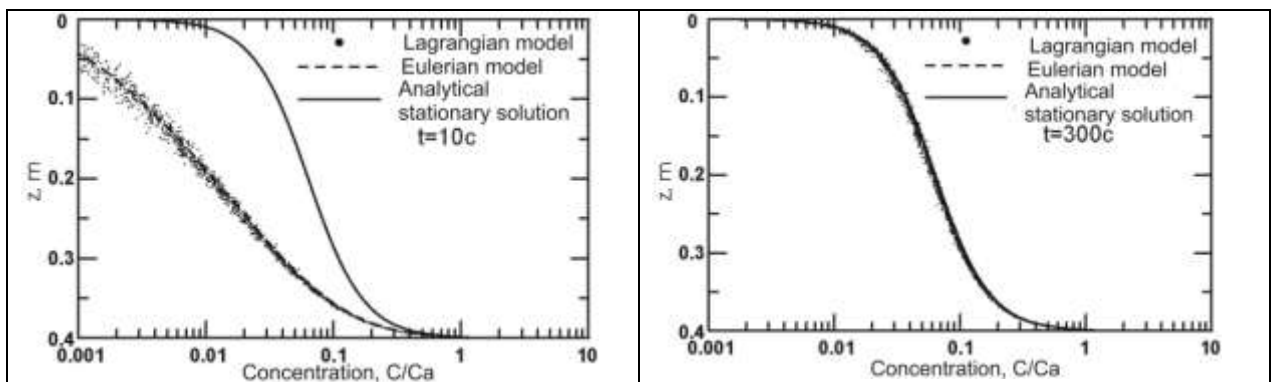


Figure 5.13. Model Testing on Analytical Solution

The Van Rijn Laboratory experiment of (1986)

The laboratory experiment on sedimentation in dredged trench [37a] was simulated using a 30 m long, 0.5 m width and 0.7 m deep flume with working length of 10 m. The bottom profile and measurement locations are given in Figure 5.16. The sediment layer on the bed consisted of fine sand $D_{50} = 160\mu m$. At the upstream boundary, flow velocity was 0.5 m/s and sand was supplied at a rate of $0.04 kg s^{-1}m^{-1}$.

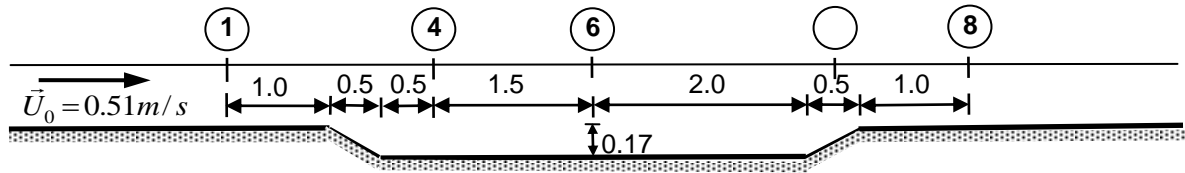


Figure 5.14. Scheme of Experiment

The experimental effective roughness was $k_s = 0.025 \text{ m}$. Currents were calculated using the 3D hydrostatic model POM [38]. In calculations, the horizontal grid size was 5cm and model used 21 sigma layer in vertical direction with refinement near bottom. The total number of Lagrangian particles during simulation was about 300000. Time step of hydrodynamic model was 0.0025 s, while time step of sediment model was 5 times lower. Figure 5.15 shows the measured and calculated profiles of concentration of suspended sediments in middle section of experimental basin. Instantaneous concentration was averaged in time during period of 100 s. The comparison of results showed good consistency between measured and calculate profiles.

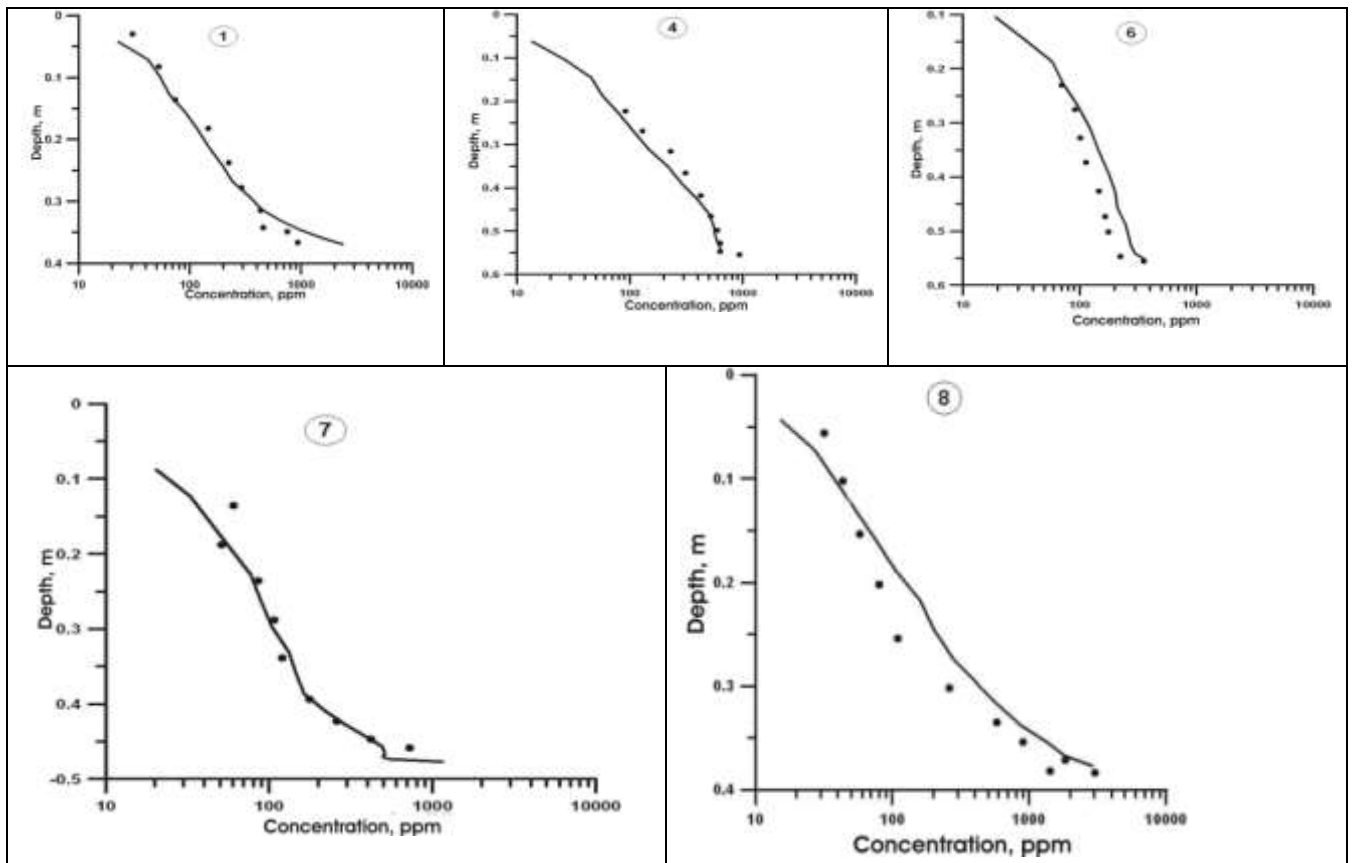


Figure 5.15. Comparison between Experimental and Calculated Data

5.2.2.5. 3D Model of Marine Currents in the Area of Seaward Access Channel

The SELFE 3D hydrostatic model is widely used to calculate hydrodynamic fields in lakes, estuaries and coastal marine waters [39]. The hydrodynamic model calculates three components of velocity field, temperature, salinity and free surface elevation. Model uses generic turbulence model which can be used in the form of $k-\varepsilon$, $k-\omega$, $k-kl$ models. Model can operate in both σ and z vertical coordinate systems.

Model equations are written in the Cartesian coordinate system (x, y, z) . The result parameters are three velocity component (u, v, w) , temperature T , salinity S and free surface elevation η . The governing equations are:

$$\frac{\partial u}{\partial x} + \frac{\partial v}{\partial y} + \frac{\partial w}{\partial z} = 0, \quad (5.5.29)$$

$$\frac{du}{dt} - fv = -\frac{1}{\rho_0} \frac{\partial P}{\partial x} + \frac{\partial}{\partial z} \left((v_t + v_f) \frac{\partial u}{\partial z} \right) + \frac{\partial}{\partial x} \left(K_m \frac{\partial u}{\partial x} \right) + \frac{\partial}{\partial y} \left(K_m \frac{\partial u}{\partial y} \right), \quad (5.5.30)$$

$$\frac{dv}{dt} + fu = -\frac{1}{\rho_0} \frac{\partial P}{\partial y} + \frac{\partial}{\partial z} \left((v_t + v_f) \frac{\partial v}{\partial z} \right) + \frac{\partial}{\partial x} \left(K_m \frac{\partial v}{\partial x} \right) + \frac{\partial}{\partial y} \left(K_m \frac{\partial v}{\partial y} \right), \quad (5.5.31)$$

$$\frac{dT}{dt} = \frac{\partial}{\partial z} \left((v'_t + v'_f) \frac{\partial T}{\partial z} \right) + \frac{\partial}{\partial x} \left(K_n \frac{\partial T}{\partial x} \right) + \frac{\partial}{\partial y} \left(K_n \frac{\partial T}{\partial y} \right) + \frac{1}{\rho_0 c_p} \frac{\partial I}{\partial z}, \quad (5.5.32)$$

$$\frac{dS}{dt} = \frac{\partial}{\partial z} \left((v'_t + v'_f) \frac{\partial S}{\partial z} \right) + \frac{\partial}{\partial x} \left(K_n \frac{\partial S}{\partial x} \right) + \frac{\partial}{\partial y} \left(K_n \frac{\partial S}{\partial y} \right), \quad (5.5.33)$$

$$\rho = \rho(T, S, P), \quad (5.5.34)$$

$$P = P_a + g \rho_0 (\eta - z) + g \int_z^\eta \rho(x, y, z', t) dz'. \quad (5.5.35)$$

Boundary conditions on the free surface $z = \eta$:

$$\frac{\partial \eta}{\partial t} + u \frac{\partial \eta}{\partial x} + v \frac{\partial \eta}{\partial y} = w, \quad (5.5.36)$$

$$v_t \frac{\partial u}{\partial z} = \frac{\tau_{AW}^{(x)}}{\rho_w}, \quad (5.5.37)$$

$$v_t \frac{\partial v}{\partial z} = \frac{\tau_{AW}^{(y)}}{\rho_w}, \quad \frac{\tau_{AW}^{(x)}}{\rho_w} = \frac{\rho_a}{\rho_w} c_{DAW} \sqrt{u^2 + v^2} u, \quad \frac{\tau_{AW}^{(y)}}{\rho_w} = \frac{\rho_a}{\rho_w} c_{DAW} \sqrt{u^2 + v^2} v, \quad (5.5.38)$$

$$v'_t \frac{\partial T}{\partial z} = \frac{1}{\rho_w c_{pw}} Q_{AW}, \quad v'_t \frac{\partial S}{\partial z} = 0, \quad k = \left(\frac{u_*^s}{c_\mu^0} \right)^2, \quad \frac{v_t}{\sigma_\varepsilon} \frac{\partial \varepsilon}{\partial z} = (c_\mu^0)^3 \frac{k^{3/2}}{\kappa (\tilde{z} + z_0)^2}. \quad (5.5.39)$$

On the bottom $z = -H$:

$$-u \frac{\partial H}{\partial x} - v \frac{\partial H}{\partial y} = w, \quad v_t \frac{\partial u}{\partial z} = C_D \sqrt{u^2 + v^2} u, \quad v_t \frac{\partial v}{\partial z} = C_D \sqrt{u^2 + v^2} v, \quad v'_t \frac{\partial T}{\partial z} = 0, \quad v'_t \frac{\partial S}{\partial z} = 0, \quad (5.5.40)$$

On the solid boundaries:

$$u = 0 \quad v = 0 \quad \frac{\partial}{\partial n} (T, S, k, \varepsilon) = 0. \quad (5.5.41)$$

On the open boundaries radiation conditions are used:

$$\frac{\partial \eta}{\partial t} + \sqrt{gH} \frac{\partial \eta}{\partial n} = \frac{\eta - \eta_{bound}}{T_*}, \quad \frac{\partial \phi}{\partial t} + u_n \frac{\partial \phi}{\partial n} = \frac{\phi - \phi_{bound}}{T_{**}}, \quad (5.5.42)$$

where $\phi = (T, S, k, \varepsilon)$ and T_* , T_{**} are relaxation parameters.

Model uses finite element approach for solving governing equations and operate on non-structured grids. It allows to specify the boundaries of a modelled area and modify/adjust the grid resolution. Semi-implicit time scheme and Eulerian-Lagrangian algorithm for inertial terms are used in the model. The bathymetry map of modelled area and location of marine dumpsite are shown in the Figure 5.16.

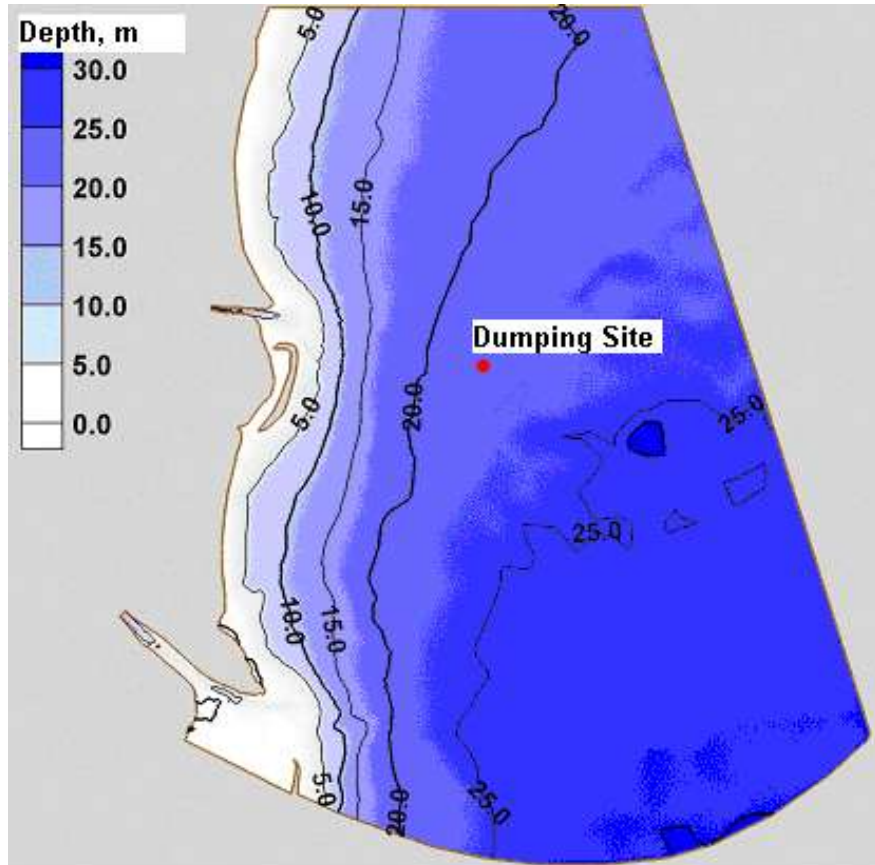


Figure 5.16. Bathymetry Map and Offshore Dumpsite

To model the sea current pattern, the unstructured finite element grid was used with 24000 nodes and 47000 triangle elements. The calculation grid is shown in Figure 5.17, it has been refined around dumping area and along the coastline. For the dumpsite, the grid resolution was about 80m, and near 250 m along the open boundaries. Model had 27 vertical sigma-layers with refinement near surface and bottom.

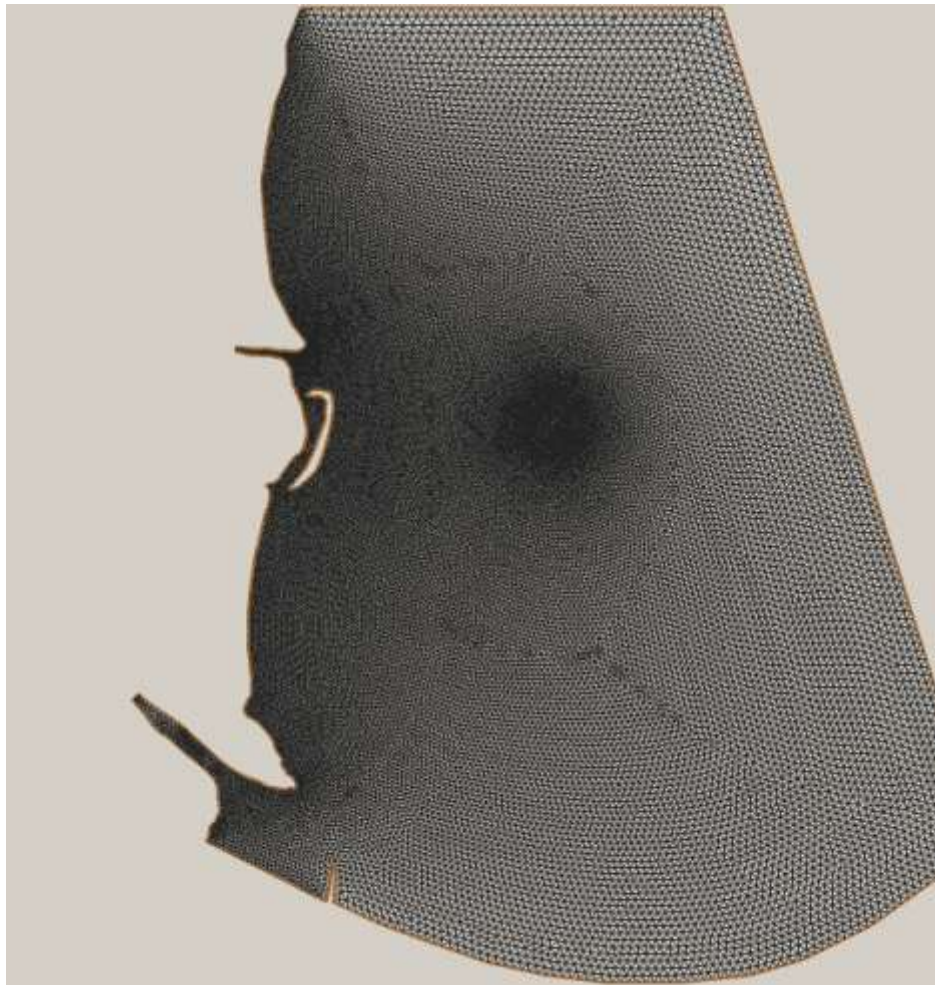


Figure 5.17. Calculation Grid of the 3D Hydrodynamic Model

The constant southward average current velocity 0.25m/s was set to calculate the current fields along the northern and eastern open boundaries. For the southern boundary, the radiation conditions were specified. The horizontal sub-grid viscosity was calculated using the Smagorinsky model with constant equal 0.4. The vertical turbulent viscosity was calculated using $k-\varepsilon$ model of turbulence. On the surface, the constant southward wind (speed 6m/s) was specified. The following discharge rates were set for the Bystre, Vostochny, Starostambulske Branches, considered to be representative for low-flow conditions: 600m³/s (Bystre), 100 m³/s (Vostochny), 750 m³/s (Starostambulske). The modelling exercise was carried out until stationary flow field was achieved after 1 day of modelling time.

Figures 5.18-5.19 show stationary surface and average velocity fields. At the dumping area, the estimated average velocity is about 0.2 m/s with the surface current of 0.3 m/s. The stationary 3D velocity field and turbulent diffusion were used to calculate sediment transport from the dumping site.

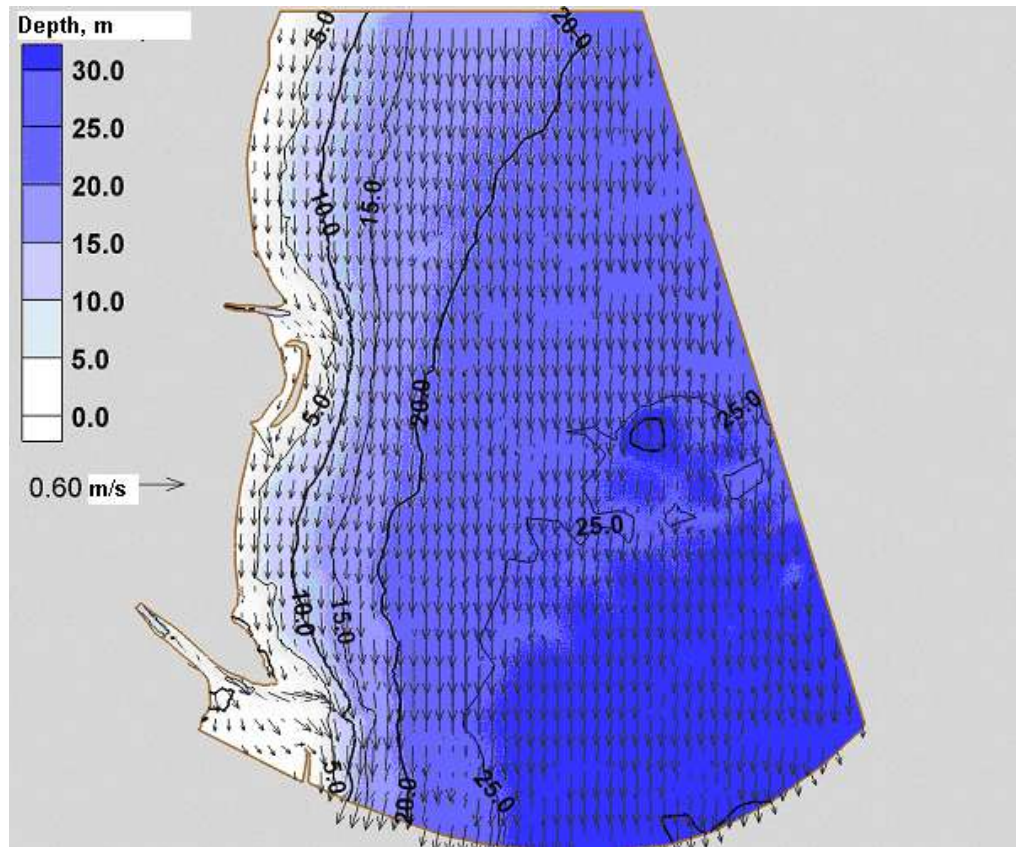


Figure 5.18. Surface Velocity Field

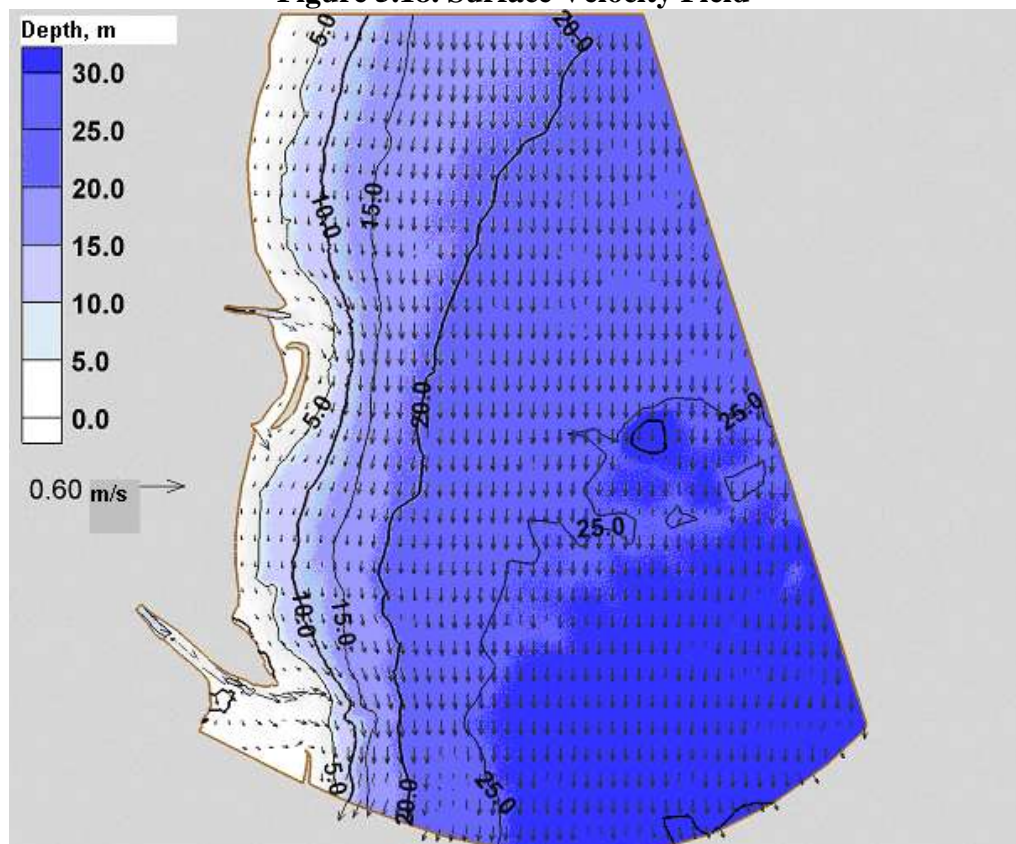


Figure 5.19. Depth Averaged Velocity Field

5.2.3. Two-Dimensional Model Used to Assess the Impact of Protective Dam Associated with the Seaward Access Channel on the Alongshore Sediment Transport

The COASTOX-MORPHO two-dimensional model was used to assess the impact of protective dam associated with the access channel on the coastal zone between the Bystre Branch mouth and the Starostambulske Branch mouth. The COASTOX-MORPHO modelling system included the model chain “waves – coastal currents – sediments transport – bed surface reformation” to help predict the bed and coastline transformation.

The results of the COASTOX-MORPHO model verification on the basis of the laboratory modelling data, and outputs produced through its application for the Danube Delta were presented in the articles [40, 41]. The COASTOX-MORPHO represents an enhanced version of the COASTOX-R [42], based on the 2-dimensional finite-volume solution of shallow water equations that take account of currents generated by sea waves.

5.2.3.1. Modelling the Coastal Current Pattern

The COASTOX-MORPHO current calculation module is based on 2-dimensional equation system averaged by time on scales essentially exceeding a “short” wave period (the storm waves, ripples) for long wavelength (hydrostatic) approximation. In explicit form these equations describe tides and the water levels oscillations concerned with window pileups. The short waves impact upon the currents and averaged level change are parameterized by the wave stresses. The equations correspondent system, where the currents averaged by time in the coastal zone are being defined by balance between window stress shift τ_w , near-bottom shift stress τ_b , vertical turbulent horizontal change averaged tensor, radiation stresses tensor S_{ij} and a force caused by free water level gradient $\partial\xi / \partial x_i$, has a following form [42]:

$$\frac{\partial d}{\partial t} + \frac{\partial q_i}{\partial x_i} = 0 \quad (5.2.37)$$

$$\frac{\partial q_i}{\partial t} + \frac{\partial}{\partial x_j} (u_j q_i) + g d \frac{\partial \xi}{\partial x_i} = \frac{\partial}{\partial x_j} \left(D_j \frac{\partial q_i}{\partial x_j} \right) - \tau_{bi} + \tau_{wi} + \tau_{Si}, \quad (5.2.38)$$

where t is time, x_i are space coordinates, $d = \xi - b$ is water depth, u_i are current velocities in x_i -coordinate direction, q_i is the water discharge in x_i -coordinate direction, $\xi(x, y, t)$ is a free water level, $b(x, y, t)$ is the bottom level, g is gravity acceleration, τ_{Si} is wave stress in x_i -coordinate direction, τ_{wi} is surface window stress, D_j is a horizontal turbulent viscosity coefficient being a wave characteristics function [43].

The near-bottom stress is made of two components: the first one is determined by quasi-steady current, and another by orbital wave motion. After near-bottom stress averaging by surface wave period we obtain a next formula [53] for near bottom stress as a result of waves and currents effect:

$$\tau_{b1} = c_b \left\{ \left(U_{wc} + \frac{\omega_b^2}{U_{wc}} \cos^2 \alpha \right) u_1 + \left(\frac{\omega_b^2}{U_{wc}} \sin \alpha \cos \alpha \right) u_2 \right\}, \quad (5.2.39)$$

$$\tau_{b2} = c_b \left\{ \left(\frac{\omega_b^2}{U_{wc}} \sin \alpha \cos \alpha \right) u_1 + \left(U_{wc} + \frac{\omega_b^2}{U_{wc}} \sin^2 \alpha \right) u_2 \right\}, \quad (5.2.40)$$

where α is wave incident angle relative to coordinate line x_1

$$U_{wc} = \frac{1}{2} \left\{ \sqrt{u_1^2 + u_2^2 + \omega_b^2 + 2(u_1 \cos \alpha + u_2 \sin \alpha) \omega_b} + \sqrt{u_1^2 + u_2^2 + \omega_b^2 - 2(u_1 \cos \alpha + u_2 \sin \alpha) \omega_b} \right\}, \quad (5.2.41)$$

$$\omega_b = \frac{\sigma H_w}{\pi \sinh[kd]}. \quad (5.2.42)$$

Here σ is angular wave frequency, H_w is the wave height, k is the wave number. The wave tensions are calculated by formulas:

$$\tau_{Si} = -\frac{1}{\rho_w} \frac{\partial S_{ij}}{\partial x_j}, \quad (5.2.43)$$

where S_{ij} are generated by waves radiation stresses. For the depth being less 0.35m the radiation stresses are defined with the relation

$$\tau'_S = \tau_S \frac{h}{0.35}. \quad (5.2.44)$$

5.2.3.2. Radiation Stresses

The HWAVE module [40] was used to calculate impulse surplus flux S_{ij} tensor. The radiation stresses represent one of the key data inputs for the COASTOX current module. Taking into account the wave motion velocity potential vertical distribution [40, 44, 45], fluid pressure distribution [54], current $\vec{U}(x, y)$ slow change on the distance comparable with character wave length L [46], and the vertical velocity w slow change on a horizontal plane as well, the radiation stress components can be formulated as follows [41]:

$$S_{11} = \rho \cdot \overline{\tilde{\varphi}_x^2} \frac{1}{g} c c_g + [-\rho \overline{\tilde{\varphi}^2} \frac{\sigma^2}{g} (1 - \frac{c_g}{c})] + \frac{\partial}{\partial x} R_{xz} + \frac{\partial}{\partial y} R_{yz} + \frac{1}{2} \rho g \overline{(\tilde{\eta}^2)}, \quad (5.2.45)$$

$$S_{12} = \rho \overline{\tilde{\varphi}_x \tilde{\varphi}_y} \frac{1}{g} c c_g, \quad S_{21} = S_{12}, \quad (5.2.46)$$

Where

$$R_{xz} = \rho \overline{\tilde{\varphi}(\tilde{\varphi}_x)} A, \quad R_{yz} = \rho \overline{\tilde{\varphi}(\tilde{\varphi}_y)} A, \quad (5.2.47)$$

$$A = \frac{h}{4 \cosh^2 k(h + \zeta_0)} [\cosh 2k(h + \zeta_0) - \frac{1}{2kh} \sinh 2k(h + \zeta_0)]. \quad (5.2.48)$$

The component S_{22} may be obtained by interchanging x and y . The over-bar denotes a period wave mean quantity. Here c, c_g are phase and group wave velocity respectively, h, η are depth

and free water surface, ζ_0 is water level change connected with waves spreading, $\tilde{\eta} = \eta - \zeta_0$. Where the fluid motion occurs, considered to be caused by a purely free surface periodic motion, $R_{xz}, R_{yz} = 0$ and the radiation stress components coincide with the relevant Longuet-Higgins components [46] being functions of the wave height and spreading angle. Notation in last terms is convenient for practice purposes and wide used in hydrodynamic models M2d [47, 55].

The radiation stresses expressed in terms of pseudo fluxes $Q^{(x)}, Q^{(y)}$ [49] were used for hyperbolic wave model of the “mild slope” equation of the hydrodynamic module Mike-21 CAMS [56]. In [40] for potential velocity $\tilde{\varphi}$ finding, the pseudo fluxes $Q^{(x)}, Q^{(y)}$ method was used similarly to [48]. Note that in [41] the components of the radiation stresses put into formulas (5.45) to (5.48) were presented in terms of the potential velocity $\tilde{\varphi}$ being the solution of the “mild-slope” equation of the hyperbolic type and not being dependent on the solution method.

5.2.3.3. Sediment Transport Equation

The wash-out, transport and soil particles deposit processes are triggered by surface water flow. The sediment transport with river flow can be described using the following convective-diffusion equation:

$$\frac{\partial(hS)}{\partial t} + \frac{\partial}{\partial x}(uhS) + \frac{\partial}{\partial y}(vhS) = \frac{\partial}{\partial x}\left(hD_x \frac{\partial S}{\partial x}\right) + \frac{\partial}{\partial y}\left(hD_y \frac{\partial S}{\partial y}\right) - (1-\phi)\rho_b \frac{\partial \eta}{\partial t}, \quad (5.2.49)$$

where ϕ is soil upper layer porosity; ρ_b is thickness soil framework; S is suspended sediment volume concentration; η is the bottom surface elevation.

5.2.3.4. Erosion/Deposition of Soil Particles

The bottom surface elevation is described by an equation:

$$\rho_b(1-\phi) \frac{\partial \eta}{\partial t} = q^s - q^b,$$

where q^s and q^b are respectively deposition and erosion rates.

The hydraulic erosion rate and deposition rate are calculated based on the approach [57] that uses the difference between suspended sediments equilibrium concentration and current local concentration:

$$q^s = \max\{0, w_0(S - S^*)\},$$

$$q^b = \max\{0, E_r w_0(S^* - S)\},$$

where S is the volumetric sediment concentration; S^* is the equilibrium sediment concentration corresponding to carrying capacity of river flow; w_0 is the particle settling velocity; E_r is an overland flux erodibility coefficient.

The equilibrium sediment concentration is defined by a relation

$$S^* = \frac{p}{h(u^2 + v^2)^{1/2}},$$

where p is transport capacity for the flax.

The flux transport capacity for a given sediment grain-size range can be calculated using one of the following five equations: Engelund-Hansen, Yalin, Einstein-Brown, Bagnold and Ackers-White [58].

5.2.3.5. Data Inputs and Assumptions Used in the Modelling Exercise

The following two scenarios were considered: (1) sediment transport pattern without the dam and access channel; and (2) sediment transport pattern with the dam and access channel. The modelled area was selected to have the dimensions 6.5×19.0 km (Figure 5.20).

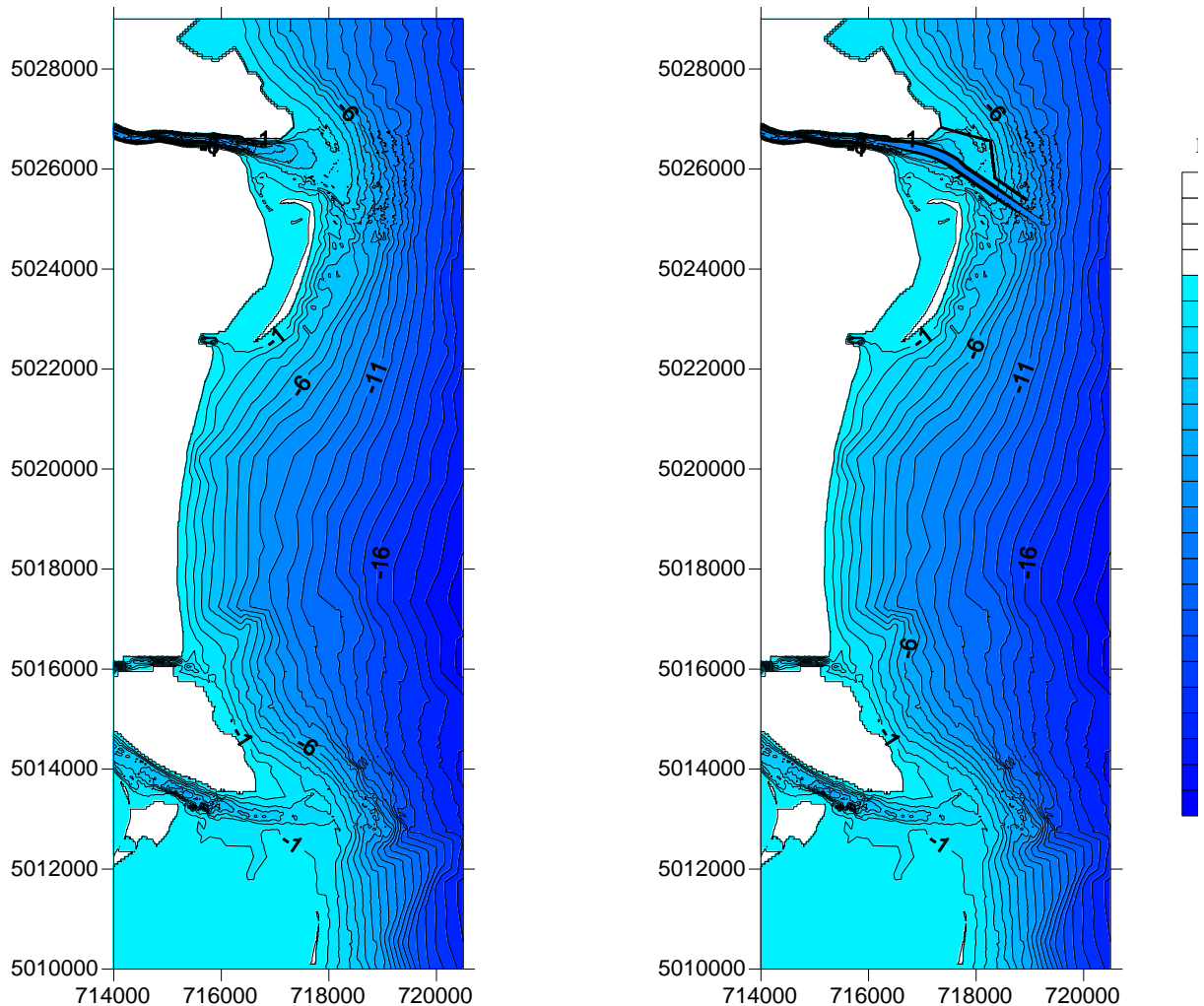


Figure 5.20. Water Depths in the Modelled Area: Before (Left) and After (Right) the Construction of Access Channel and Protective Dam

Flow discharge rates in the Bystre Branch and Starostambulske Branch were assumed to be at 2409 m³/s and 2130 m³/s, respectively. The concentrations of suspended solids were assumed to be at 180 g/m³ in the Bystre Branch, and 160 g/m³ in the Starostambulske Branch. The upper boundary of the modelled area was assumed to have the flow velocity of 0.3 m/s and sediment concentration at 20 g/m³. At the initial instant of modelling time, the concentration of sediments in water was assumed to be nil.

The modelled area was overlain with irregular rectangular grid with steps ranging between 10 to 100 m. both horizontally and vertically. Figure 5.21 demonstrates the shape and layout of velocity fields associated with radiation stresses generated by north-eastern wind.

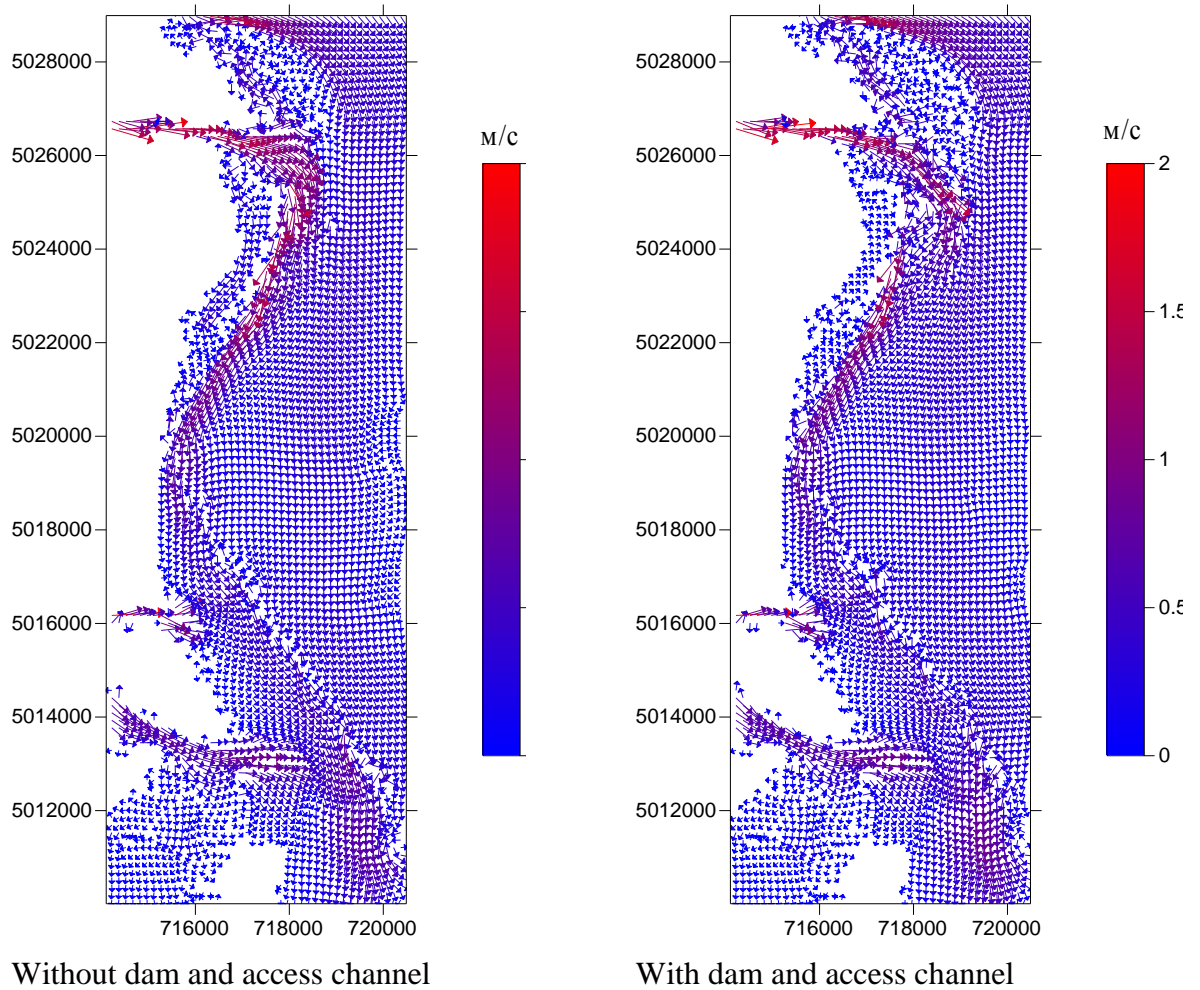


Figure 5.21. Velocity Fields Associated with Waves Induced by the North-Eastern Wind

5.2.4. Technique Employed to Calculate Increments in the Concentrations of Suspended Solids Downstream of Dredging Locations

In order to assess the transboundary impact of increased water turbidity in the Danube caused by dredging activities within the fluvial section of proposed navigation route, a special calculation exercise has been carried out to provide estimates on the distribution of fine suspended solids along the Chilia and Starostambulske Branches, i.e. along the state border between Ukraine and Romania.

The calculation technique developed by the Tallinn Polytechnic Institute (TPI) [50] has been used to estimate the distribution of suspended solids in those sections of the Danube Branches that are located immediately downstream of dredging locations, where the relationship between a flow discharge rate within the contaminated plume (q) and total flow discharge rate within a river branch (Q) can be described as $q \ll Q$ [59]. This technique evolves around the turbulent diffusion equation:

$$\frac{dC}{dx} = \frac{D}{v_{cp}} \left(\frac{d^2C}{dy^2} + \frac{d^2C}{dz^2} \right), \quad (5.2.50).$$

where C is a concentration of pollutant; x is a longitudinal coordinate; y is a vertical coordinate; and z is a lateral coordinate. It is assumed that a normal distribution curve is applied to describe the distribution of pollutant concentration over the stream width at a sufficient distance from the discharge. In this situation, the maximum concentration of a substance C_{maxc} at the control location can be described by the following equation:

$$C_{maxc}(t) = C_{\phi} + (C_{cm} - C_{\phi}) \cdot \exp(k_n \cdot x / v) / [H \sqrt{\pi \cdot v \cdot D_z} \cdot l \cdot \Phi(\xi \sqrt{2})],$$

where C_{cm} and C_{ϕ} refer to the pollutant concentration within the contaminated plume and background concentration of this pollutant within a stream, respectively; k is a factor characterizing the non-conservativeness of a substance; v and H refer, respectively, to the stream velocity and average depth; D_z is the lateral dispersion factor; ξ is a value calculated by the following formula:

$$\xi = B \sqrt{v} / (4 \sqrt{D_z} \cdot l),$$

where B is the average stream width; and Φ is the likelihood integral:

$$\Phi(\xi \sqrt{2}) = \frac{2}{\sqrt{\pi}} \int_0^{\xi \sqrt{2}} e^{-t^2} dt.$$

The dispersion factor D_z is calculated using the following formula:

$$D_z = \frac{H \cdot v}{3524} \cdot \left(\frac{B}{H} \right)^{1,378}.$$

For more remote sections of the Danube Branches, located further downstream of dredging sites, where flow discharge rates within the contaminated plume are comparable with those of the river branch, the Karaushev's method has been employed to calculate concentration fields. This method is also based on the turbulent diffusion equation, though features its numerical solution. To this effect, the equation (5.2.50) is to be rewritten in the finite difference form as follows:

$$\frac{\Delta_x C}{\Delta x} = \frac{D}{v_{cp}} \left(\frac{\Delta_y^2 C}{\Delta y^2} + \frac{\Delta_z C}{\Delta z^2} \right).$$

The turbulent diffusion factor D is calculated by the following formula:

$$D = \frac{g \cdot H \cdot v}{MC_u},$$

where g is the gravitational acceleration; C_u is the Chezy factor; M refers to a value calculated by the following formula:

$$M = \begin{cases} 0,7C + 6, & C < 60, \\ 48 = const, & C \geq 60. \end{cases}$$

The Δz interval is set at discretion, the longitudinal interval for a plane problem is defined as follows:

$$\Delta x = 0,5 \cdot \Delta y^2 / D.$$

In this situation, the concentration of a substance at each grid point equals:

$$C_{k+1,m} = 0,5 \cdot (C_{k,m-1} + C_{k,m+1}), \quad (5.2.51)$$

where k and m are the grid cell numbers along the x and y axes, respectively.

To calculate the concentrations of a substance at the boundary points, the formula (5.2.51) is modified by replacing $C_{k,m+1}$ and $C_{k,m-1}$ with, respectively, $C_{k,1}$ and $C_{k,K}$, where K is the number cells in the lateral direction.

As can be seen from the above, the equation (5.2.51) enables the calculation of the approximate concentration of a substance at any point of a watercourse. For the purposes of the calculation exercise, it was assumed that fine suspended solids within the modelled sections of the Danube Branches behaved themselves essentially the same as conservative compound, being not prone to sedimentation, which represented the worst-case scenario in ecological terms. The following sections were included in the exercise: Section 1 (from the Chilia Branch rift planned to be dredged on the 47th kilometre of the route to the bifurcation of the Chilia Branch and Babyna Branch); and Section 2 (from the Starostambulske Branch rift planned to be dredged at the Bystre Branch outflow on the 11th kilometre of the route to the bifurcation of the Chilia Branch and Musura Branch) (Figure 5.22).

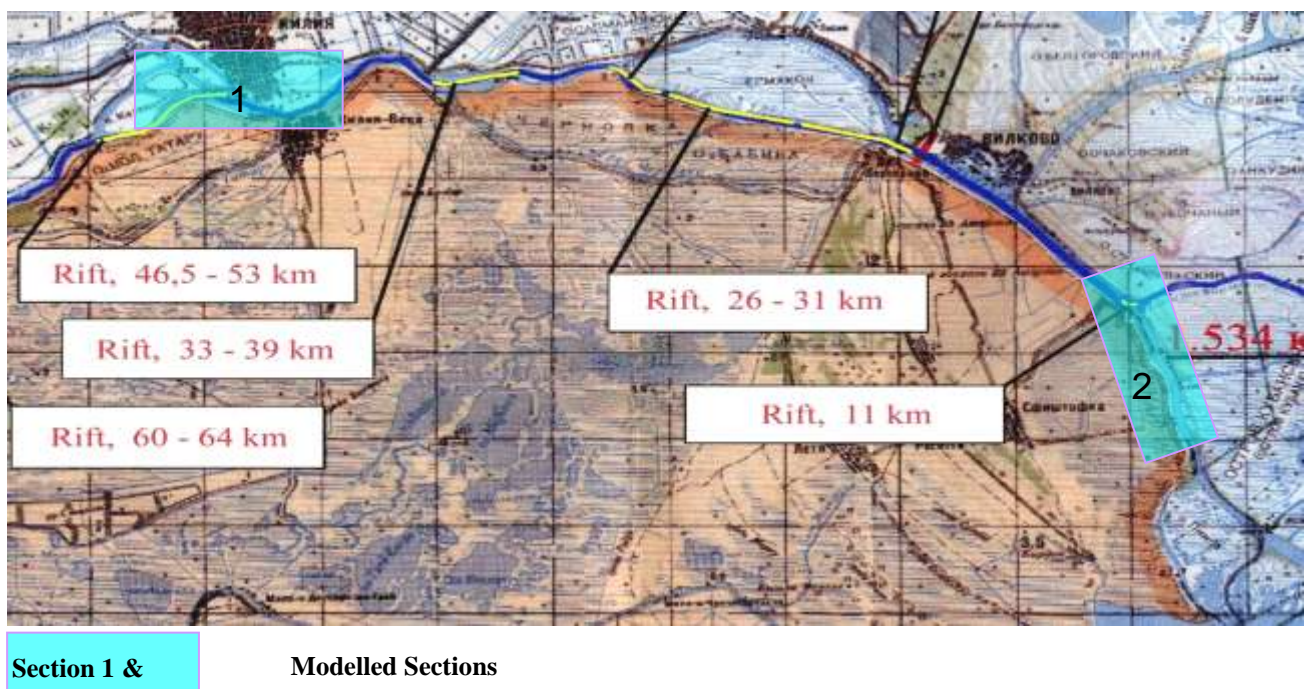


Figure 5.22. Modelled Sections of the Chilia and Starostambulske Branches Included in the Calculation of Turbidity Increments Due to Dredging

These are the sections where the transboundary impact of increased water turbidity in the Danube due to dredging operations is likely to be manifested most obviously. For the Section 1, this is explained by the fact that the Babyna Branch flows into the territory of Romania. For the Section 2, this is attributed to a decrease in flow discharge rates in the Starostambulske Branch downstream of the Bystre Branch outflow, resulting in the increased proportion of turbid water in the total water flow discharged via the Starostambulske Branch.

All modelling calculations assume the existing flow distribution pattern and minimum yearly flow discharge rates at the 95% confidence level [60] (Table 5.3).

Table 5.3. Minimum Yearly Flow Discharge Rates at the 95% Confidence Level

Branch	Proportion (%) of the Chilia Branch Flow	Flow Discharge Rate, m ³ /s
Chilia (downstream of Kilia)	100	1350.0
Babyna	32.0	432.0
Ochakiv	22.1	298.3
Bystre	39.3	530.6
Starostambulske (downstream of the Bystre Branch outflow)	36.1	487.4

Taking into account that the river flow at the bifurcation of the Chilia and Babyna Branches is distributed between separate streams in a smooth and gradual manner, it is assumed that the Babyna Branch receives that part of river flow which runs along its right bank, and this part is comparable to the proportion accounted for by the Babyna Branch in the total river flow discharged via the Chilia Branch upstream of the bifurcation.

The extent and layout of each dredging site were selective relative to the existing navigable channel, which implies that these dredging sites tend to be concentrated along the right bank of the river within the Chilia and Starostambulske Branches (as per the detailed design).

The modelling scenario features two dredges in operation for the Section 1 (the 47th Kilometre), with design capacity 1000 m³ of earth material per hour each, and design loss of earth material at 2%. The total volume of soil dredged by both dredges (w) is assumed to be 1200 m³/year, taking into account their unsynchronized operation and equipment wear. For the Section 2 (the 11th Kilometre), the modelling scenario features one dredge in operation, with design capacity 800 m³/year. The density of loose dredged soil (ρ) is assumed to be 1.6 g/cm³. It is also assumed that the dredged material contains bottom sediments tending to remain in the suspended state, and their fraction is estimated at 5%.

For the calculation of initial (baseline) concentrations of suspended solids in the immediate vicinity of a dredging site with two dredges in operation, it was assumed that these dredges are located at the same distance from the riverbank, and there is 50 m distance between them along the river channel, and any short-term movements/changes in the position and layout of various parts of each dredge are limited to a 10 m zone around each dredge. Under this scenario, maximum estimated hourly concentration of suspended solids downstream of a dredging site was 50 mg/l, taking into account the background concentration of suspended solids, assumed to be about 30 mg/l under summer low-flow conditions.

5.3. The Updated Assessment of the Scale and Magnitude of Likely Transboundary Impacts, to Take Account Additional Survey Results

5.3.1 Summary of Modelling Results: Estimated Changes in Flow Discharges and Water Levels in the Starostambulske Branch

One-dimensional model was used to examine the impact of the navigation route on flow discharges and water levels in the Starostambulske Branch for low-water, average and high-water conditions defined on the basis of systemic hydrologic research data available [60].

The minimum flow discharge rate in the Chilia Branch near Vylkove was set at 1,500 m³/s, which is consistent with mean minimum monthly discharge data available for the low-water period (August/September) of the most dry year (1990).

The average flow discharge rate in the Chilia Branch near Vylkove was specified at $3,300 \text{ m}^3/\text{s}$, which is the mean flow discharge rate recorded over 2001-2003.

The maximum flow discharge rate in the above mentioned section of the river was set at $7,000 \text{ m}^3/\text{s}$, which reflects the mean maximum monthly discharges recorded in the high-water period (May/June) of the most water-abundant years (1980, 1999).

Flow discharge estimates produced with the one-dimensional model for the Bystre and Starostambulske Branches (the latter – downstream of bifurcation point) for the three flow availability scenarios are presented in Table 5.4. Comparisons of changes in water levels along the Starostambulske Branch under various flow conditions are presented in Figures 5.23-5.25. The Bystre Branch bifurcation point, located in 12.7 km from Vylkove, is marked by ‘x’.

Table 5.4. Flow Distribution among the River Branches Before and After the Implementation of the Navigation Route Project

Branch	Scenario	Discharge, m^3/s	Difference between Scenarios, %	Discharge, m^3/s	Difference between Scenarios, %	Discharge, m^3/s	Difference between Scenarios, %
Chilia		1500		3300		7000	
Bystre	Before	575	5.22%	1170	5.98%	2390	5.86%
	After	605		1240		2530	
Starostambulske	Before	550	-3.64%	1340	-2.99%	2900	-3.45%
	After	530		1300		2800	

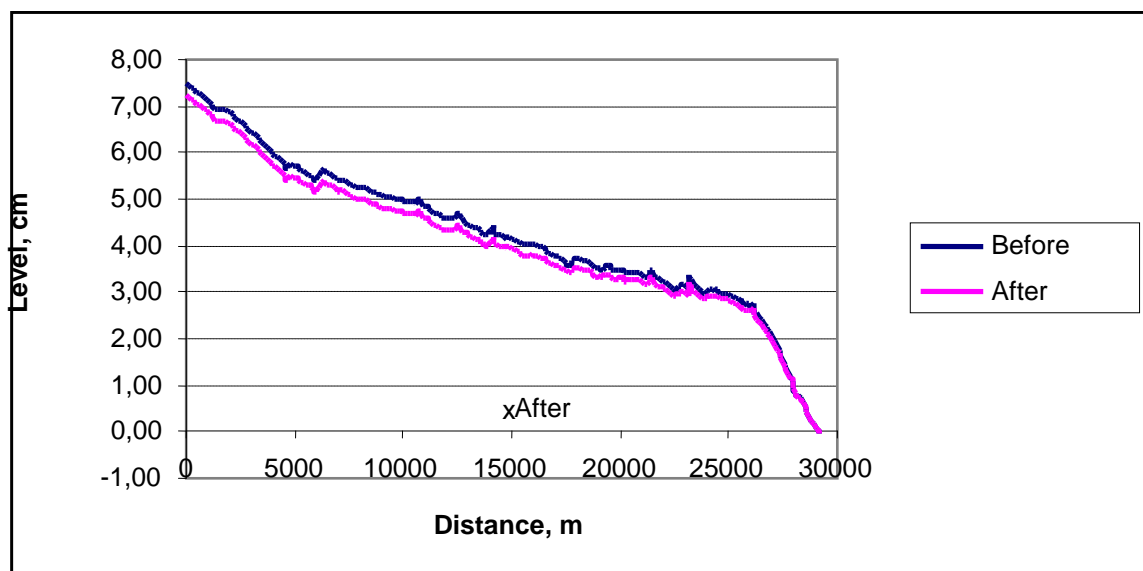


Figure 5.23. Changes in Water Plane Levels along the Starostambulske Branch Downstream of Vylkove under ‘Before’ and ‘After’ Scenarios, Flow Discharge Rate near Chilia at $1,500 \text{ m}^3/\text{s}$

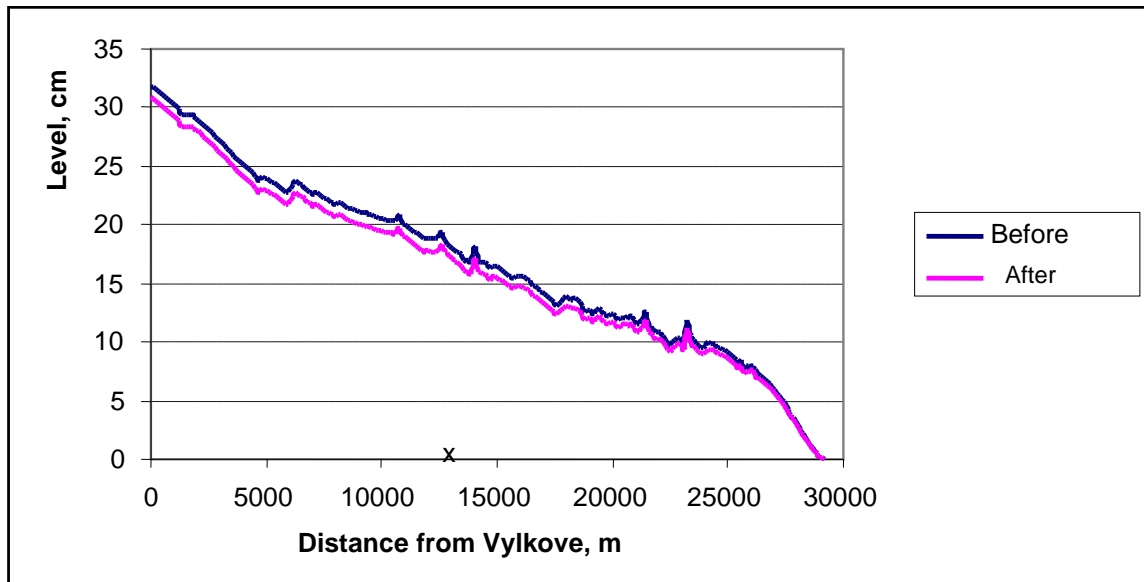


Figure 5.24. Changes in Water Plane Levels along the Starostambulske Branch Downstream of Vylkove under ‘Before’ and ‘After’ Scenarios, Flow Discharge Rate near Chilia at 3,300 m³/s

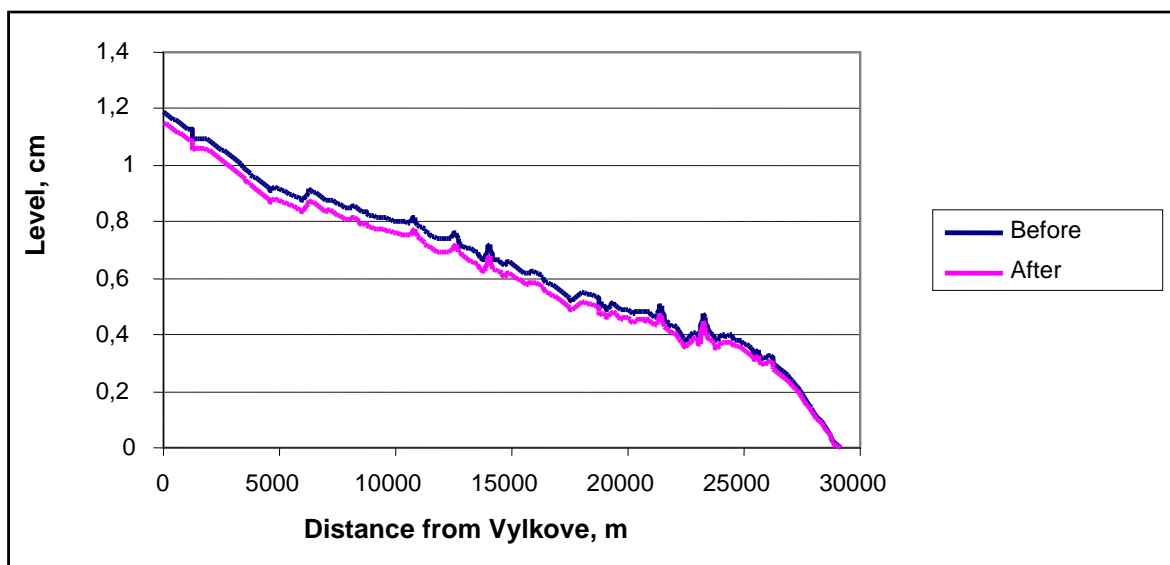


Figure 5.25. Changes in Water Plane Levels along the Starostambulske Branch Downstream of Vylkove under ‘Before’ and ‘After’ Scenarios, Flow Discharge Rate near Chilia at 7,000 m³/s.

Based on the modelling results, maximum margins of decrease in water levels in the Starostambulske Branch were estimated as follows: 0.2 cm at the 1,500 m³/s flow discharge rate; 1.5 cm at the 3,300 m³/s flow discharge rate; and 4 cm at the 7,000 m³/s flow discharge rate.

The two-dimensional model was used to examine the following 3 scenarios:

Before the commencement of the project: based on the 2003 bathymetry;

After the commencement of the project (D): a long retaining dam in the Bystre Branch mouth and the navigation route along the Bystre and Starostambulske Branches are in place and operational;

After the commencement of the project (D+FD): the same as in the previous “D” scenario plus a flow guide dam at the bifurcation of the Bystre and Starostambulske Branches (see Figure 3.7).

Figures 5.26 to 5.31 show the bathymetric estimates for various options and sections of the navigation route.

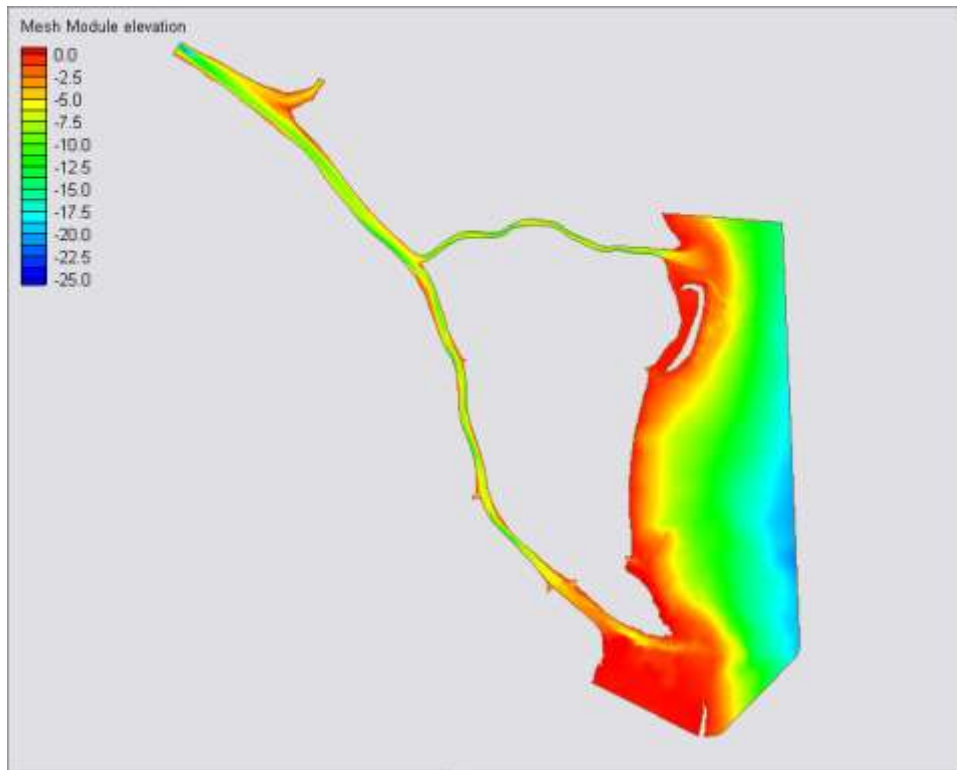


Figure 5.26. Bottom Levels – the ‘Before’ Scenario

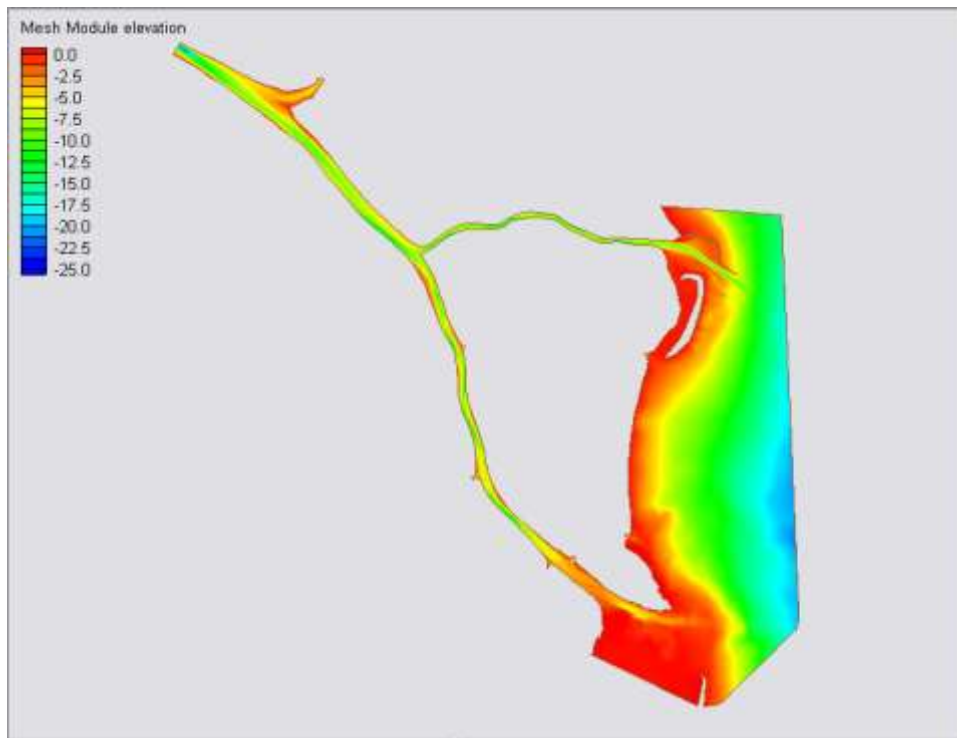


Figure 5.27. Bottom Levels – the ‘D’ Scenario

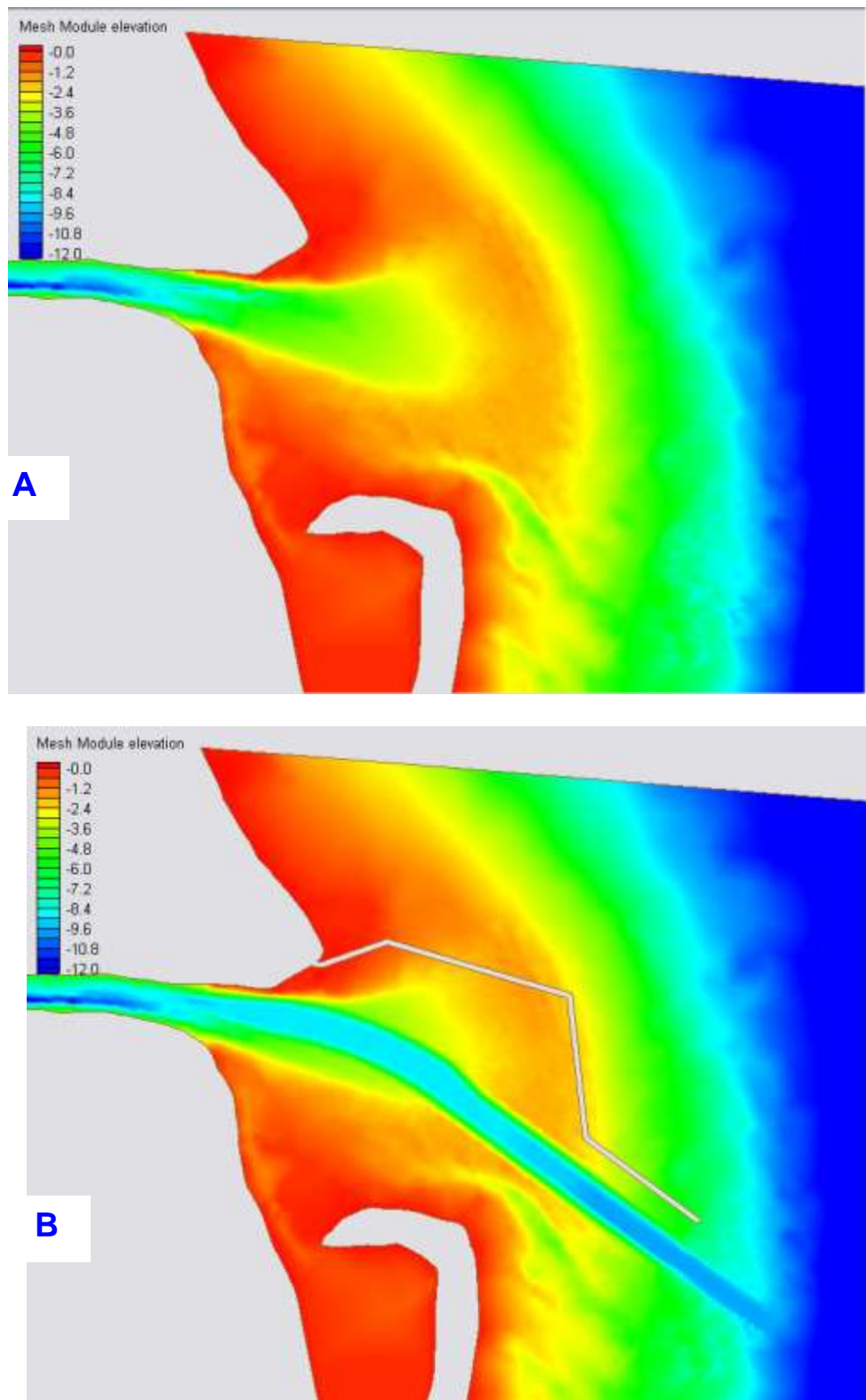


Figure 5.28. Bottom Levels (Bystre Branch Mouth): A – the ‘Before’ Scenario; B – the ‘D’ Scenario

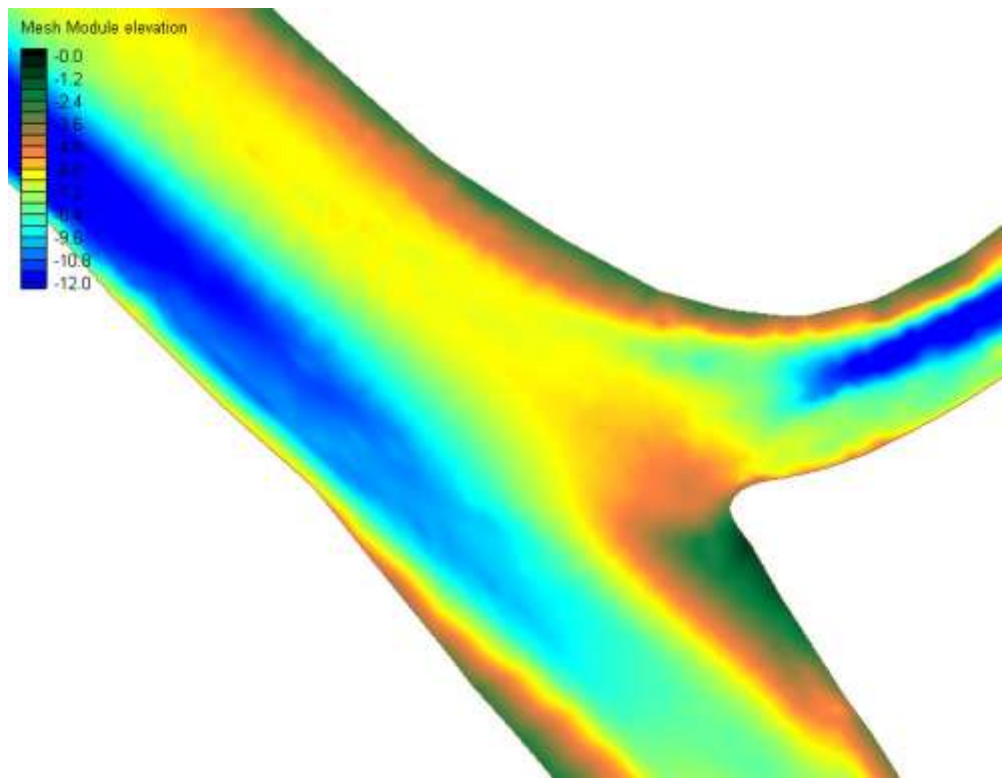


Figure 5.29. Bottom Levels Near the Bifurcation of the Bystre and Starostambulske Branches (the 'Before' Scenario)

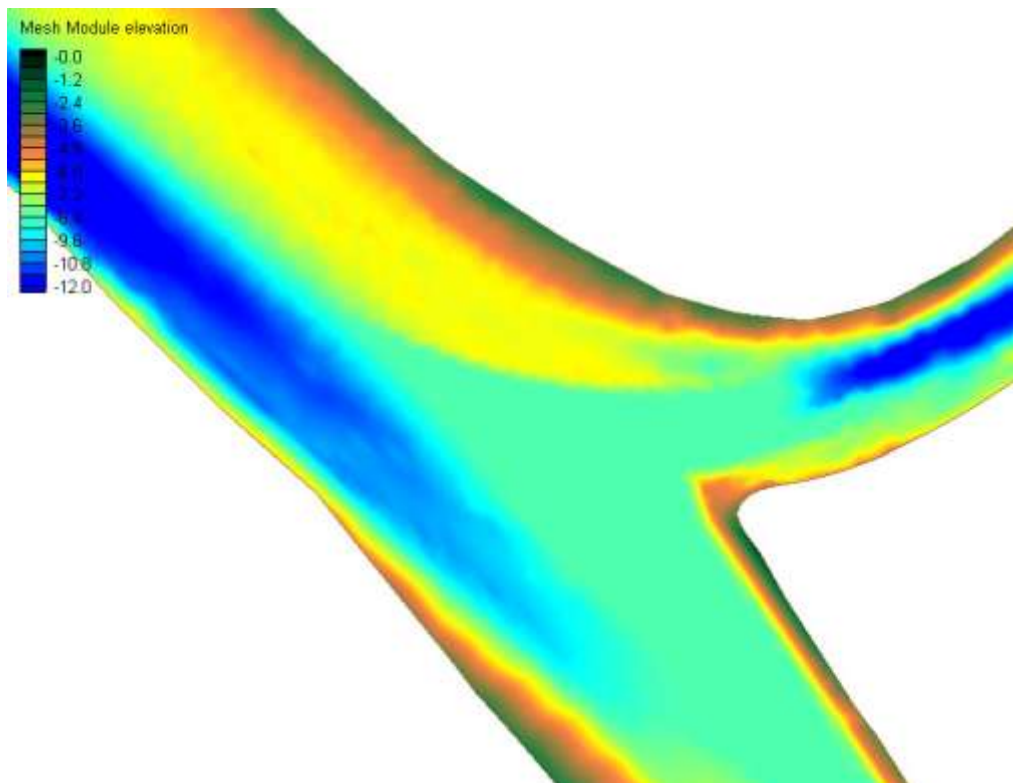


Figure 5.30. Bottom Levels Near the Bifurcation of the Bystre and Starostambulske Branches (the 'D' Scenario)

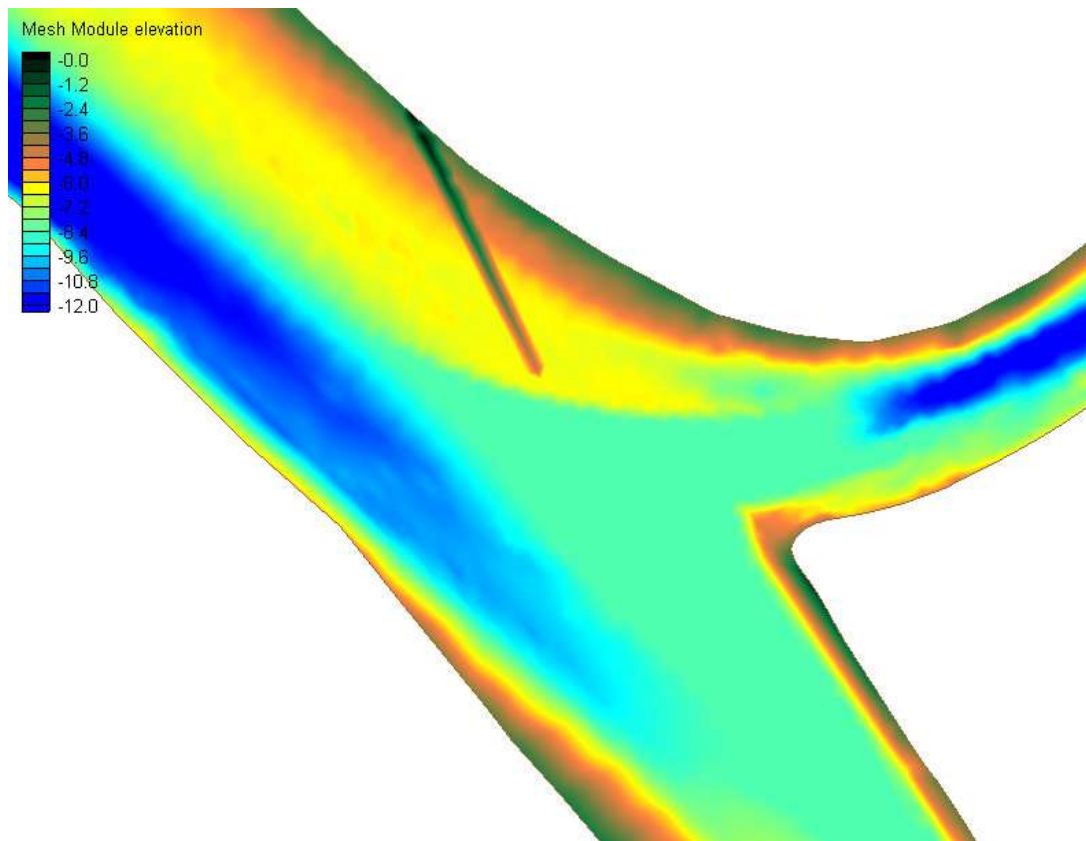


Figure 5.31. Bottom Levels Near the Bifurcation of the Bystre and Starostambulske Branches (the ‘D+FD’ Scenario)

The two-dimensional modelling exercise examined changes in water levels at 3 various flow discharge rates in the Chilia Branch near Vylkove:

Maximum: 6,000 m³/s,
 Average: 3,400 m³/s,
 Minimum: 1,800 m³/s.

Overall, taking into account 3 bathymetric scenarios and 3 flow discharge scenarios, the total number of scenarios for the modelling exercise was 9.

Figures 5.32-5.36 graphically illustrate water level and flow velocity estimates for various options of the navigation route and in its various sections at the flow discharge rate at the Chilia Branch being 6,000 m³/s.

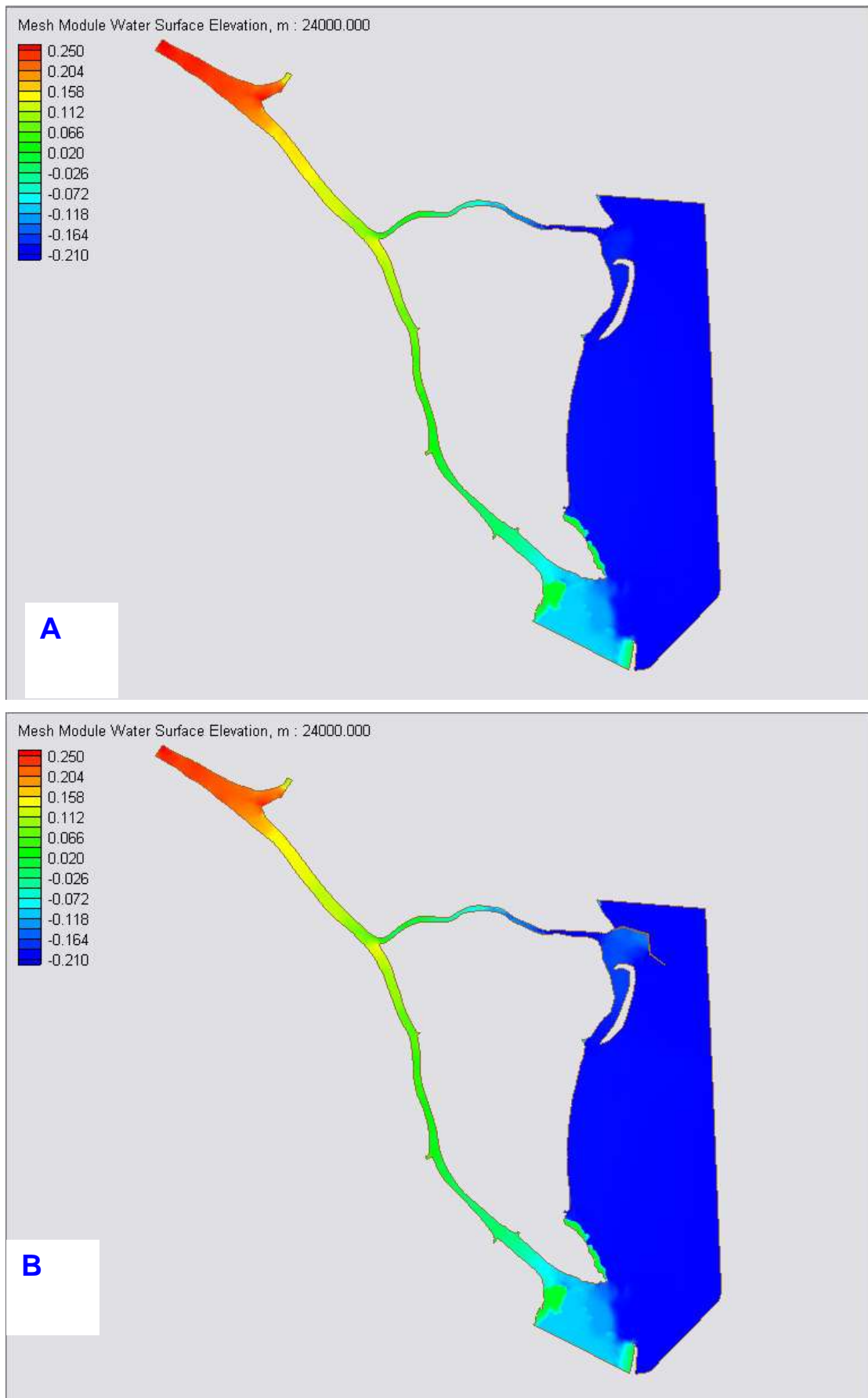


Figure 5.32. Flow Velocities in the Project Area: A– the ‘Before’ Scenario; B – the ‘D’ Scenario

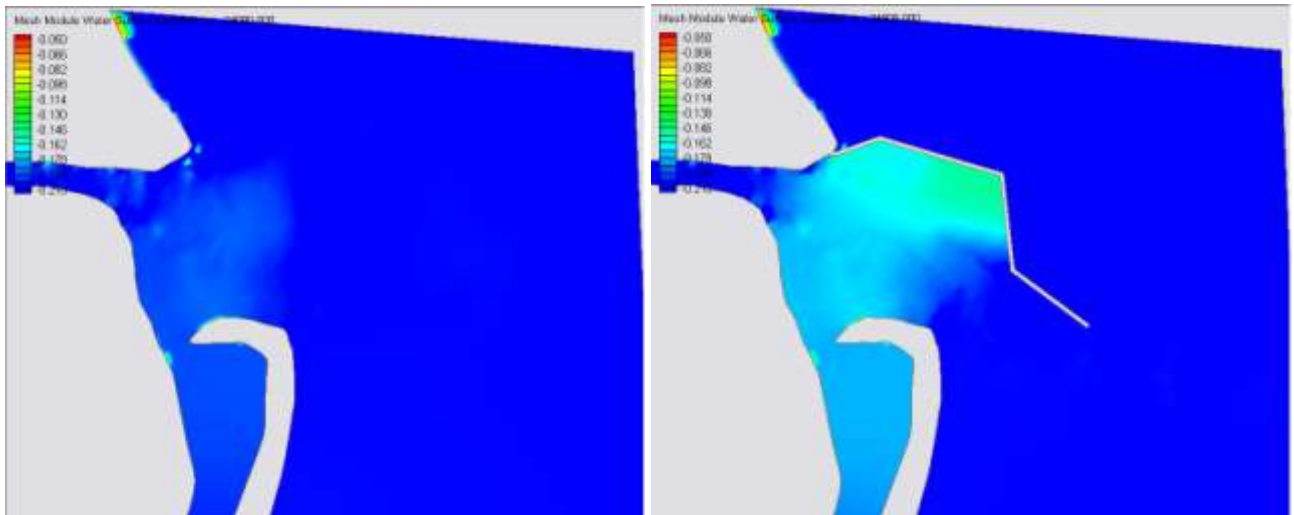


Figure 5.33. Water Levels at the Bystre Branch Mouth: the 'Before' Scenario (Left) and the 'D' Scenario (Right)

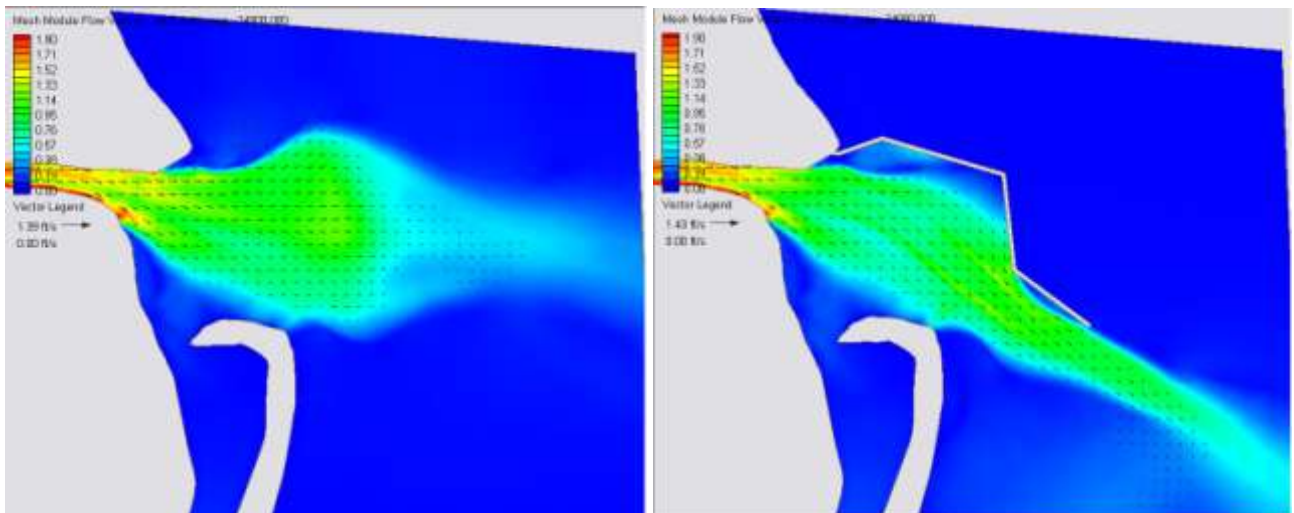


Figure 5.34. Flow Velocities at the Bystre Branch Mouth: the 'Before' Scenario (Left) and the 'D' Scenario (Right)

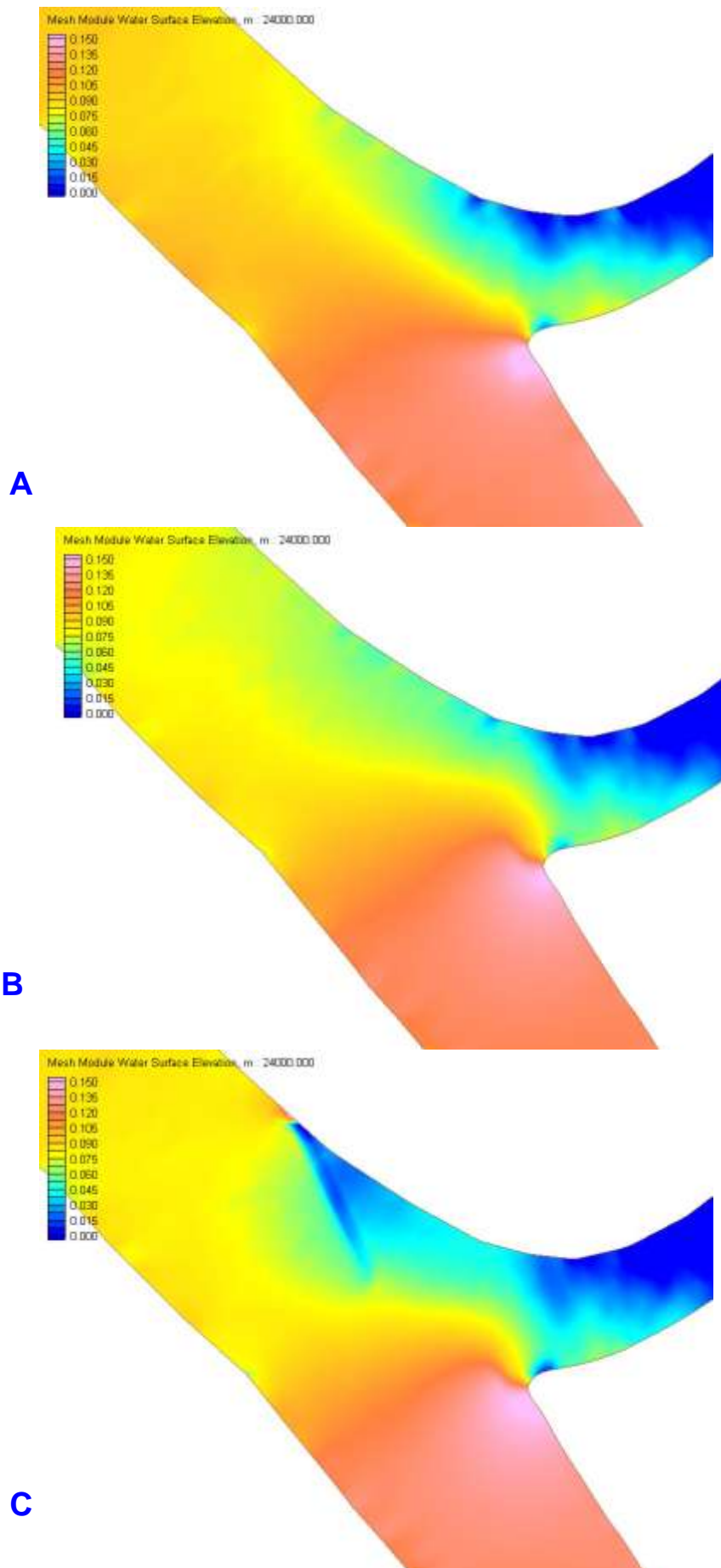


Figure 5.35. Water Levels at the Bifurcation of the Bystre and Starostambulske Branches: A – the ‘Before’ Scenario, B – the ‘D’ Scenario, and C – the ‘D+FD’ Scenario

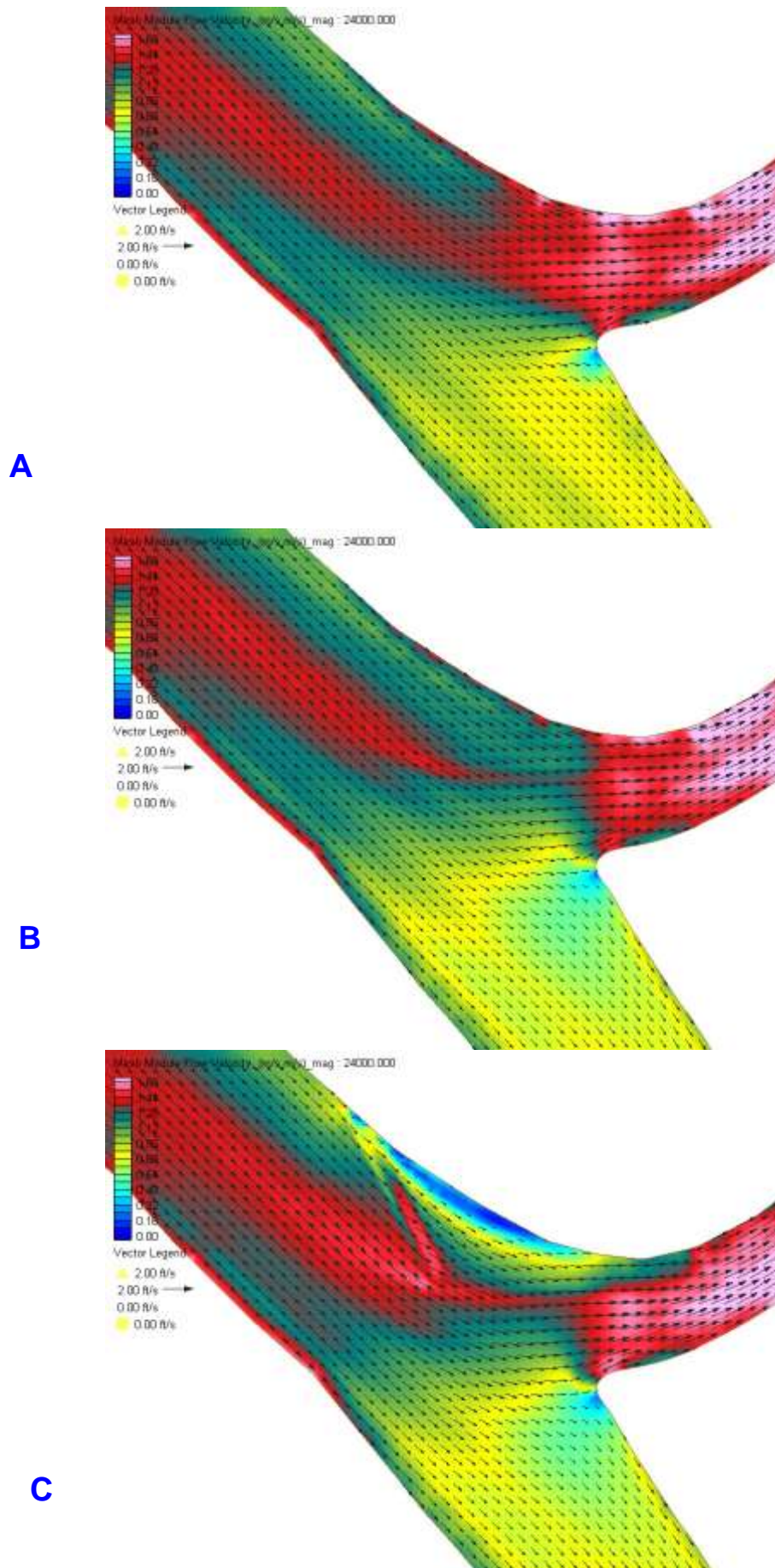


Figure 5.36. Flow Velocities at the Bifurcation of the Bystre and Starostambulske Branches: A – the 'Before' Scenario, B – the 'D' Scenario, and C – the 'D+FD' Scenario

Table 5.5 presents data on estimated changes in water levels in the Bystre and Starostambulske Branches relative to the 'Before' Scenario. Table 5.6 presents similar estimates on changes in flow velocities. These estimates indicate that the maximum margin of change in water levels and flow velocities in the Starostambulske Branch (10 km) due to the implementation of the project will be below one centimetre at maximum flow discharge rate. This margin shrinks as flow discharges decrease, the impact of the route on these parameters is thereby diminished.

Table 5.5. Changes in Water Levels Relative to the 'Before' Scenario (in cm)

	Q=6000			Q=3400			Q=1800		
	Before	D	D+FD	Before	D	D+FD	Before	D	D+FD
Starostambulske Branch (10 km)	11.43	10.71	11.13	-10.11	-10.39	-10.25	-17.97	-17.99	-17.94
Margin of change		-0.72	-0.30		-0.28	-0.14		-0.02	0.03

Table 5.6. Changes in Flow Velocities Relative to the 'Before' Scenario (in m/s)

	Q=6000			Q=3400			Q=1800		
	Before	D	D+FD	Before	D	D+FD	Before	D	D+FD
Starostambulske Branch (10 km)	0.927	0.894	0.897	0.545	0.526	0.528	0.299	0.289	0.289
Margin of change		-0.032	-0.030		-0.019	-0.018		-0.010	-0.009

At the 6,000 m³/s flow discharge in the Chilia Branch, the water level at the Bystre Branch mouth was at -21.01 cm before the commencement of the project, and at -22.01 cm after the development of the navigation route, i.e. the decrease in water level was 1.0 cm. At the average to minimum flow discharges, the margin of decrease would be at 0.7 cm and 0.5 cm, respectively. These changes are within the error margin and very minor. Table 5.7 shows estimated changes in flow discharges in the Bystre and Starostambulske Branches relative to the 'Before' Scenario.

Table 5.7. Changes in Flow Discharges Relative to the 'Before' Scenario (in m³/s)

	Q=6000			Q=3400			Q=1800		
	Before	D	D+FD	Before	D	D+FD	Before	D	D+FD
Starostambulske Branch (10 km)	2133	2110	2121	1206	1192	1198	650	644	647
Bystre Branch	2408	2431	2419	1398	1412	1406	775	782	779
Margin of change		-23	-12		-14	-8		-7	-4

As can be seen from the above table, the development of the navigation route would result in an increase in flow discharged via the Bystre Branch. The margin of increase at maximum, average and minimum flow rates would be at 23, 14 and 7 m³/s, respectively. In the Starostambulske Branch, the percentage of change in flow discharges relative to the baseline levels would be at 1.1%, 1.1% and 1.0% at the maximum, average and minimum flow rates, respectively.

The overall picture emerging from the modelling exercise undertaken to estimate project-related changes in flow discharges and water levels in the Starostambulske Branch indicates that the margin of change will be between 1% to 3% (depending upon the choice of a calculation method), still considered to be significantly smaller than the estimate provided by the Inquiry Commission. This impact can therefore be hardly considered as a major one.

5.3.2. Summary of Modelling Results: Estimated Distribution of Turbidity Plume from the Offshore Dumping Site under the Impact of Alongshore Southerly Currents

This modelling exercise was undertaken in order to provide more precise estimates in response to the conclusion made by the Inquiry Commission concerning the scale and magnitude of transboundary impact likely to arise from the offshore disposal of dredging spoils. To ensure comparability, this exercise used the same calculation parameters as those adopted by the experts of the Inquiry Commission.

For the purposes of modelling, soil density was assumed to be at 1,500 kg/m³. Based on the available information on grain-size composition (Table 5.8), it was assumed that the fine silt fraction (particle sizes below 0.005 mm) accounts for 10% of the total mass of soil.

Table 5.8. Soil Density and Grain Size Composition According to Data Provided in [61]

Area	Km	Dominant GEU ¹	Fraction < 50 um (%)	Fraction < 5 um (%)	Density (t/m ³) or porosity (%)
Maikan Island	35.5-38.0	2	80	32	25%
Katenka/Mashenka Island	47.0-53.1	2	80	32	30%
Bolshoy Daller Island	63.4-69.7	1/3/4	35	16	<i>n.a.</i>
		2	80	32	40%
Kislitsky	70.2-74.5	1	<3.5	<3.5	1.32
		5	72	23	45%
Kislitsky Arm	75.6-76.8	5	72	23	31%
Bystre sandbar		3	17	8	1.26
		6	49	20	33%
		7	37	12	28%
Sandbar section (annex 24)			10-50	3-23	1.8-1.9
Sandbar section (annex 26)				1	1.4
Starostambulske branch (annex 26)	11.0			14	1.3

It was also assumed that as a turbidity plume develops, the entire fine soil fraction with particle sizes below 0.005 mm enters the marine environment near the dumping site, accounting for 10% of the total soil mass. The following data inputs were used by the Inquiry Commission for modelling purposes: surface current velocity in the area of the offshore dumpsite at about 0.25 m/s; horizontal diffusion coefficient at 3 m²/s; fine silt deposition rate at 0.1 mm/s; and 16 km distance between the offshore dumpsite and the Romanian border.

5.3.2.1. Modelling Results Illustrating the Estimated Movement and Dispersion of Turbidity Toward the Romanian Territory Plume for the Continuous Dumping Scenario

It is assumed that dumping activity takes place over a certain period of time, in this case 30 days. Table 5.9 provides data on the volumes of soil dumped that can be used as a basis for calculating the average dumping rate during the construction of the seaward access channel, which is in the order of 500 kg/s.

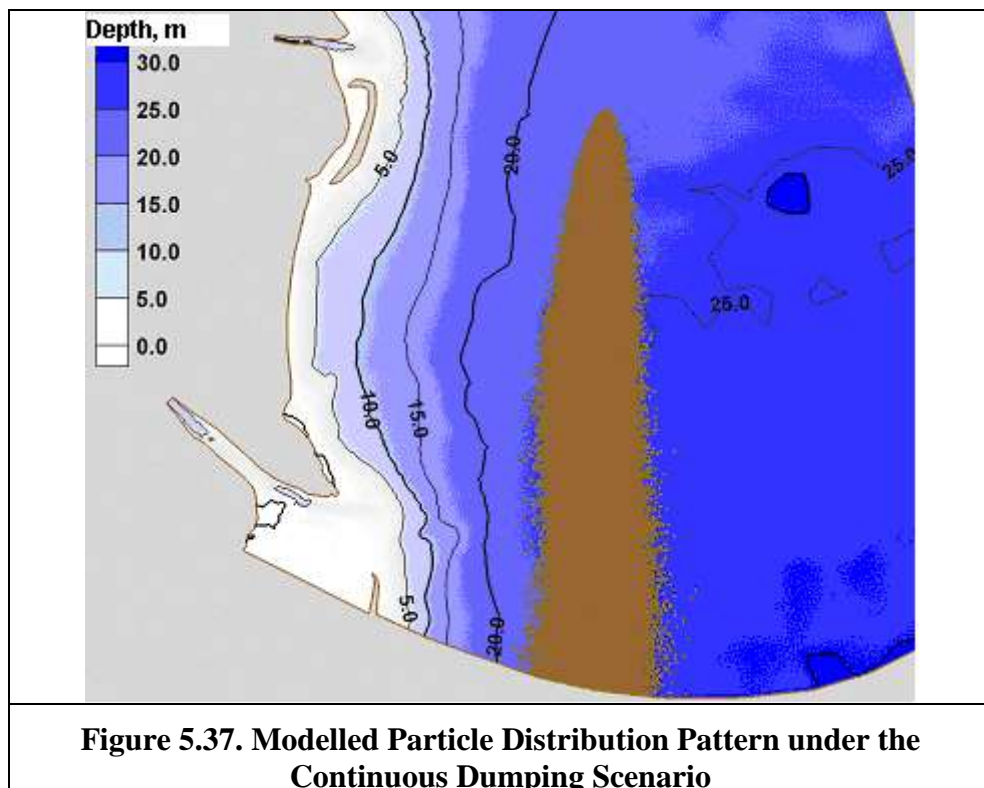
Table 5.9. Data on Soil Volumes Dumped at the Marine Dumpsite

Project Phase	Volume (10 ⁶ m ³)	Sediment Mass (10 ⁶ t)	Duration of Dumping, days	Average Dumping Rate (kg/s)	Dumping rate for fine fraction <0005 (10%) (kg/s)
Phase 1	1.9	1.6	30	611	61
Phase 2	1.7	1.4	30	547	55
Annual maintenance	1.0	0.83	30	322	32

The following parameters were included in the model calculation: continuous release of fine silt matter with particle size of 0.005 mm at the rate of 50 kg/s. The corresponding mass of each Lagrangian particle included in the modelling is 15 kg; total number of particles is 600,000; modelling time step is 1 second; modelling period is 30 hours. The horizontal diffusion coefficient is $3 \text{ m}^2/\text{s}$. The characteristics pertaining to the stationary 3D current fields and vertical diffusion were the same as those included in the previous hydrodynamic modelling exercise. Figure 5.37 graphically illustrates the distribution of Lagrangian particles, and modelled sediment concentration fields are presented in Figures 5.38 to 5.40.

The surface and near-bottom concentrations of sediments were defined as the average sediment concentration within the 4-m surface layer and the average sediment concentration recorded at the depths of over 18 m.

As can be seen from Figures 5.38 to 5.40, the estimated maximum sediment concentration at the Romanian border is 2 mg/l under this modelling scenario. It is also obvious from these Figures that the surface concentration is somewhat higher than the average and near-bottom concentrations, ranging around 3 mg/l. This is attributed to very slow sediment settling rates, especially in the upper turbulent layer where the sediment may remain suspended for longer time. The modelling result produced by the Inquiry Commission expert was that the estimated sediment concentration at the distance of 16 km from the emission source would be 5 mg/l. The difference in estimates is can be explained by the fact that the present modelling procedure takes into account a number of additional factors (vertical mixing, 3D structure of currents that promotes the settling process, and variable bottom topography).



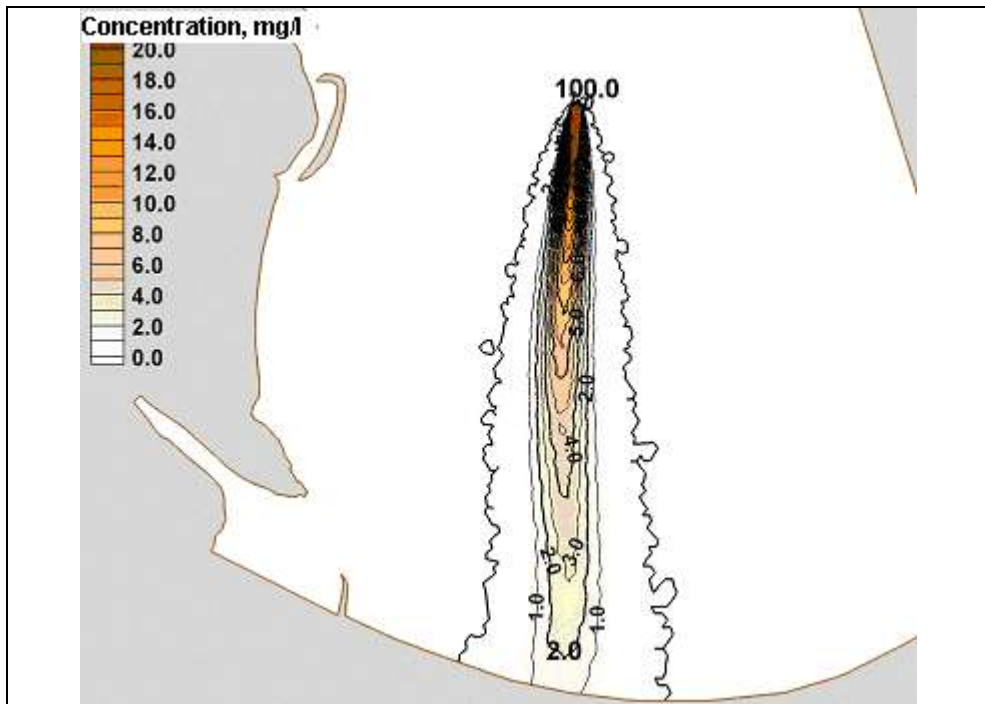


Figure 5.38. Estimated Suspended Sediment Concentrations Averaged Over Depth

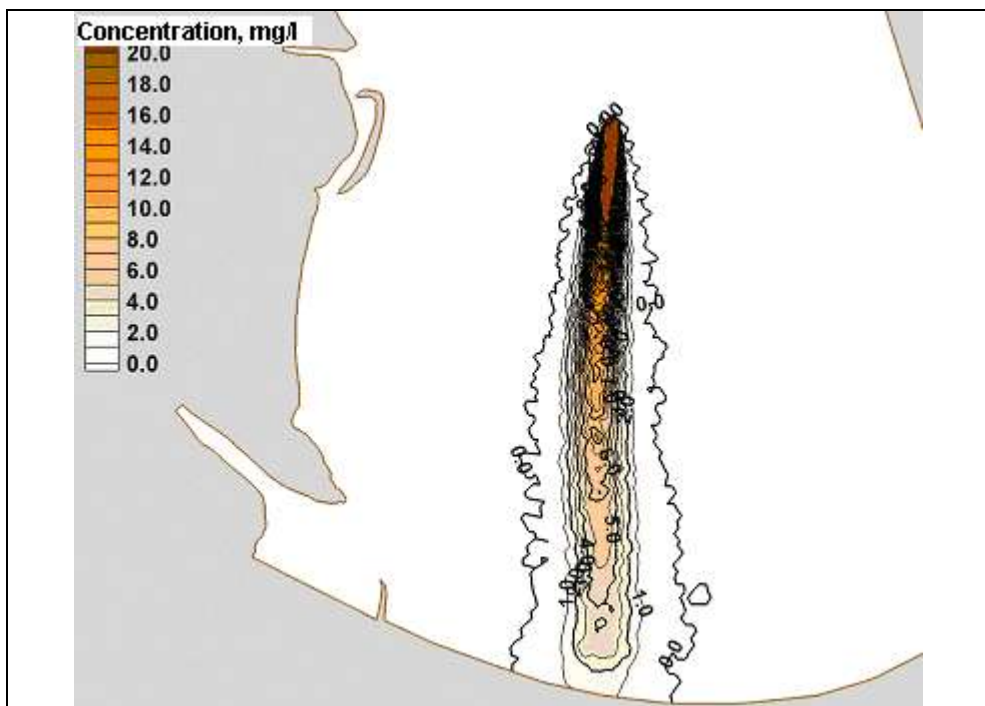
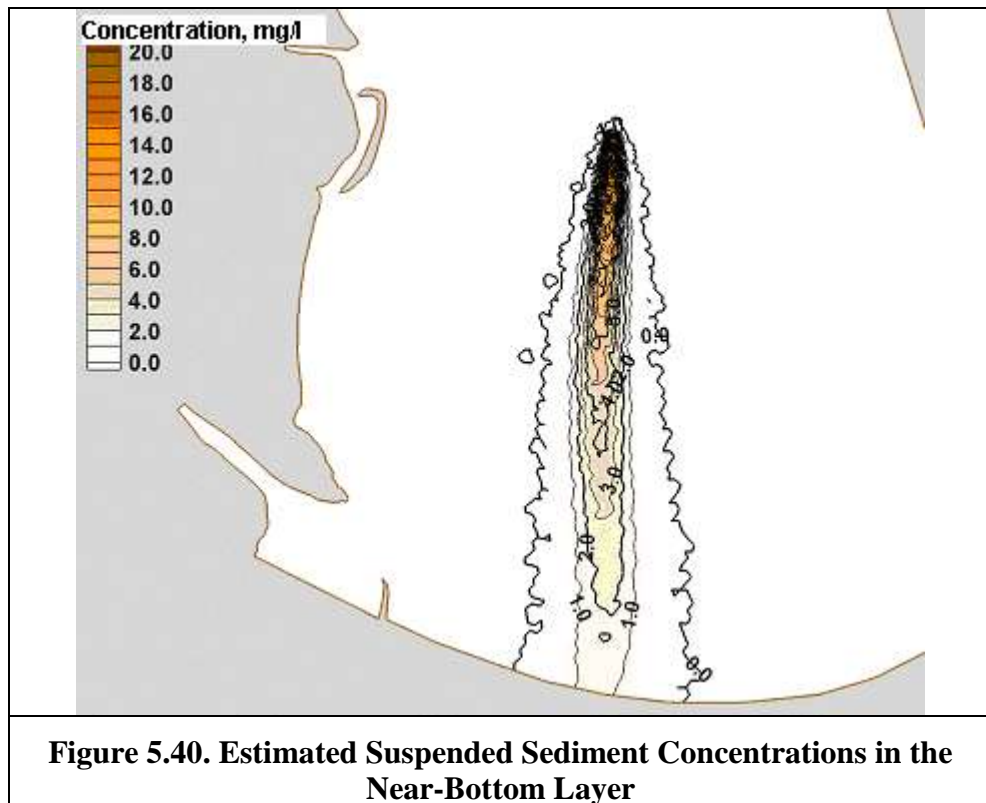


Figure 5.39. Estimated Suspended Sediment Concentrations in the Surface Layer



5.3.2.2. Modelling Results Illustrating the Estimated Movement and Dispersion of Turbidity Toward the Romanian Territory Plume for the Instantaneous Dumping Scenario

The design as proposed features the use of barges with the capacity of 500-600 m³ of sludge to deliver and dump dredged spoils to the offshore dumpsite. Based on this, the estimated instantaneous sediment load dumped from one barge is about 420 tonnes, where about 42 tonnes is accounted for by the fine silt fraction with particles sizes below 0.005 mm. The model was used to simulate and examine the turbidity pattern for a scenario where 42 tonnes of fine matter is dumped instantaneously at the offshore dumpsite.

The following assumptions and parameters were included in the model calculation: the instantaneous dumping of fine silt matter with particle size of 0.005 mm, total mass load 42 tonnes. The corresponding mass of each Lagrangian particle included in the modelling is 0.1 kg, the total number of particles is 420,000. Modelling time step is 1 second; modelling period is 1 day. The horizontal diffusion coefficient is 3 m²/s. The characteristics pertaining to the stationary 3D current fields and vertical diffusion were the same as those included in the previous hydrodynamic modelling exercise.

Figures 5.41 to 5.44 graphically illustrate the distribution of average suspended solid concentrations at various instants of time as the turbidity plume develops after the dumping of the dredged spoils load carried by one barge. Under this scenario, the estimated maximum concentration of suspended sediments in the marine water at the Romanian border is 0.08 mg/l.

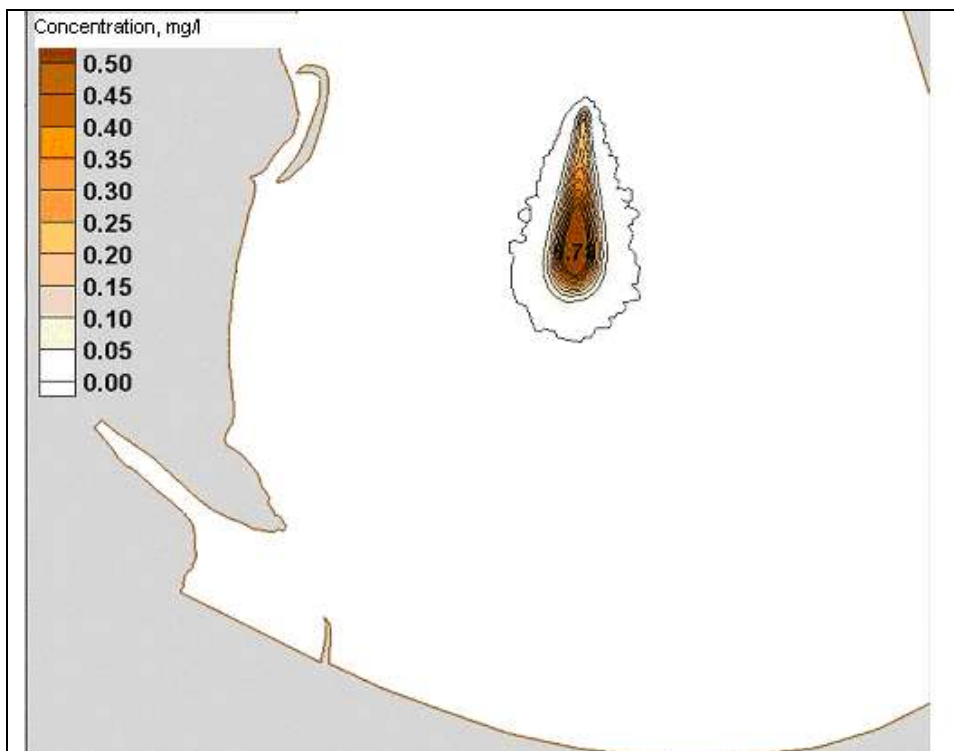


Figure 5.41. Estimated Suspended Sediment Concentration Averaged Over Depth, 6 Hours After the Dumping

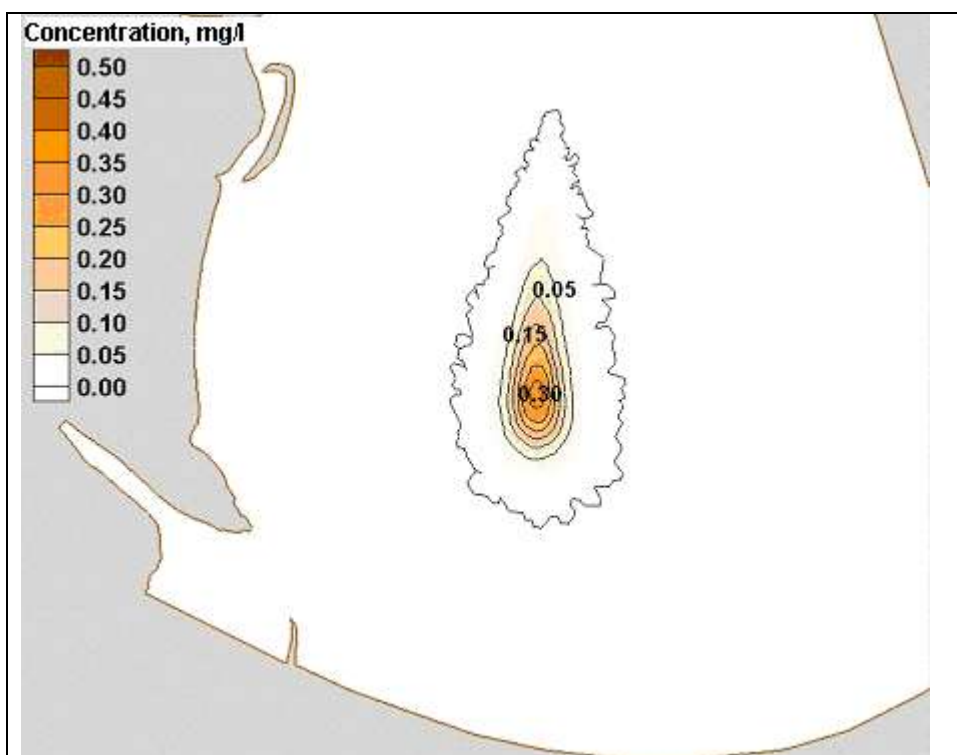


Figure 5.42. Estimated Suspended Sediment Concentration Averaged Over Depth, 12 Hours After the Dumping

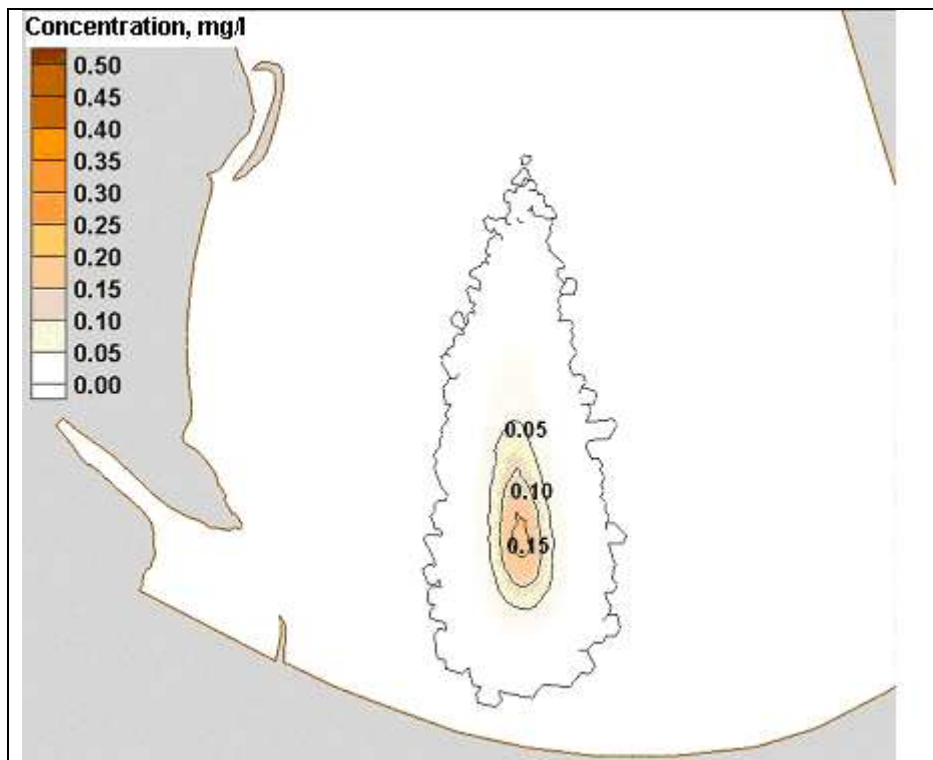


Figure 5.43. Estimated Suspended Sediment Concentration Averaged Over Depth, 18 Hours After the Dumping

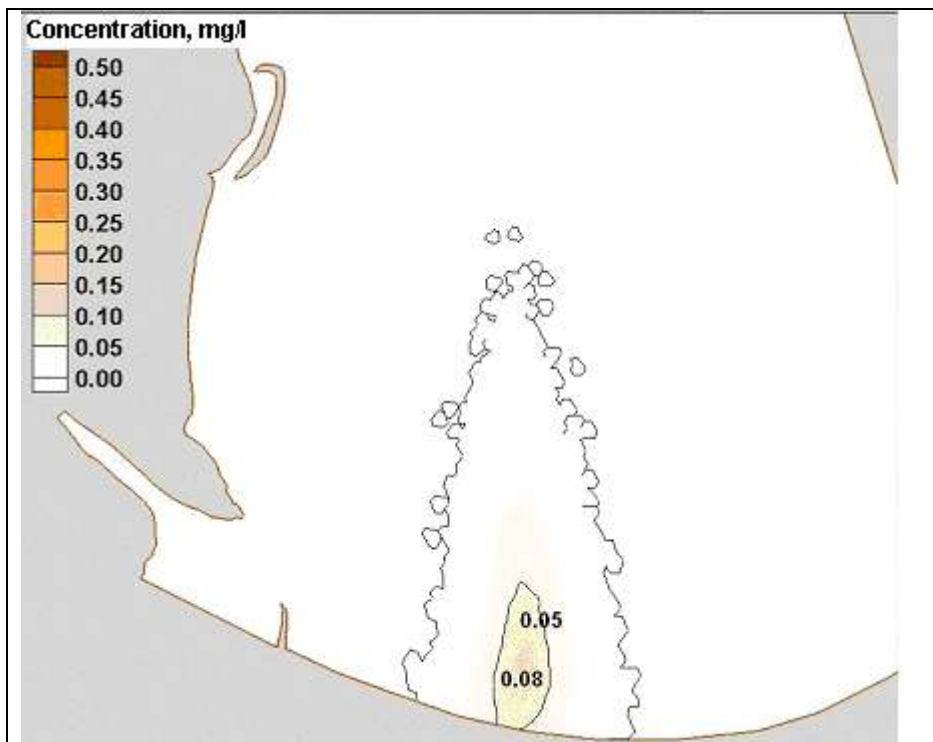


Figure 5.44. Estimated Suspended Sediment Concentration Averaged Over Depth, One Day After the Dumping

Overall, the picture emerging from the present modelling exercise that has used the same parameters as those defined in the Final Expert Report to the Inquiry Commission is one of much lower estimated concentrations of suspended sediments under the continuous dumping scenario, which appear to be twice as low compared to the estimates included in the Inquiry Commission Report.

5.3.3. Results of Modelling Exercise Examining the Impact of Retaining Dam on the Alongshore Sediment Transport

This modelling exercise was undertaken to examine the impact of retaining dam associated with the seaward access channel on the alongshore transport of sediment and enable a more complete analysis of potential transboundary aspects of this impact. The methodological framework for this analysis is described in the Section 5.2.3, and modelling results are graphically illustrated in Figures 5.45-5.46. Sediment concentrations in water, estimated for the modelling period of 3.5 days, are presented in Figure 5.45. Figure 5.46 illustrates changes in the bottom topography for the modelling period of 3.5 days. The modelling results are presented relative to the sea bottom datum $z_0 = 2$ m.

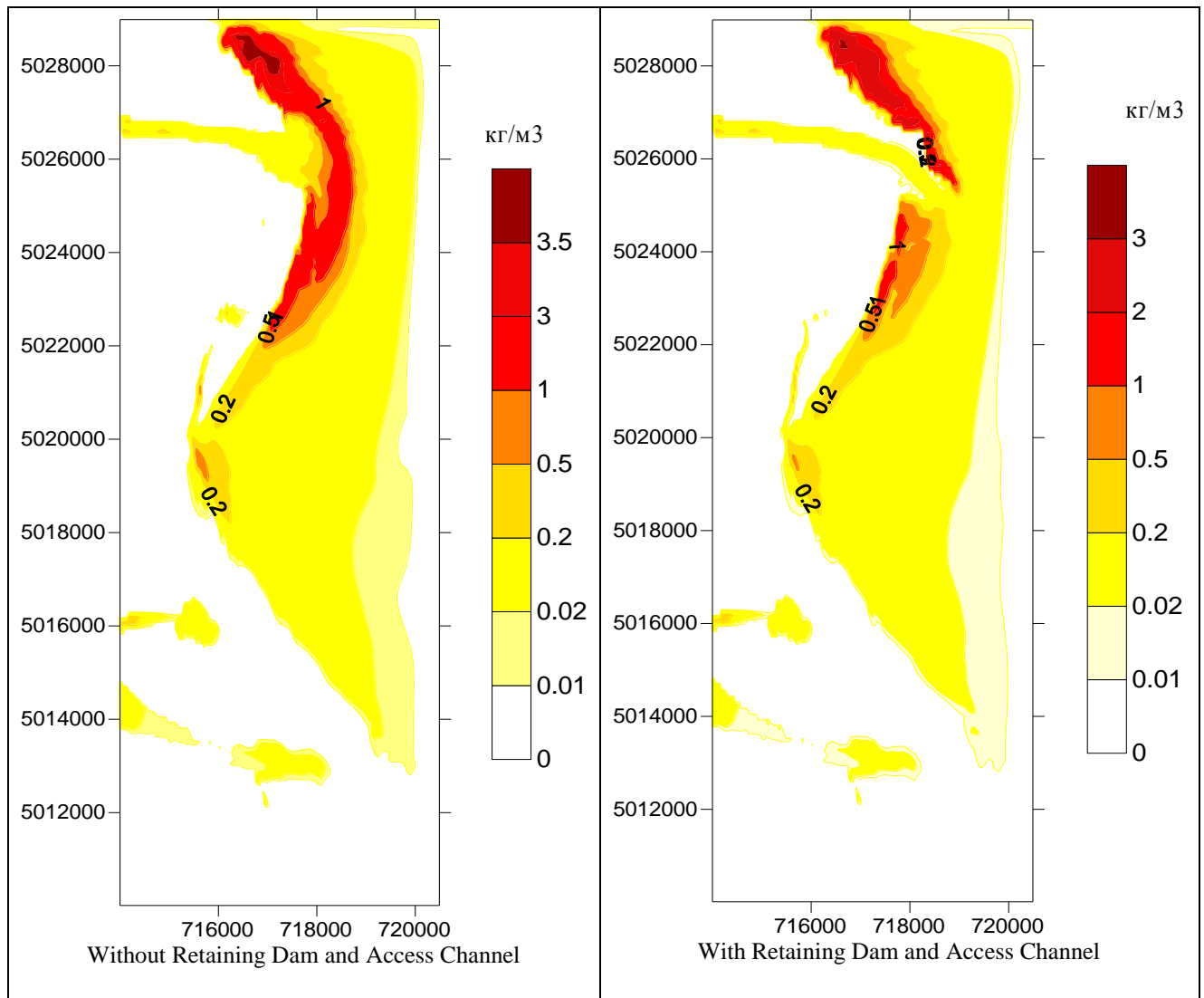


Figure 5.45. Estimated Concentrations of Suspended Sediments in Water

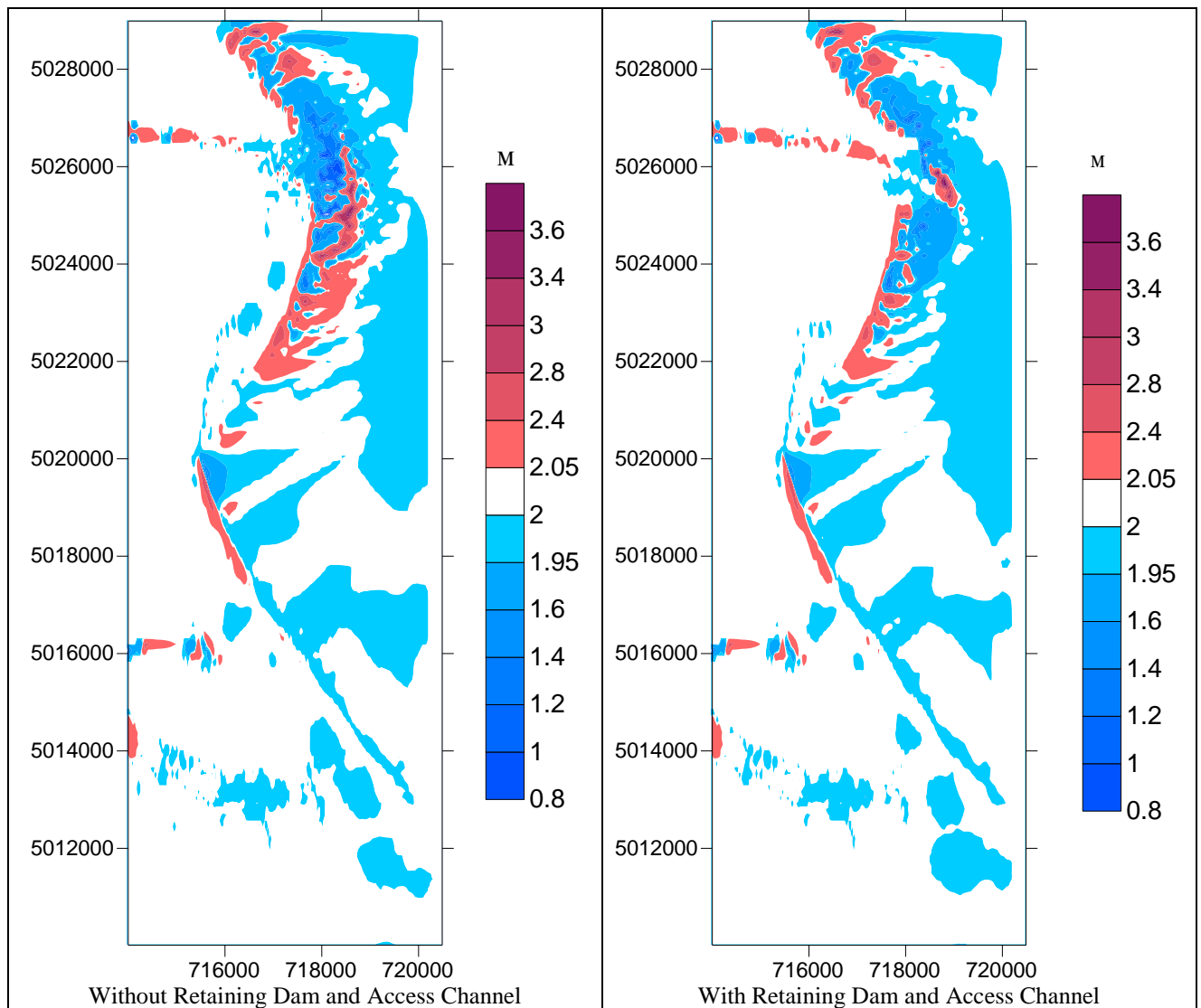


Figure 5.46. Changes in the Bottom Topography

The main outcome of this modelling exercise is an obvious demonstration of the fact that the anticipated impact of the seaward access channel and related facilities on the coastal morphodynamics is localized in nature, being limited to a small area near the Bystre Branch mouth, and this impact will completely fade away at the distance of 6 km from the Bystre Branch mouth, while the distance from the Bystre Branch mouth to the Starostambulske Branch (state border with Romania) is 16 km.

5.3.4. Summary of Modelling Results: Estimated Increments in the Concentrations of Suspended Solids Downstream of Dredging Locations

The results of modelling exercise, described in the Section 5.2.4 and carried out to predict the distribution of turbid water plume downstream of dredging sites located along the Chilia and Starostambulske Branches, are graphically presented in Figures 5.47 and 5.48.

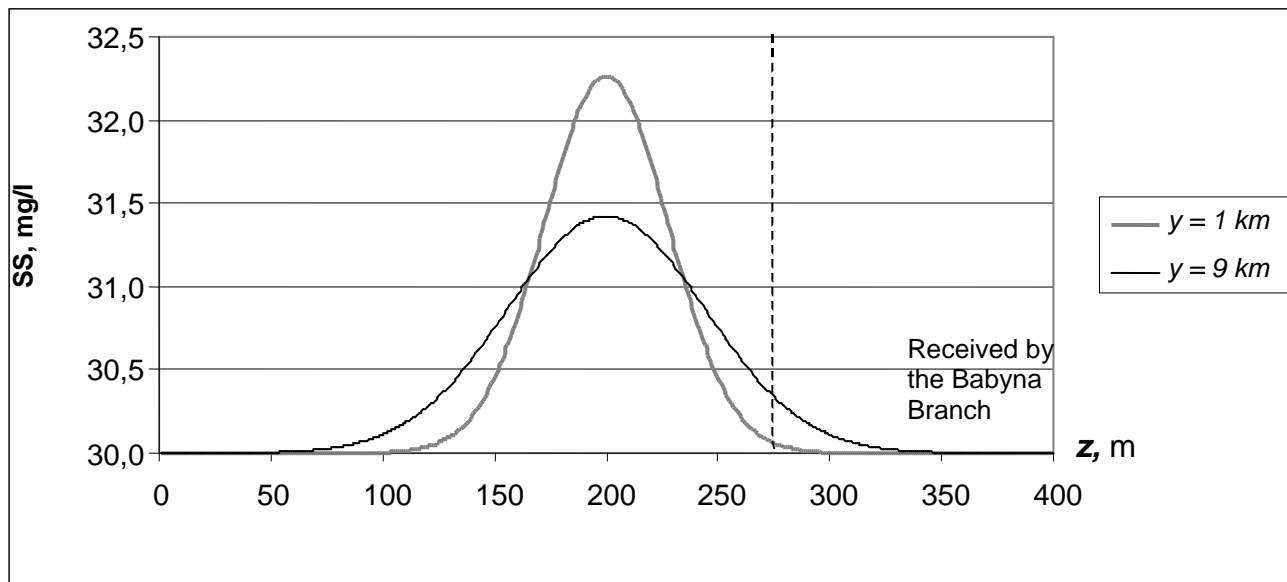


Figure 5.47. Projected Distribution of Fine Suspended Solids over the Cross Section of the Chilia Branch at the Distances of 1 and 9 Kilometres Downstream of Two Dredges Operated at the 47-km Section of the Navigation Route

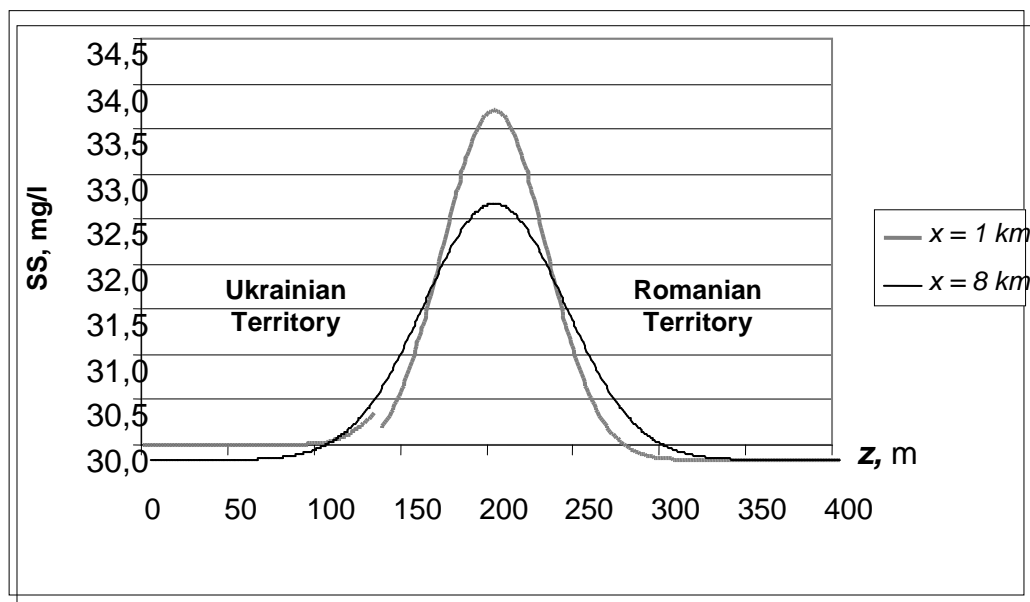


Figure 5.48. Projected Distribution of Fine Suspended Solids over the Cross Section of the Chilia Branch at the Distances of 1 and 8 Kilometres Downstream of One Dredge Operated at the 11-km Section of the Navigation Route

As can be seen from Figure 5.47, the modelling results suggest that dredging operations would cause an increase in the levels of fine suspended solids in the Chilia Branch, measured 1 km downstream of a dredging site with two dredges in operation, but the margin of increase would be rather small (less than 2.5 mg/l along the turbid plume axis relative to the recorded background

concentration of 30 mg/l). At the distance of 9 km, where the Babyna Branch splits off the main branch, the margin of increase would be less than 1.5 mg/l. This increment is considered to be too insignificant to be able to affect the water quality and habitat conditions for fish populations.

The major proportion of sediments re-suspended in the water as a result of dredging operations carried out within the navigable channel of the river will remain within the modelled mainstream section of the Chilia Branch, i.e. at the distance of over 100 m from the riverbanks. **Therefore the part of flow diverted from the Chilia Branch to the Babyna Branch would show a very minor increase in the levels of suspended solids, expected to be below 0.1 mg/l under the pessimistic scenario assuming that a dredge operates in the maximum design-specified proximity to the bifurcation point. This transboundary impact is considered to be minor.**

According to the proposed design, only one dredging site is anticipated to be established and maintained in the Starostambulske Branch, to be located on the 11th kilometre of the navigation route, where the Bystre Branch splits off the Starostambulske Branch. Figure 5.48 illustrates turbidity modelling results for this dredging site with one dredge in operation. Under this scenario, the projected increase in concentrations of fine suspended solids at the distance of 1 km downstream of the dredging site would be at or below 4 mg/l along the navigable section of the river channel, and would be below 3 mg/l at the distance of 8 km downstream of the dredging site (i.e. where the Musura Branch splits off the main branch. Similar to the previous modelling scenario, the turbid plume would be aligned along the central section of the river channel and would not approach the riverbanks closer than 100 m, the Romanian territory would therefore remain unaffected. **In this situation, the transboundary impact of project-related dredging activities is also considered to be minor.**

A series of control measurements of suspended solid concentrations, carried out as part of the comprehensive environmental monitoring programme, with the control sampling sites located 0.5 km downstream of dredges operating in the Chilia Branch, did not provide any decisive evidence of any increase in downstream concentrations relative to the upstream concentration measured at the control station located upstream of the dredging site, and this fits well with the design assumption suggesting that the project-related dredging activities would represent a very minor impact, especially in the context of turbidity pattern prevailing in the Chilia Branch.

5.3.5. Updated Assessment of Transboundary Aspects of Some Project Activities (Dredge Spoils Dumping, Dredging and Riverbank Strengthening) and Their Habitat Loss Impact on Fish and Bird Fauna, Based on the Recent Field Survey Results

According to information provided by the Delta Pilot State Company, some revisions and amendments have been made in the initial organization and management arrangement for dredge spoils dumpsites located along the left bank of the Chilia Branch. According to the revised arrangement, some dumpsites are planned to be closed and decommissioned for various reasons (Table 5.10).

Table 5.10. Recent Amendments and Revisions in the Initial Arrangement Outlined in the Project Phase 1 and 2 Design for the Organisation and Management of Riparian Dumpsites

Riparian Dumpsite	Coordinates Relative to the Navigation Route Alignment, km	Area, ha	Long-Term Management Arrangement
Dredge Spoils Pond 3, Kyslytsky Island	76.2-74.6	11.88	Not planned for future use due to the landlord refusal to extend the lease on the site
Dredge Spoils Pond 13a	39.00-39.5	1.93	Not planned for future use due to limited storage capacity

Riparian Dumpsite	Coordinates Relative to the Navigation Route Alignment, km	Area, ha	Long-Term Management Arrangement
Dredge Spoils Pond 14	36.7-35.5	6.61	Not planned for future use due to the imposition of sanitary and environmental restrictions
Dredge Spoil Pond 15, Yermakiv Island	31.1-30.00	14.82	Not planned for future use due to the landlord refusal to extend the lease on the site
Dredge Spoil Pond 16, Yermakiv Island	29.5-27.40	28.23	Not planned for future use due to the landlord refusal to extend the lease on the site
In-Stream Spoil Storage	60.50-59.60	0.78	Not planned for future use due to the imposition of sanitary and environmental restrictions
Protoka In-Stream Spoil Storage			Not planned for future use due to the imposition of sanitary and environmental restrictions

As can be seen from the above table, both spoil ponds located on the Yermakiv Island are planned to be closed and decommissioned, and these are exactly those sites whose operation is considered by environmental NGOs as being detrimental to bird communities present on the island. Furthermore, the in-stream storage arrangement for dredge spoils, initially anticipated in the Full-Scale Project Design, has been completely rejected for purely environmental reasons, since this arrangement is considered to represent a potential adverse impact on fish fauna. Remaining riparian dumpsites that are planned to be used in the future lie along the left bank of the Chilia Branch outside the protected area, and these are not likely to cause any significant adverse transboundary impact.

The system of riverbank protection structures as proposed in the Full-Scale Project Design comprises a flow guide dam, to be located on the left bank of the Starostambulske Branch immediately upstream of the bifurcation point where the Bystre Branch splits off (please see Figure 3.7) and four riverbank sections planned to be strengthened (with Sections 1 and 2 lying at the bifurcation of the Bystre Branch and Starostambulske Branch (Figure 3.7), and Section 3 and 4 located further downstream along the Bystre Branch). The latter two sections are not considered as the most urgent construction priorities, and their feasibility and final layout will be decided at a later stage based on the monitoring results.

Riverbank strengthening measures are planned to be implemented in those riparian sections that show obvious signs of erosion caused by the natural river channel development processes. It is therefore considered that the risk of degradation of riparian benthic communities and biocoenoses associated with these sections remains credible even under the no-project ('zero') scenario. Weak and scarce benthic communities are typical of these areas, which are not very attractive as habitats for fish and bird communities, therefore any natural or manmade disturbance caused to these areas is not considered to represent a significant adverse impact to fish and bird fauna, and it is even less likely to have any transboundary dimension.

The majority of dredging sites located in the Chilia Branch and identified in the Detailed Design for both Phase 1 and Full-Scale Development of the Project are also characterized by a relatively weak development of zoobenthic communities. This is attributed to higher flow velocities and periodic re-deposition of bottom sediments (mainly sand) that are typical to these sections. This can be illustrated by the results of the seasonal macrozoobenthic survey carried out within the framework of the Comprehensive Environmental Monitoring Programme by the Institute of Hydrobiology of the National Academy of Sciences of Ukraine between October 2004 through November 2005. A summary of results produced during this survey is presented in the Table 5.11. It can be seen from the table that samples taken in the shallow areas and other sections with similar conditions (i.e. the depths between 5 to 8 m) show relatively low species diversity and abundance, regardless of dredging activities and/or presence/absence thereof. On the other hand, these field survey results are

obviously insufficient to provide a reliable assessment of impact caused by dredging activities to benthic communities, especially considering their mosaic pattern and the fact that it is virtually impossible to use and maintain precise sampling locations over seasons.

In the light of the above, the next field survey planned under the Comprehensive Environmental Monitoring Programme will involve the pairwise sampling exercise, i.e. collection of parallel samples at paired sampling sites, to be located within and outside the dredging areas.

Table 5.11. Results of Macrozoobenthic Community Survey Carried Out Along the Navigation Route in the Danube Delta Within the Framework of Environmental Monitoring Programme

Station No.	Station Description	Depth, m	Substrate	Abundance and Biomass of Key Macrozoobenthic Communities (above the line: population (individuals/m ²), below the line: biomass (g/m ²).												
				Total	Oligochaeta	Polychaeta	Gammaridae	Corophiidae	Misidacea	Cumaceae	Isopoda	Bivalvia	Gastropoda	Chironomidae	Ceratopogonidae	Heteroptera
October-November 2004																
S14	Chilia Branch upstream of Ismail, 103 km	16	Sand	<u>13900</u> 144,36	<u>5300</u> 8,3		<u>6380</u> 23,56						<u>2220</u> 112,5			
S13	Downstream of Ismail, 89.9 km	16	Sand	<u>20500</u> 34	<u>17300</u> 16,3								<u>3200</u> 17,7			
S12	Chilia Branch upstream of Kilia, 49 km	6	Clay and sand	<u>17300</u> 412,34	<u>5400</u> 5,5							<u>100</u> 24,74	<u>11800</u> 382,1			
S11	Chilia Branch downstream of Kilia, 39 km	16	Clay	<u>2000</u> 148,9			<u>320</u> 2,7					<u>1680</u> 146,2				
S10	Chilia Branch downstream of Kilia, 32 km	6-8	Sand	<u>22000</u> 1314,3	<u>20400</u> 13,1								<u>1600</u> 1301,2			
S09	Chilia Branch upstream of Vylkove, 21 km	7-12,5	Sand	–												
S05	Bystre Branch outflow, 9.3 km			<u>7000</u> 75,9				<u>6800</u> 3,8				<u>200</u> 72,1				
S04	Bystre Branch mouth, 0 km	5	Silty sand	–												
May 2005																
4	Chilia Branch upstream of Ismail, 103 km	5	Sand	<u>160</u> 2,26	–	–	<u>160</u> 2,26									
7	Downstream of Ismail, 89.9 km	5	Silt	<u>440</u> 0,58	<u>320</u> 0,42	<u>100</u> 0,12	–	<u>20</u> 0,04								
8	Downstream of Ismail, 78 km	8	Sand	<u>1360</u> 6,1	<u>820</u> 0,6	<u>440</u> 0,3	<u>80</u> 3,26	<u>20</u> 1,94								
9	Rift I, 69 km	9	Sand	<u>340</u> 2,92	<u>320</u> 0,22	–	–	–			–	–	<u>20</u> 2,7	–	–	–
10	Rift II, 61 km	4	Sand	<u>1000</u> 0,76	<u>980</u> 0,74	<u>20</u> 0,02	–	–			–	–	–	–	–	–

Station No.	Station Description	Depth, m	Substrate	Abundance and Biomass of Key Macrozoobenthic Communities (above the line: population (individuals/m ²), below the line: biomass (g/m ²).													
				Total	Oligochaeta	Polychaeta	Gammaridae	Corophiidae	Misidacea	Cumaceae	Isopoda	Bivalvia	Gastropoda	Chironomidae	Ceratopogonidae	Heteroptera	Trichoptera
11	Upstream of Kilia, Rift III, 49-50 km	7	Sand	$\frac{1460}{2,24}$	$\frac{1420}{1,32}$	–	$\frac{40}{0,92}$	–			–	–	–	–	–		–
12	Downstream of Kilia, 32 km	5	Clay	$\frac{500}{2,96}$	–	$\frac{20}{0,02}$	$\frac{200}{1,6}$	$\frac{260}{0,52}$			–	–	–	–	–		$\frac{20}{0,82}$
13	Upstream of Vylkove, 21 km	5	Silt, sand	$\frac{1780}{6,14}$	$\frac{1760}{5,68}$	–	–	–			–	–	$\frac{20}{0,46}$	–	–		–
15	Bystre Branch outflow, 11 km	6	Silt, sand, shell sand	$\frac{1060}{28,14}$	$\frac{740}{15,12}$	–	$\frac{200}{0,88}$	$\frac{20}{0,06}$			–	–	$\frac{100}{12,08}$	–	–		–
16	Bystre Branch mouth, 0 km	6	Sand	$\frac{160}{18,52}$	$\frac{20}{0,04}$	$\frac{20}{0,04}$	$\frac{80}{1,14}$	–			–	–	$\frac{20}{17,26}$	$\frac{20}{0,04}$	–		–
17	Sea section facing the Bystre Branch, 0.5 km	7	Sand	$\frac{40}{0,12}$	$\frac{20}{0,04}$	–	$\frac{20}{0,08}$	–			–	–	–	–	–		–
18	Bystre Branch, 0.5 km	6	Sand	$\frac{180}{5,02}$	$\frac{20}{0,08}$	$\frac{20}{1,24}$	$\frac{120}{3,66}$	$\frac{20}{0,04}$			–	–	–	–	–		–
19	Bystre Branch, 4 km	9	Sand	$\frac{60}{2,14}$	–	–	$\frac{40}{0,52}$	–			–	–	$\frac{20}{1,62}$	–	–		–
20	Bystre Branch, 6 km	4	Silt	$\frac{10280}{37,06}$	$\frac{20}{0,06}$	$\frac{40}{0,36}$	$\frac{680}{5,3}$	$\frac{9160}{22,44}$			$\frac{20}{0,06}$	–	–	–	–		$\frac{360}{8,84}$
August 2005																	
3	Upstream of Ismail, 103 km	16		$\frac{520}{0,97}$	$\frac{420}{0,5}$		$\frac{60}{0,16}$	$\frac{20}{0,03}$									$\frac{20}{0,28}$
6	68.3 km, upstream of the DN-60 dredge	8,5		$\frac{180}{0,66}$	$\frac{100}{0,04}$		$\frac{80}{0,62}$										
5	68 km, the DN-60 dredge site	6,3		$\frac{320}{0,28}$	$\frac{300}{0,1}$		$\frac{20}{0,18}$										
4	67 km, downstream of the DN-60 dredge site	11		$\frac{1620}{18,76}$	$\frac{1460}{4,58}$								$\frac{160}{14,18}$				
8	65.7 km, upstream of the E. Kolodochka dredge site	8		$\frac{80}{0,24}$			$\frac{80}{0,24}$										
7	65.5 km, the E. Kolodochka dredge site	7		$\frac{40}{0,24}$	$\frac{40}{0,24}$												
9	Downstream of Kilia, 39 km	17,5		$\frac{1100}{5,43}$	$\frac{60}{0,02}$		$\frac{820}{4,98}$	$\frac{80}{0,03}$									$\frac{140}{0,4}$

Station No.	Station Description	Depth, m	Substrate	Abundance and Biomass of Key Macrozoobenthic Communities (above the line: population (individuals/m ²), below the line: biomass (g/m ²).													
				Total	Oligochaeta	Polychaeta	Gammaridae	Corophiidae	Misidacea	Cumaceae	Isopoda	Bivalvia	Gastropoda	Chironomidae	Ceratopogonidae	Heteroptera	Trichoptera
10	Downstream of Kilia, 32 km	8		<u>440</u> 28,92	<u>170</u> 1,89		<u>20</u> 0,045	<u>10</u> 0,005			<u>10</u> 0,01	<u>20</u> 3,6	<u>50</u> 22,4				<u>160</u> 0,97
11	Upstream of Vylkove, 21 km	16		<u>340</u> 2,15	<u>120</u> 0,04		<u>180</u> 2,08							<u>40</u> 0,03			
15	Bystre Branch, 0 km	4,5		<u>1705</u> 9,25		<u>6</u> 0,05	<u>1666</u> 8,8					<u>33</u> 0,4					
16	Bystre Branch, -0.5 km	5,5		<u>40</u> 0,04		<u>20</u> 0,02	<u>20</u> 0,02										
17	Bystre Branch, -1 km	10		<u>60</u> 0,12		<u>60</u> 0,12											
18	Bystre Branch, 0.5 km	6		<u>60</u> 0,24		<u>40</u> 0,18	<u>20</u> 0,06										
19	Bystre Branch, 2 km	10		<u>1880</u> 4,964			<u>840</u> 3,6	<u>1000</u> 1,3	<u>20</u> 0,04			<u>20</u> 0,024					
22	Starostambulske Branch, 11 km	9		<u>760</u> 4,92	<u>720</u> 4,86		<u>40</u> 0,06										
November 2005																	
4	Chilia Branch upstream of Ismail, 103 km			<u>60</u> 0,88			<u>60</u> 0,88										
5	Downstream of Ismail, 89.9 km			<u>120</u> 0,316	<u>40</u> 0,02	<u>40</u> 0,006	<u>20</u> 0,28							<u>20</u> 0,01			
7	69 km, upstream of dredge site			<u>440</u> 0,07	<u>180</u> 0,01			<u>20</u> 0,03			<u>40</u> 0,01			<u>200</u> 0,02			
6	69 km, rift			<u>460</u> 1,962	<u>20</u> 0,002		<u>200</u> 1,88	<u>180</u> 0,06						<u>60</u> 0,02			
8	62 km, rift			<u>2600</u> 0,986	<u>2280</u> 0,96			<u>20</u> 0,006						<u>300</u> 0,02			
9	52 km, rift			<u>4100</u> 36,24			<u>700</u> 4,28	<u>960</u> 24					<u>20</u> 0,8				<u>2420</u> 7,16
10	Upstream of Kilia, 49 km			<u>100</u> 0,54			<u>0,42</u> 0,42	<u>60</u> 0,12									

Station No.	Station Description	Depth, m	Substrate	Abundance and Biomass of Key Macrozoobenthic Communities (above the line: population (individuals/m ²), below the line: biomass (g/m ²).													
				Total	Oligochaeta	Polychaeta	Gammaridae	Corophiidae	Misidacea	Cumaceae	Isopoda	Bivalvia	Gastropoda	Chironomidae	Ceratopogonidae	Heteroptera	Trichoptera
11	Downstream of Kilia, 39 km			<u>1500</u> 10,28	<u>120</u> 0,02		<u>180</u> 7,2	<u>740</u> 0,58				<u>60</u> 0,78	<u>20</u> 1	<u>60</u> 0,002			<u>320</u> 0,7
12	Downstream of Kilia, 32 km			<u>420</u> 0,64	<u>320</u> 0,04		<u>60</u> 0,58										<u>40</u> 0,02
14	Upstream of Vylkove, 21 km			<u>100</u> 0,86	<u>60</u> 0,48		<u>40</u> 0,38										
18	Bystre Branch, -1 km			<u>60</u> 0,02		<u>40</u> 0,01				<u>20</u> 0,01							
19	Bystre Branch, 0 km			<u>300</u>		<u>300</u> 0,14											
20	Bystre Branch, 0.5 km			<u>120</u>		<u>120</u> 0,08											
21	Bystre Branch, 1 km			<u>120</u>	<u>80</u> 0,02	<u>40</u> 0,04											
22	Bystre Branch, 2 km			<u>1760</u> 42,14	<u>40</u> 0,02		<u>340</u> 1,92	<u>220</u> 0,16			<u>80</u> 0,04			<u>20</u> 0,002			<u>1060</u> 40
23	Starostambulske Branch			<u>20</u> 0,2			<u>20</u> 0,2										

6. MITIGATION MEASURES DESIGNED TO MINIMISE THE LIKELY ADVERSE TRANSBOUNDARY ENVIRONMENTAL IMPACT OF THE PROJECT

Table 6.1 presents a suite of environmental mitigation measures included in the detailed design for the full-scale development of the Navigation Route Project. All relevant details and description of these measures can be found in the EIA Report [1].

Table 6.1. A Suite of Planned Environmental Protection and Mitigation Measures

Category	Description
Resource-Saving	<ul style="list-style-type: none"> • The siting of riparian dumpsites in the scarcely used, bush and reed overgrown areas of low ecological that are waterlogged and/or periodically flooded. • The restoration of dumpsites, including improvements in soil fertility and water regime (in order to restore original agricultural uses). • The environmentally reasonable siting of marine dumpsite in a manner that facilitates the minimization of damage to bottom communities, safe disposal of dredging spoils, and prevention/avoidance of re-contamination of estuarine and coastal waters. • The provision of floating navigation signs in order to avoid the use of riparian land for the installation of these signs.
Protective	<ul style="list-style-type: none"> • The provision of engineered structures combining both navigation and environmental protection functions: <ul style="list-style-type: none"> ➢ Flow guide dam at the bifurcation of the Bystre and Starostambulske Branches, designed to regulate the distribution of river flow between the branches and compensate any potential transboundary impact on the hydrological regime of the Starostambulske Branch; ➢ Riverbank strengthening measures designed to prevent/avoid bank erosion along the navigation route; ➢ Retaining dam along the seaward access channel, designed to minimize siltation processes caused by sea storms; ➢ Settling basins and on-site dikes established at the riparian dumpsites in order to clarify generated drainage flow and minimize water contamination in the Danube River. • Technology measures: <ul style="list-style-type: none"> ➢ Restricting/reducing, as much as possible, the amount of project-related construction and maintenance activities in the period of fish spawning and downstream migration of young fish; ➢ Restricting/reducing, as much as possible, the amount of project-related construction and maintenance activities in the area of the seaward access channel in the bird nesting period; ➢ Restricting ship traffic speeds in order to minimize/prevent the destructive impact of waves on the riparian levees, and meet the established noise limits; ➢ Careful planning, distribution and regulation of mobile plant and machinery; adjusting the number of mechanisms operated simultaneously (a suite of air quality management measures designed to ensure compliance with existing air quality standards); ➢ Introducing the ban on honking and loud music relaying to the ship deck while a ship moves through the protected area; scheduling ship traffic properly so that to ensure that the major proportion is handled in day-time (a suite of measures designed to minimize disturbance to local fauna and reduce damage to fisheries caused by losses in fish catches).
Restorative	<ul style="list-style-type: none"> • River channel deepening along the navigation route as a measure designed to promote the partial restoration of water regime in the Delta, disturbed/alterd by past human activities (river channel straightening and flow guide dam construction by the Romanian party).
Compensatory	<ul style="list-style-type: none"> • The provision of financial compensation for unmitigable damage and utilization of compensation funds for financing appropriate and comparable environmental improvements (for example, compensation of damage to fish stocks through the construction of fish breeding farm; compensation of damage arising from disturbance to bird communities through the implementation of bird habitat improvements in the adjacent areas).
Protective	<ul style="list-style-type: none"> • Implementing a comprehensive environmental monitoring programme in order to enable the prompt and early detection of any potential adverse trends associated with the proposed activities.

All these measures should be considered in the transboundary context since they aim to ensure the conservation and normal functioning of the entire Danube Delta by preventing/minimizing any adverse impact on the biodiversity of the bilateral Danube Biosphere Reserve.